DRY COATING – A CHARACTERIZATION AND OPTIMIZATION OF AN INNOVATIVE COATING TECHNOLOGY

DRY COATING – CHARAKTERISIERUNG UND OPTIMIERUNG EINER INNOVATIVEN COATING TECHNOLOGIE

INAUGURAL – DISSERTATION

zur
Erlangung des Doktorgrades der
Mathematisch-Naturwissenschaftlichen Fakultät der
Heinrich-Heine-Universität Düsseldorf

Vorgelegt von
Caroline Désirée Kablitz
aus Köln

Düsseldorf 2007

Aus dem Institut für Pharmazeutische Technologie und Biopharmazie der Heinrich-Heine-Universität Düsseldorf

Gedruckt mit der Genehmigung der Mathematisch-Naturwissenschaftliche Fakultät der Heinrich-Heine-Universität Düsseldorf

Referent: Frau Juniorprof. Dr. Nora Anne Urbanetz
Korreferent: Herr Professor Dr. Peter Kleinebudde

Tag der mündlichen Prüfung: 1. Juni 2007

INDEX

LIST OF FIGURES

LIST OF TABLES

LIST OF ABBREVIATIONS

Abbreviations	Meaning
AFM	Atomic force microscope
A_H	Hamaker constant [J]
AMG	Acetyl monoglyceride
API	Active pharmaceutical ingredient
A_s	Surface area [m^2]
C	Van der Waals coefficient [Jm^6]
CCF	Central composite face design
CE	Coating efficiency [%]
CI	Confidence interval [%]
d	Diameter [m]
D	Distance [m]
DOE	Design of experiments
DR	Drug release [%]
DSC	Differential scanning calorimetry
E	Young's modulus [N/m^2]
F_c	Capillary force [N]
F_{el}	Electrostatic force [N]
F_f	Static friction [N]
F_g	Resistance force [N]
ff_c	Flowability
F_n	Normal force [N]
F_p	Laplace force [N]
F_r	Line force [N]
F_t	Traction Force [N]
F_{vdw}	Van der Waals force [N]
g	Earth's gravity [9,80665 m/s^2]
G	Gravity [N]
G_t	Shear modulus [Pa]
GPCG	Glatt Particle Coater Granulator
HPMCAS	Hydroxypropyl methylcellulose acetate succinate
HPMCP	Hydroxypropyl methylcellulose phthalate
HPMC	Hydroxypropyl methylcellulose
h_v	Planck's constant [$6.63 \bullet 10^{-34}$ J•s]

$h\varpi$	Lifshitz constant [eV]
k	Spring constant [N/m]
l	Length [m]
MFT	Minimum film formation temperature [°C]
MICA	Monoclinic silicate minerals
M_r	Molecular weight [kg/mol]
pk_s	Logarithm of acid dissociation constant
pH	potentia hydrogenii
p_k	Laplace pressure [Pa]
p_k	differential pressure [Pa]
p-Value	Probability value
Q^2	Measure of prediction
r,R	Radii [m]
$R^2_{adj.}$	Coefficient of determination
RH	Relative humidity [%]
SEM	Scanning electron microscope
T	Temperature [K]
t	Time [s]
TEC	Triethyl citrate
Tg	Glass transition temperature [°C]
TMA	Thermo mechanical analysis
Ts	Softening temperature[°C]
U	Contact potential [V]
USP	United States Pharmacopoeia
VC	Variation coefficient
W	Potential energy [J]
w	Width [m]
wg	Weight gain [%]
x	Median

LIST OF GREEK LETTERS

α	Coefficient of thermal extension
α	Angle of capillary [°]
α_P	Polarizability [C^2/Jm^2]
β	Regression coefficient
δ	Deflection of cantilever
ε_0	Permittivity of free space [$8.85 \bullet 10^{-12}$ C^2/Jm^2]
ε_R	Relative permittivity [C^2/Jm^2]
γ_S / γ_L	Surface tension [N•m]
γ_{SL}	Interfacial tension [N•m]
η	Viscosity [Pa•s]
μ	Dipole moment [C•m]
μ	Coefficient of friction
ν	Materials frequency [s^{-1}]
θ	Contact angle [°]
θ^2	Contact angle [°] (section A 3.2)
σ_1	Unconfined stress [Pa]
$\sigma_{A,B}$	electron density [$e/\mu m^2$]
σ_C	Consolidation stress [Pa]
σ_h	Horizontal stress [Pa]
σ_v	Vertical stress [Pa]
σ_α	Normal stress [Pa]
τ_α	Shear stress [Pa]

A INTRODUCTION

Coating of solid oral dosage forms is a common technique in order to protect the active pharmaceutical ingredient (API) against environmental impact and the body fluids or rather to protect the body against adverse effect of the API. The origin of the coating technology of the modern times is the coating process based on organic polymer solutions which have been replaced gradually by aqueous dispersions in order to avoid the disadvantages of organic solvent based processes like toxicity and environmental pollution [60, 68]. However aqueous dispersions have the disadvantage that the energy input to evaporate the dispersion medium water is high due to the high latent heat of evaporation [84]. Also slow spraying rates must be employed to prevent water from penetrating the surface of the substrate enhancing processing time [33]. Furthermore, the API may interact with the water and i. e. hydrolysis may occur.

A further development of the coating technology is the coating without the uses of organic solvent respectively water, namely the dry coating process, where polymer powder particles and liquid plasticizer are layered on the pellet. This innovative alternative is still in the stage of development and needs further optimization and characterization. Different interpretations of the process are performed and introduced in literature [31, 101, 107-109, 153], however, little information about the coating mechanism and the storage stability of the coated oral dosage form is documented [125]. A certain drawback of the dry coating process is that its coating efficiency is below the coating efficiency of the conventional coatings.

The process is composed of two phases, applying in the first phase the coating material, and curing the coated oral dosage form in the second phase. It is assumed that the critical phase for the coating efficiency is the coating phase whereas the curing phase is decisive for the film formation occurring mainly during this phase. This is in contrast to conventional coating where material application and film formation takes place concurrently. Several parameters are influencing the process which have to be characterized since they differ from the key parameters of the conventional coating like the minimum film formation temperature [77]. As dry coating polymer powders are applied to the dosage form, interparticle forces will take place during the coating phase of the process. Their influence has to be regarded assuming that high interparticle forces will lead to an increase of the coating efficiency. Furthermore, due to the absence of a dispersion media, film formation differs considerably from film formation of aqueous dispersion based processes. Thus, the film formation mechanism needs to be analyzed and the key parameters have to be identified.

First, investigations with respect to the functionality of the film and the storage stability of the dry coated dosage form were used to characterize the process. Drug loaded pellets were coated with micronized polymer powders and liquid plasticizers by the dry coating technique. The drug release of the coated pellets was investigated in order to evaluate the functionality of the film, and the storage stability was investigated by monitoring the drug release after different storing times. Different formulations were composed and compared to each other.

Afterwards the formulations were used for characterizing the two phases of the process. Contact angle measurements and atomic force microscopy gave information about the interparticle forces occurring during the coating phase. Further, thermal analysis was used to describe the coating material with regard to the glass transition temperature. With respect to the film formation it is expected that the Tg affect film formation of the polymer particles. In order to define the curing temperature, which is needed for film formation the pellets are cured at different temperatures. Scanning electron microscopy gave information about the morphology of the film.

After the key parameters of the dry coating process have been determined with regard to the coating efficiency and the functionality of the film, the process parameters of the equipment were characterized using a factorial design. This elucidated the critical factors of the process and lead to an optimization of the process settings. Finally, the process was transferred on larger coating equipment in order to demonstrate the suitability of this innovative coating technology.

1 Aim of film coating

Early in the history the first steps of coating technology is passed on from the 9th century B.C. when the Egyptians began to coat hand-shaped spheres using beside talc and gelatin, silver and gold as coating material demonstrating affluence and political reputation. Coating with honey and sugar was further developed in order to mask the unpleasant and bitter taste encountered as the pill was taken into the buccal cavity and swallowed. In the 19th century, sugar became a major ingredient for coating candy products, which were also used for pharmaceutical coatings. Other natural products such as shellac, zein, and gum arabic were commonly used in the pharmaceutical industry. However, such materials were replaced predominantly by semi- or fully-synthetic substances last century, which are available on the market today. In 1954 Abbott Laboratories produced the first commercially available film coated tablet, although the first film coating appeared in 1930. Compared to sugar coating, film coating provides more flexibility with the ability to coat a variety of substrates [9, 33, 146]. Today the pharmaceutical development and production of solid dosage forms is inconceivable without film coating.

The purpose of film coating can be categorized into three main groups examining it from three different points of view. The first group regards film coating from the point of the patient and stands for safety due to easy identification and for compliance due to visual attractiveness as well as for taste masking which enhances palatability describing the possible reasons why people started to coat oral dosage forms in earlier centuries. The pharmaceutical aspects are found in the second group which results in the increase of the stability of an active drug substance during exposure to light, moisture and atmospheric oxygen and the increase of the mechanical integrity of the oral dosage form during manufacturing and packaging. Additionally, it is possible to avoid incompatibility of active drug substances by physical separation of the incompatibles into the core and coat. Biopharmaceutical rationales display the third group where enteric coatings, sustained release coatings or osmotic pump systems are used to modify the drug release profile. Furthermore, side effects of the active drug substance can be avoided as preventing gastric irritation by employing an enteric polymer coating [9, 16, 33, 124]. Considering these aspects it is self-evident that the development of coating processes and coating materials continues consequently.

2 Coating processes

The early coating techniques were extemporaneous and rather crude often performed on individual pills by picking them up one at time, either on the point of a needle or with a pair or forceps, and dipping them into a coating solution [5]. In the last century, the first steps of liquid coating development were performed using organic solvents. Solutions of polymeric coating material were sprayed onto pellets and the solvent was evaporated subsequently. Later on the organic solvent-based processes have been replaced by aqueous coatings applying aqueous based solutions respectively dispersions onto the pellets. In order to overcome the time consuming processes due to the evaporation of the media the development of new coating technologies proceeds constantly resulting in coating techniques conducted without any media named dry coating or rather dry powder coating.

2.1 Solution based coatings

Film coating in the early 1950s coatings was performed by applying polymers dissolved in organic solvents [119]. The use of such polymer solutions benefits of several advantages like short processing times due to the rapid evaporation of the solvent. Furthermore, the possibility to produce thin, smooth continuous films with 5% - 30% coating material based on weight of the core was an innovation compared to sugar coatings where 50% - 150% coating material had to be applied [8].

Film formation using organic polymer solutions is easily achieved due to the dissolved polymer that after deposition builds the film on the substrate surface by undergoing sol to gel transition as the organic solvent evaporates [86]. Upon evaporation, the polymer molecules approach each other and finally form a homogenous film with a high degree of polymer chain interpenetration [81] (Figure 1). However, the use of organic solutions holds various disadvantages, such as that the toxicity of the solvent requires its recovery combined with high costs and environmental concerns. Nevertheless, organic coatings experience a revival today due to their less problematic stability on storage. Residual solvent or chemical respectively structure changes are few reasons for instabilities of the API whereas coats applied from aqueous dispersions often reveal changes in the drug release after storage due to incomplete film formation during the process [87].

Figure 1: Film formation of solution based coatings

An alternative coating technology is the aqueous solution based coating where water-soluble polymers are applied on solid dosage forms [96]. The major application of such systems is for protective coatings as the films will be water soluble without any functional effect. The coating process is similar to the organic based process; however, the high energy demand of the process has to be considered. Higher coating temperatures and lower spraying rates due to the relatively high latent heat of vaporization of water (540 kcal/g for water vs. 204 kcal/g for ethanol) [84] must be employed to ensure sufficient evaporation of solvent. The low polymer concentration, which is limited by the viscosity of the solution, extends the process time which is disadvantageous for both, the organic and the solvent based coatings. Therefore, the improvement to coat oral dosage forms with polymer dispersions was a major step in the history of coating technology.

2.2 Dispersion based coatings

Organic solution based coatings of water-insoluble polymers were predominately replaced by aqueous dispersion based coatings. The use of aqueous polymer dispersions is of interest due to the high amount of polymer in the dispersion resulting in shorter process times compared to aqueous solution based processes. The dispersion with up to 30% (w/w) solids including the polymer with a colloidal size is sprayed on the cores similar to the coating solution, however, the film formation differs completely since water-insoluble solid polymer particles are used. The mechanism is a complex process [75] and is still discussed in literature [137].

The film formation of aqueous polymer dispersions using latex or pseudolatex polymer materials is driven by the evaporation of water and subsequent coalescence of the polymer particles [45]. The process of film formation using aqueous polymer dispersions is usually divided in three phases [3, 137]. Phase I is the evaporation of water. The density of the dispersion increases until the colloidal particles come into contact with each other and, subsequently, form close-packed arrays. The particles then undergo deformation to polyhedra [103] without interparticle spaces in phase II, induced by an increase in temperature above the minimum film formation temperature (MFT), one of the most important parameters of film formation from aqueous dispersion based coatings. It is

defined to be the minimum temperature at which a cast film becomes crack-less and clear [40]. Below this temperature, the dried dispersion appears opaque and powdery [45]. Increasing the temperature above the glass transition temperature (Tg) in stage III, the boundaries between the particles disappear through interdiffusion of polymer chains developing a continuous film without distinguishable particles [114]. The micromechanical process of the coalescence is still not completely analyzed, however, several models are discussed. Dillon et al. [36] explained the film formation mechanism introducing the dry sintering hypothesis which postulates that the surface tension of the polymer is the driving force accompanied by viscous flow and particle deformation. An analogous mechanism based on the polymer-water interfacial tension was suggested by Vanderhoff et al. [69] known as wet sintering. An alternative theory was developed by Brown et al. [20] termed the capillary theory. Capillary forces exerted by the liquid facilitate the deformation of the particles in the interstitial capillary system between particles during drying.

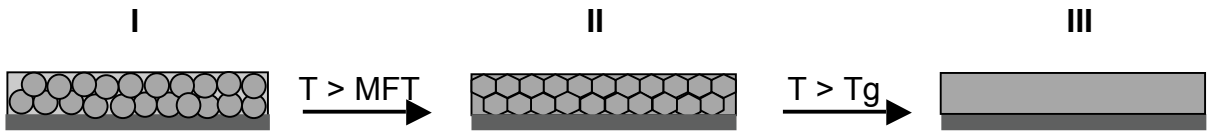

Figure 2: Film formation of aqueous dispersion based coatings

Film formation of aqueous polymer dispersions usually takes several minutes up to hours depending on film thickness and environmental conditions [152]. Temperature has an important effect on the rate of polymer diffusion and film formation [17, 103] and is highly affecting the quality of the resulting film. Recently Siepmann et al. reported that additionally to heat, humidity enhances film formation of HPMCAS coatings. Furthermore film formation was shown to be dependent on the particle size of the polymer. Additionally, it is described in the literature that film formation begins at the upper surface of the coating and proceeds from top to bottom progressively during drying or rather curing [57]. The formation of a thin surface layer of coalesced particles is assumed, through which the residual water needs to diffuse during the progress of drying [132].

Like organic based processes aqueous based process exhibit several disadvantages. Since water is used as dispersion media it has to be evaporated which is time and energy consuming. A simple way to shorten coating time is to use a coating dispersion of higher concentration, but this approach is limited by the risk of spray nozzle blocking caused by agglomerated particles, which can be transported to the nozzle. Furthermore, nozzle blocking is caused by premature coalescence of the polymer in the dispersion. Hence, the use of dry powders as coating material is a new challenge of the coating technology.

2.3 Dry coating

Initially, redispersible powders were developed for the preparation of aqueous polymer dispersions. Enteric polymers contain esters in their chemical structure which may be hydrolyzed if stored as aqueous dispersion. Thus, redispersible dry powders were offered by the manufacturers in order to be dispersed in the dispersion media prior to the application [120]. These redispersible powders were adopted to develop new coating technologies.

Coating with polymer powders is an innovative and promising alternative to the conventional coating technology with organic polymer solution or aqueous polymer dispersion. Conducting organic solvent based processes the solvent needs to be recovered due to environmental pollution. Coating processes with aqueous dispersions are very time and energy consuming [148] caused by the low concentration of coating polymer and large amounts of water which need to be evaporated. Compared to both the dry coating method is favourable regarding environmental friendliness and safety. It is a coating process without any use of water or organic solvent. Because of their absence, water or organic solvent do not need to be evaporated which leads to shorter processing times. It might be a very suitable coating method in order to coat drugs which are sensitive to organic solvents or water.

Different variations of the dry coating process have been developed layering polymer powder particles on the pellet or tablet surface by simultaneously feeding/spraying polymer powder and plasticizer followed by a curing phase at increased temperatures. By using a CF granulator (centrifugal coater) tablets were coated by adding polymer powder and plasticizer composition separately by a powder feeder and a spray nozzle. The powder is dosed onto the tablets and the liquid is sprayed. Afterwards film formation was induced by spraying a small amount of water on the coated beads and by increasing the temperature facilitating coalescence. The tablets were cured in an oven [101]. In an other study, pellets were coated with polymer powder and plasticizer mixed to an emulsion with HPMC solution using a Wurster insert with a powder feeder and separate spray nozzle [108, 109]. However, these processes do not meet exactly the conditions of the dry coating process using a small amount of water. It was demonstrated that dry powder coating compared to aqueous coating procedures generally required higher coating levels, higher plasticizer concentrations, and higher processing temperatures. Recently, soft-gelatin capsules were coated applying the dry powder and the liquid plasticizer separately but simultaneously meeting the process conditions of the dry coating process [30] without any use of water.

An alternative was performed by Zhu et al. conducting the dry coating process in a patented electrostatic pan coater achieving powder adherence due to the electrostatic charging without any water [154]. Furthermore, tablets were coated with polymer powder which prior to the coating process had been preplasticized by mixing polymer powder with plasticizer and sieving afterwards [31] or rather by a hot-melt extrusion process of polymer, plasticizer and thermal lubricant followed by cryogenically grinding of the extrudate [147, 153]. Sauer et al. coated tablets containing a highly water soluble drug applying primers before the powder coating in order to achieve better adhesion of the polymer powder [125]. The disadvantages of these processes are the small batch size of 50 g and the need of additional processing time and equipment for preparation of the coating material. Moreover, prolonged-release microparticles were developed composed of core particles with multi-layer coat of binder, drug and polymeric nanopowder using a high-speed elliptical-rotor powder mixer [65]. Recently, Ando et al. examined the use of a different approach to the making of compressed tablets containing pellets. A double-structure punch (center punch and outer punch) compressed and dry coated the pellets in a single run [2].

In contrast to the research work in literature, in this study the dry coating process is carried out applying the dry powder using a rotary fluid bed equipment. The polymer is passed as dry powder via a powder feeder to the three way nozzle which is able to transport separately but closely together the plasticizer composition and the dry powder into the pellet bed [71]. This method secures an efficient application of the coating material onto the pellets compared to separate addition which was performed by Obara et al. and Pearnchob et al. [101, 109] and does not require any addition of water. Additionally, the dense spiral movement of the fluid bed enhances the layering of the polymer particles by clinging them tightly to the pellet, which minimizes the loss of powder. Furthermore, it does not need any pre-steps as hot-melt extrusion.

First steps of process optimization of the dry coating process is described in the literature by Genovesi et al. who demonstrated that lower feeding/spraying rates results in an increase in coating uniformity not defining if the uniformity between complete batches or the uniformity of the pellets' film is meant [53]. Generally, process optimization can be performed using factorial designs. The significant process parameters and interactions between them can be determined and consequently used to optimize ad scale up process [79, 97]. With respect to the production of pellets in the rotary fluid bed, there is one study describing the optimization of a process using factorial design [19]. The results indicated that the pellet mean particle size was negatively affected by the rotor speed, while the binder spray rate had a positive effect on size; pellet flow properties were enhanced by

operating at increased air flow rate and deteriorate with increased binder spray rate. Nevertheless, an optimization of the dry coating process is still pending.

Compared to conventional coatings the dry coating process differs in its way of material application and film formation. Due to the missing dispersion media the adhesion of powder particles to the pellets surface at the beginning of the process and film formation turned out to be especially critical steps and will be introduced in the following chapter.

3 Application and film formation of coating material performing the dry coating process

The dry coating process can be divided in two phases, the coating and the curing phase. During the coating phase polymer powder and plasticizer are added separately but simultaneously to the pellets and adhere on their surface achieving a homogeneous application of the coating material onto the pellets. During the curing step film formation is achieved by an increase in temperature [71]. In contrast to conventional coatings the vehicle, used to apply the polymer, is missing. Hence, the polymer particles stick to the pellets due to the interparticle forces. Alike, the film formation is based on a different mechanism since no vehicle exerting capillary forces and promoting coalescence is used. It can be assumed that by using a liquid plasticizer capillary forces will still play a certain role as well as the viscous flow of the polymer particles will promote the film formation.

3.1 Material application

During powder processing and handling, individual particles are in contact with each other and with the surface of any equipment used. The degree of interaction between the particles and between the particles and the surfaces determines the properties of the powder bulk, e.g. during mixing, powder flow, granulation, compaction and drug delivery to the lungs. Thus, interparticle forces are influencing the interaction between the particles and play an important role for the development of dry powder inhalers [44, 88, 89, 117] as well as for the development of solid pharmaceutical dosage forms [116, 136].

Interparticle forces depend on the one hand on the particle size and the distance between the two acting partners and on the other hand on the shape including surface properties and deformation, as well as the chemical identity and adsorbed materials [59, 115-118]. The most important interparticle forces are van der Waals forces and electrostatic forces and, when magnetic materials are used, magnetic forces. Additionally, due to the presence of liquids capillary forces can appear. In the following sections the different forces will be introduced and the parameters influencing the forces will be described. Miscellaneous approaches to calculate the forces will be shown, however, it has to be considered that the calculations are theoretically and based on ideal geometries. In chronology to the performance during the material application the interparticle forces will be described.

3.1.1 Capillary forces

Capillary forces exceeds when the liquid has a certain volume. Capillary forces are commonly encountered in nature because of the spontaneous condensation of liquid from surrounding vapor, leading to the formation of a liquid bridge [24, 121]. Furthermore they can be exerted by simply adding small amounts of liquid to dry powders as during granulation [28]. In the beginning of the dry coating process during the material application the powder will get in contact with the liquid plasticizer, which is able to build up capillary forces between the solid material prior to its penetration into the polymer (see A 5.2).

The capillary force F_C, which acts due to the liquid bridges, is the sum of F_P and F_R (Eq. 1), whereas F_P is based on the Laplace pressure (p_K) and F_R is the force at the three-phase point between solid, liquid and gas.

$$F_C = F_P + F_R \qquad \textbf{Eq. 1}$$

The Laplace pressure is calculated using the Young-Laplace equation (Eq. 2), which relates the pressure difference between the two phases [34] and the curvatures of the surface:

$$p_K = \gamma_L \left(\frac{1}{R_1} + \frac{1}{R_2} \right) = \frac{2\gamma_L}{R_m} \qquad \textbf{Eq. 2}$$

γ_L = surface tension of the liquid

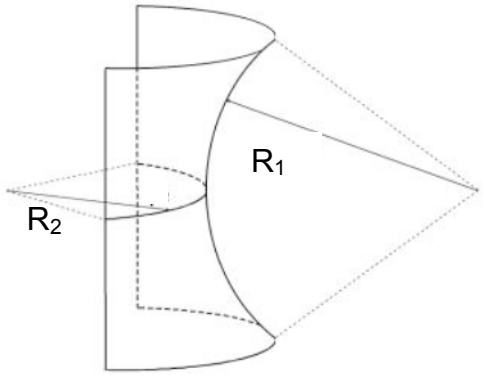

Figure 3: Radii R_1 and R_2 of the curvature of a liquid bridge

R_1 and R_2 are the two principle radii of the curvature (Figure 3) and stand in a fix relation to each other (Eq. 3):

$$R_m = \frac{2R_1R_2}{R_1 + R_2} \qquad \textbf{Eq. 3}$$

As long as $|1/R_1| > |1/R_2|$, the Laplace pressure contributes positively the capillary force (F_C). The force F_P resulting from the Laplace pressure is described by the following equation (Eq. 4):

$$F_P = p_k \frac{\pi d_K^2}{4} \sin^2 \alpha = \gamma_L \left(\frac{1}{R_1} - \frac{1}{R_2} \right) \frac{\pi d_K^2}{4} \sin^2 \alpha \qquad \textbf{Eq. 4}$$

whereas α stands for the angle of the liquid bridge as illustrated in Figure 4.

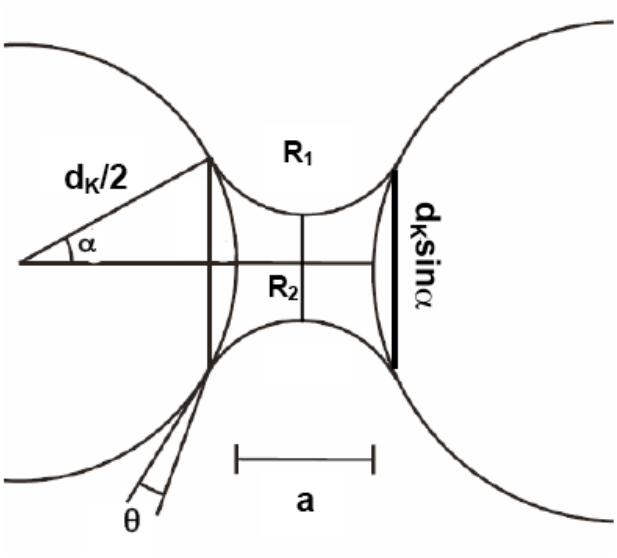

Figure 4: Scheme of a liquid bridge, a = distance between the spheres

The force F_R is calculated using the following equation (Eq. 5):

$$F_R = \gamma_L \sin(\alpha + \vartheta) \pi d_K \sin \alpha \qquad \textbf{Eq. 5}$$

Combining both equations, F_C can be defined as (Eq. 6):

$$F_C = \pi \gamma_L d_K \sin^2 \alpha \left[1 + \frac{d_K}{4} \left(\frac{1}{R_1} - \frac{1}{R_2} \right) \right] \qquad \textbf{Eq. 6}$$

Hence, the capillary forces depend among other parameters on the curvature of the solid particles and on the surface tension (Figure 4). In literature different approaches for the calculation of capillary forces are performed considering the geometry of the particles [100, 121, 132, 141]. A critical distance is described depending on the volume of the liquid bridge. By overstepping this distance the capillary will shear and the force will disappear.

This phenomenon can be observed in granulation when the amount of liquid binder is too high [8]. In this study, it is not expected as the plasticizer penetrates into the particles and, consequently, the amount of liquid decreases.

3.1.2 Van der Waals forces

After the plasticizer has been penetrated into the particles the remaining forces are van der Waals forces beside electrostatic forces which will be described in the next section. Van der Waals forces are a class of intermolecular forces which arise when molecules are polarized becoming dipoles or multipoles. Between molecules three different van der Waals forces exist, namely Keesom forces, Debye forces and London forces. The Keesom forces are the attractive forces between permanent dipole molecules. The Debeye forces are the attractive forces between a permanent dipole molecule and an induced dipole molecule. An induced dipole molecule is a nonpolar molecule which was induced to become a dipole molecule by the attractive force of another dipole molecule. London forces are attractive forces between two nonpolar molecules. Because of the constant motion of the electrons, an atom or molecule can develop a temporary (instantaneous) dipole when its electrons are distributed asymmetrically about the nucleus. A second atom or molecule, in turn, can be distorted by the appearance of the dipole in the first atom or molecule which leads to an electrostatic attraction between the two atoms or molecules. They are also called induced dipole-induced dipole forces. Hydrogen bonds are high dipole-dipole attractions that occur between a hydrogen atom and any of oxygen/fluorine/nitrogen.

The potential energy (W_{AB}) of the interaction between the molecules A and B is (Eq. 7)

$$W_{AB}(D) = -\frac{C_{AB}}{D^6} \qquad \textbf{Eq. 7}$$

The potential energy (W_{AB}) stands in a reciprocal relation to the distance (D) to the power of 6 between molecules. C_{AB} (van der Waals coefficient) is the interaction between the molecules and sums up contributions of all three dipole-dipole interactions. The potentials of the three different van der Waals forces are shown in Table 1.

VAN DER WAALS FORCES	POTENTIAL W (J)	INTERACTION
Keesom	$W_K = -\frac{C_{orient}}{D^6} = -\frac{\mu^4}{3(4\pi\varepsilon_0)^2 k_B T}$	permanent dipole – permanent dipole
Debye	$W_D = -\frac{C_{ind}}{D^6} = -\frac{\alpha_P \mu^2}{(4\pi\varepsilon_0)^2 D^6}$	permanent dipole - induced dipole
London	$W_L = -\frac{C_{disp}}{D^6} = -\frac{3}{2} \cdot \frac{h_v \nu {\alpha_P}^2}{(4\pi\varepsilon_0)^2 D^6}$	induced dipole – induced dipole

Table 1: Interaction potentials of van der Waals forces

C = van der Waals coefficient (Jm^6), α_P = polarizability (C^2/m^2J), μ = dipole moment (Cm), ε_0 = permittivity of the free space ($8.85 \cdot 10^{-12}$ C^2J/m), k_B = Boltzmann konstant ($1.38 \cdot 10^{-23}$ J/K), K = temperature (K), h_v = Planck's constant ($6.63 \cdot 10^{-34}$ Js), ν = materials frequency (s^{-1}) [25]

In order to determine the interaction between solids respectively particles two different approaches are described in literature. The microscopic approach is based on the interactions between atoms and molecules. As the forces of molecules and atoms will sum up, the interaction can be calculated by integrating of the molecular density over the entire volume of the solids. The calculation is performed using the Hamaker constant (A_H).

$$A_H = \pi^2 C_{AB} \sigma_A \sigma_B \qquad \textbf{Eq. 8}$$

whereas σ_A and σ_B stands for the molecular (electron) density ($e/\mu m^2$) of molecule A and B.

Using this approach the influence of neighboring molecules on the interaction between any pair of molecules is not considered. In reality the van der Waals forces between two molecules changes by the presence of a third molecule. This problem of additivity is completely avoided in the macroscopic theory developed by Lifshitz [85]. Lifshitz neglects the discrete atomic structure and the solids are treated as continuous materials with bulk properties (Eq. 9).

$$h\varpi = \frac{4}{3}\pi A_H \qquad \textbf{Eq. 9}$$

Generally, the Hamaker constant (A_H) has a value around 10^{-20} – 10^{-18} J which results in a Lifshitz constant ($h\omega$) of 0.2 – 9 eV being equal to 3.2 x 10^{-20} – 1.44 x 10^{-18} J (1 eV = 1.6 x 10^{-19} J).

In the following Table 2 the different models are shown considering the surface geometry of the two partners (flat surface/flat surface, flat surface/sphere, sphere/sphere). It is presumed that the surfaces are smooth and do not undergo any changes respectively deformation and that the distance is between 0.4 nm and 100 nm. Above 100 nm the van der Waals forces will be lower than calculated and below 0.4 nm the Born repulsion force will act.

MODEL	MICROSCOPIC CALCULATION	MACROSCOPIC CALCULATION
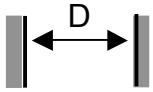	$\frac{F_{vdW}}{A_S} = \frac{A_H}{6\pi D^3}$	$\frac{F_{vdW}}{A_S} = \frac{h\varpi}{8\pi^2 D^3}$
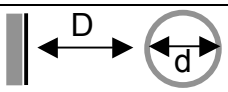	$F_{vdW} = \frac{A_H d}{12D^2}$	$F_{vdW} = \frac{h\varpi d}{16\pi D^2}$
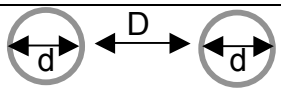	$F_{vdW} = \frac{A_H d}{24D^2}$	$F_{vdW} = \frac{h\varpi d}{32\pi D^2}$

Table 2: Van der Waals forces (F_{vdW}) between model partners
A_S = surface area (m^2), d= diameters (m), D = distance (m)

3.1.3 Electrostatic forces

Electrostatic forces (Coulomb forces) (F_{el}) emerge between charged particles. When the particles are both either positively or negatively charged, the force is repulsive. When they are of opposite charge, it is attractive. The force can result from friction or even by contacting solid surfaces and building up an electric potential. Due to electron transfers between the particles the potential emerges. The particle, which needs less energy to release the electrons, delivers them to the other particle. The charging of isolators and electronic conductors is depending on the electron surface density. In Table 3 according to Table 2 the equations needed for calculating the electrostatic force of the different models are shown differing between isolators and electronic conductors.

MODEL	ELECTRIC ISOLATOR	ELECTRIC CONDUCTOR
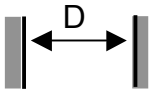	$\frac{F_{el}}{A_S} = \frac{1}{2}\varepsilon_r\varepsilon_0 U^2 \frac{1}{D^2}$	$\frac{F_{el}}{A_S} = \frac{1}{2}\frac{\sigma_1\sigma_2}{\varepsilon_r\varepsilon_0}$
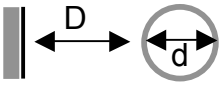	$F_{el} = \pi\varepsilon_r\varepsilon_0 U^2 \frac{d}{2D}$	$F_{el} = \frac{\pi}{2}\frac{\sigma_1\sigma_2}{\varepsilon_r\varepsilon_0} d^2$
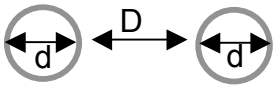	$F_{el} = \pi\varepsilon_r\varepsilon_0 U^2 \frac{d}{4D}$	$F_{el} = \frac{\pi}{8}\frac{\sigma_1\sigma_2}{\varepsilon_r\varepsilon_0}\frac{d^2}{\left(1+\frac{2D}{d_1+d_2}\right)^2}$

Table 3: Electrostatic forces (F_{el}) between model partners
ε_r = relative permittivity (C^2J/m), ε_0 = permittivity of the free space (C^2J/m), U = contact potential (V), σ = electron density (e/µm) A_S = surface area (m^2), d= diameters (m), D = distance (m)

However, the electron density of surfaces is inhomogeneous and cannot be determined as well as the charging can be influenced by adsorbed impurities covering the surfaces. Thus, the calculation of F_{el} is difficult and often an approximate value. The equations of electric conductors is valid if D<d. F_{el} of electric isolators can be calculated for the models flat surface/flat surface and flat surface/sphere if the charge is distributed homogeneously without considering the relation between the interaction and the distance. Nevertheless, the probability of a homogeneously distributed electron density is small and a dependency on the distance has to be expected.

3.1.4 Dependency of interparticle forces on different parameters

In Figure 5 the dependency of the forces on the distance between the partners flat surface and sphere is shown. The diameter of the sphere is 10 µm.

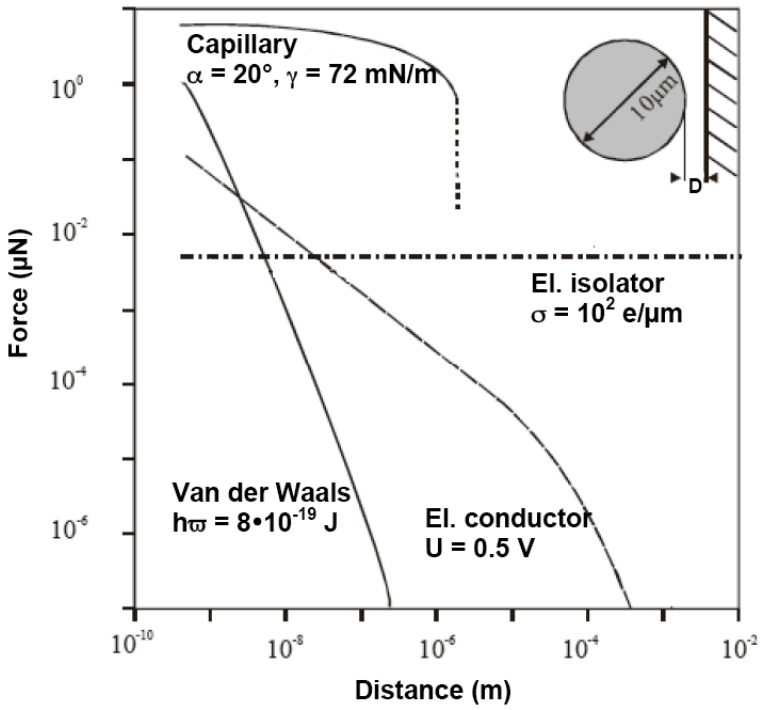

Figure 5: Dependency of forces on the distance between a flat surface and a sphere d = 10 µm [90, 127]

Capillary forces are the strongest forces with an acting range up to 10^{-6} m. They are the predominated forces when liquid bridges can be build up. By increasing the distance between the partners, the capillary will be pulled off and the force will vanish. In contrast, the other forces decrease by increasing the distance between the sphere and the flat surface. The acting range of van der Waals force is the shortest. Almost at distances above 10^{-7} m the van der Waals force becomes weak and is negligible. The electrostatic forces have a more extensive acting range. However, by separating the partners the charge of the electric conductors gets reduced whereas the isolator has a constant force. The electrons responsible for the charge of the conductor are located in the first layers of the surface with a range to the inside of 1 nm, which enables charge equalization during the separation of the partners (tunnel effect). In contrast, the electrons of isolators are located in the surface layers up to 1µm to the inside. By separating the two partners the electrons of the isolator are not able to equalize and remain on the surface. For an equalization of isolators the separation has to be arranged extreme slowly in order to give

the material time to delocate the electrons. However, this applies only, if the electron density is distributed homogeneously on the flat surface.

With regard to the same model system the dependency of the force on the particle's diameter is described (Figure 6):

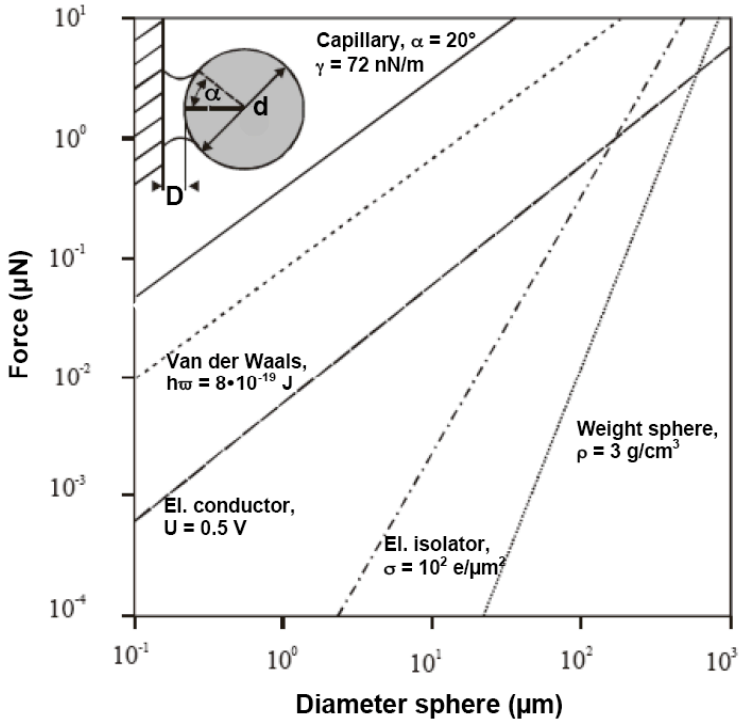

Figure 6: Dependency of the forces on the particle diameter [90, 127]

Small particles are more strongly affected by interparticle forces as larger particles. With respect to the small diameter, capillary forces are the strongest forces followed closely by the van der Waals forces. The force of the conductors is decreased one potency compared to the van der Waals forces still having an influence on the small particles. This is caused by the higher contact potential since the charge of the conductors is close to the surface and higher in comparison to isolators. The force of the isolator becomes more attractive on larger particles. By increasing the diameter of the sphere above 100 µm the relation between the force and the weight of the sphere or rather gravity (G) changes. This is an important phenomenon for the flowability of powders. The gravity is calculated using Eq. 10:

$$G = \frac{\pi}{6} \rho_S g d^3 \qquad \textbf{Eq. 10}$$

whereas ρ_S is the density and d the diameter of the solid.

According to the volume of a sphere the weight increases with the cubic diameter of the sphere in contrast to the interparticle force, which is in a linear relation to the diameter. Thus, the force increases by decreasing the diameter of the sphere leading to a stronger adhesion. Consequently, the flowability of the smaller particles is impeded. This phenomenon is the reason, why fine powders flow worse than coarse powders.

A further parameter influencing the interparticle forces is the surface roughness. The effect is demonstrated in Figure 7 using the model of the flat surface and the sphere. The sphere has a certain surface roughness, which is increasing the distance between the partners. The capillary force depends on the volume of the liquid. When the volume is high enough, the liquid will surround the roughness and the force of the capillary will be based on the diameter of the particle and will be slightly decreased by the increase of the roughness' diameter. When the volume is smaller, the capillary will be build up between the roughness and the flat surface of the partner. Hence, by increasing the diameter of the roughness the force will be decreased. Above a certain diameter of the roughness the capillary force increases linearly with the log diameter of the roughness. The capillary broadens which results in a larger angle α and an increase in the capillary force.

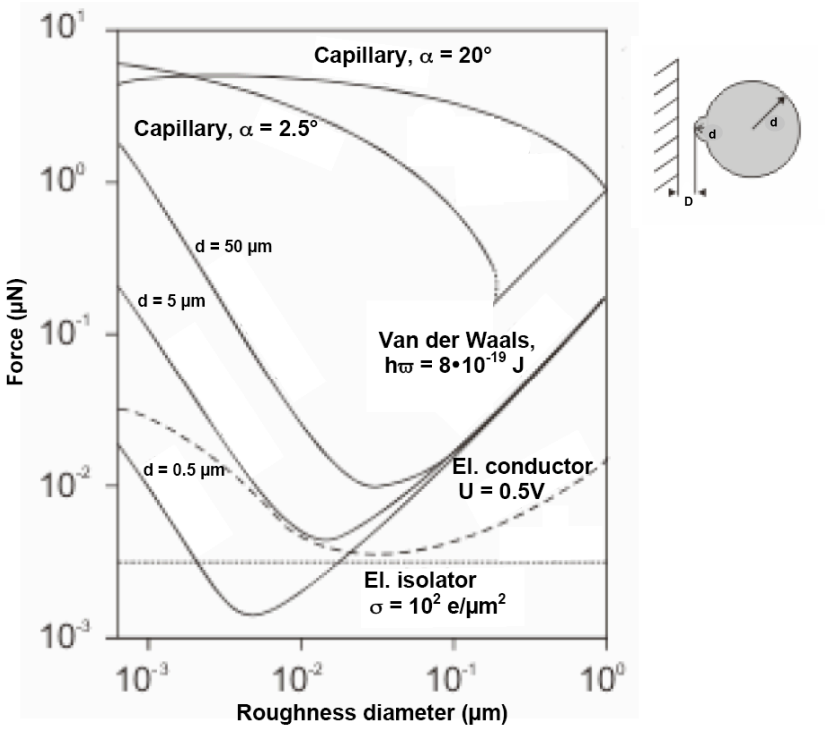

Figure 7: Dependency of the forces on the surface roughness [90, 127]

Van der Waals forces are very sensitive on changes in the diameter. They strongly decrease by increasing the surface roughness passing through a minimum and increase since the roughness is the only parameter responsible for the development of the

interparticle forces. By increasing the diameter of the roughness of the sphere the amount of the forces of the basic sphere is decreased as the distance between the sphere and the flat surface enlarges. In contrast the amount of the force built up by the roughness increases. The relation between the different diameters and the interparticle force are shown in Figure 7 detecting the proportional relation of the sphere's diameter and the interparticle forces. The forces exerted by the roughness increase as the diameter of the roughness increases. Finally, the curves of the different diameters meet after passing through the minimum due to the fact that the forces in this diagram are solely depending on the model roughness with a constant diameter. The force of the conductors show a similar effect passing a minimum at a certain diameter, however, the effect is less intensive as the slope of the conductor is decreased compared to the slope of the van der Waals forces. As the electrostatic force of an isolator is independent from the distance, the increase in roughness has no influence on the force.

In literature the determination of the roughness on real systems like interactive mixtures is described [66, 115]. Thereby the surface roughness of spherical particles is investigated as well as flat, rough surfaces. In the majority of cases, it is observed that by an increase of the roughness the interparticle forces decrease. When the diameter of the particle is larger than the space between the elevations of the roughness, the particle will get in contact solely with the top of the elevation and the interparticle force will decrease. However, the opposite can be observed as well. Smaller particles, which fit in between the elevations, have a higher contact area with the partner and though the interparticle force will increase [90].

With regard to the technology of bulk materials a certain roughness is desired. Mixing smaller particles to bulk materials the particles adhere on the surface of the bulk particles, which has a similar effect as an increase of the surface roughness itself. The interparticle forces are reduced and accordingly the agglomeration tendency, resulting in a better flowability [140].

3.1.5 Frictional force

By the detachment of particles in tangential orientation friction may occur between the partners. The frictional force is the force which acts against the displacement. It is distinctive with respect to static friction and kinetic friction. The initial force to get an object moving is often dominated by static friction whereas the kinetic friction is responsible to keep on the movement. The force of friction is always exerted in a direction that opposes movement (for kinetic friction) or potential movement (for static friction) between two

surfaces. The static friction (F_f) is related by the coefficient of friction (μ) with the normal force N (F_N) (Eq. 11).

$$F_f = \mu \cdot F_N \qquad \textbf{Eq. 11}$$

During the detachment of particles the static friction force and the interparticle force act against the traction force (F_t). Additionally, the lifting force of the particle and the particle weight has to be considered. However, regarding small particles below 10 µm the particle weight and the lifting force are negligible and $F_t > F_f$. Thus the force needed for detachment is F_f and can be calculated with the given equation (Eq. 11).

3.2 Film formation

Film formation of polymer coatings is crucial with respect to the functionality of pharmaceutical coatings of solid oral dosage forms like enteric resistance or modified release. Film formation using organic polymer solutions is easily achieved, as mentioned in section A 2.1, due to the dissolved polymer that after deposition builds the film on the substrate surface by undergoing sol to gel transition as the organic solvent evaporates. The film formation of aqueous polymer dispersions using latex or pseudolatex materials is driven by the evaporation of water and subsequent coalescence of the polymer particles [45]. The micromechanical process of the coalescence is still discussed in the literature [20, 36, 144].

The film formation of solvent free dry coating processes occurs predominantly during the curing step [108]. Before the curing step, the coating consists mainly of adhered polymer particles and agglomerates. Obara et al. suggested to spray a small amount of water to the coated spheres triggering film formation by acting as a plasticizer [101]. Film formation can be achieved without water by adjusting higher curing temperatures, thereby decreasing the polymer's melt viscosity, one resisting force for film formation [153]. Further film formation can be enhanced by increasing the plasticizer concentration [107]. Studies of Terebesi et. al. [138] showed that the addition of different plasticizers also affect the film formation. Since dry coating is conducted without any dispersion media it may be assumed that the film formation follows the theory of dry sintering [36]. However, the application of the liquid plasticizer has to be considered influencing the film formation by temporarily building capillary forces between the polymer particles before the polymer will have taken up the plasticizer.

The film formation process of the dry coating can be described as followed: as the plasticizer is applied simultaneously with the polymer, the polymer is not homogenously plasticized at the time point it hits the surface of the dosage form. Thus, prior to the penetration into the polymer the plasticizer may exert capillary forces ensuring adhesion of the polymer particles on the cores [72]. However, the plasticizer will be able to soften or even dissolve the surface of the particles. Expecting that the capillary forces will disappear after the penetration of the plasticizer film formation will occur according to the dry sintering theory. Dillon et al. introduced the dry sintering theory where film formation of colloidal lattices is described [36]. The mechanism of coalescence is based on the viscous flow of the polymer which leads to particle deformation (Figure 8). Caused by the viscoelastic behaviour of polymers, applied stress induces a combined response of elastic deformation and viscous flow [40].

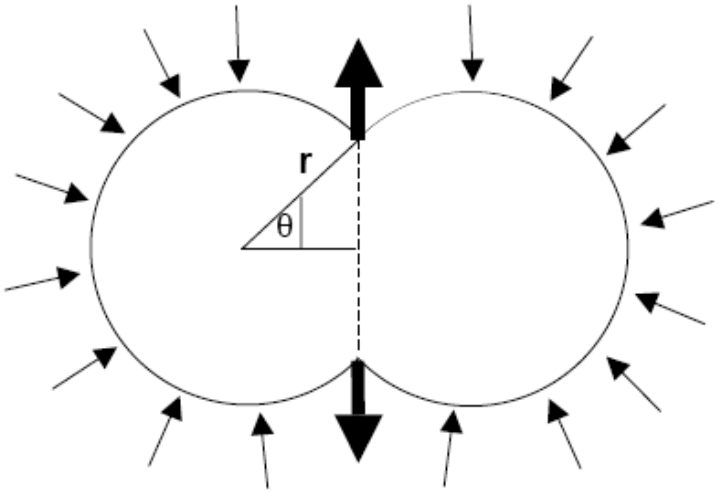

Figure 8: Shear stress leading to coalescence of two polymer particles, r = radius, θ = half contact angle

The driving force is the shear stress, to which the polymer particles are exposed. The polymer surface tension tends to minimize the surface area in order to reduce the free surface energy. The differential pressure p_k, which is acting over the circle of the junction, can be calculated by the following equation:

$$p_K = \frac{2\gamma_p}{r} \qquad \textbf{Eq. 12}$$

whereas γ_P is the surface tension of the polymer and r the radius of the polymer particle. A high pressure (p_k) is achieved by decreasing the particles radii r or increasing the surface tension γ_P. The contact angle θ is depending on the time t expressed by the Frenkel equation (Eq. 13):

$$\theta^2 = \frac{3\gamma_p}{2\pi \cdot \eta \cdot r} \cdot t \qquad \textbf{Eq. 13}$$

The time necessary for complete coalescence was calculated to be between less than one second and a few hours depending on the viscosity of the particle [50, 69]. Improved coalescence results in an increase of the angle of contact θ. With respect to Frenkel's equation (Eq. 13) it can be derived that θ increases by increasing the polymer surface tension γ_P or rather decreasing the viscosity η or the particle radius r. Considering the decreased viscosity and modulus of the polymer particle the deformation and the resulting film formation is facilitated by the addition of a plasticizer since a softer polymer is able to

deform and flow easier than a harder one [75]. Thus, the complete coalescence of the polymer will occur in a shorter time [36]. In order to induce the viscous flow and film formation the temperature needed is supposed to be close to the Tg of the polymer [145].

As during the material application the plasticizer builds up capillary forces between the polymer particles, the capillary theory has to be considered as well as a mechanism of the film formation of the dry coating process. However, since the amount of plasticizer is small and as a function of time the plasticizer will penetrate into the polymer, the capillary theory is of minor importance. After the introduction of the dry sintering theory, Brown et al. criticized the mechanism of film formation from aqueous dispersion by solely viscous flow since the film formation occurs already during the evaporation of the dispersion media of aqueous coatings [20]. He supposed that the polymer-water interfacial tension is the driving force for the coalescence as it is generally lower than the polymer's surface tension. Furthermore, it was shown that incomplete coalescence was obtained after the temperature during the process was kept below a critical value. It was considered that capillary forces developed by the evaporation of the aqueous dispersion media were the main reason for coalescence (Figure 9) [40].

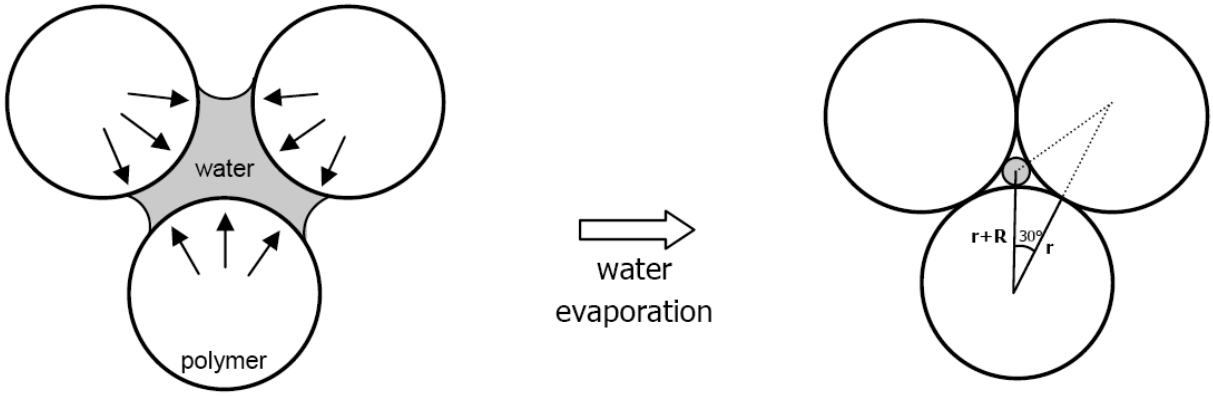

Figure 9: Capillary forces exerted by a liquid between polymer particles during evaporation of the liquid

Several forces promote or inhibit the coalescence of adhered particles, however, the main forces competing with each other are finally F_C and F_G. F_C is the capillary force as described in section 3.1.1. F_G denotes the resistance of the polymer sphere to deform. In order to achieve coalescence F_C has to be larger than F_G ($F_C > F_G$). The Laplace pressure, arising from the concave water surface, deforms the particle and initiates the coalescence. However, a polymer with certain rigidity will resist the deformation and water will evaporate without particle coalescence. When viscous flow is possible, the particle will undergo

stress relaxation and deformation with the required stress being a function of the complex modulus of the polymer.

Regarding Figure 9 with respect to the depicted geometrical array r/(r+R) = 30° cos, with r as the radius of the polymer particle and R the radius of the capillary, the Laplace pressure can be described as:

$$p_K = \frac{12.9\gamma_L}{r} \qquad \textbf{Eq. 14}$$

The resistance to deformation is depending on the time-related elastic shear modulus G_t of the polymer and is determined to be:

$$p_G = 0.37 \cdot G_t \qquad \textbf{Eq. 15}$$

Since the pressure p_K and p_G are assumed to be proportional to the forces F_C and F_G, they result in:

$$G_t \langle \frac{35 \cdot \gamma_L}{r} \qquad \textbf{Eq. 16}$$

In literature it is described that at the minimum temperature required for film formation, the modulus G_t will be less than the calculated maximum value for film formation [20]. Additionally, the equation (Eq. 16) reveals that at a given temperature affecting the modulus of the polymer, coalescence only occurs up to a certain particle size.

Later, a third theory in addition to Brown et al. and Dillon et al. has been introduced proposing that the physical contact of two polymers is not sufficient to ensure a stable film formation. Moreover, polymer chains have to diffuse through the boundaries from one particle to another leading to an interpenetrating network [145]. Only with this presumption the needed mechanical strength is achievable allowing to swell but not to redisperse after getting in contact with water.

These proposed mechanisms gave reason to discuss the phenomenon of coalescence almost for 50 years. Finally, it was proofed experimentally that capillary forces alone are insufficient for explaining the film formation. In combination with the interfacial tension as driving force coalescence is facilitated [40]. Furthermore, it was observed that film

formation occurs under conditions where water is not evaporating and consequently no capillary forces are exerted [37].

A deviating mechanism of particle coalescence and film formation is discussed in literature. Due to the larger particle size of HPMCAS in comparison to other dispersed polymers film formation from aqueous dispersions containing HPMCAS differ slightly [99]. A suggested theory of film formation from the aqueous dispersions of HPMCAS is that the plasticizer is separated from the water phase during the drying process and it dissolves or gelates the particle of HPMCAS. The particles then fuse to form a film. However, solid parts of HPMCAS particles are still detectable [134].

4 Coating equipment

Coating of spherical beads can be conducted in varied equipments. The very first industrial equipment for coating pellets was the top spray fluid bed. With top spray coating in the fluid bed (Figure 10 (a)), particles are fluidized in the flow of heated air, which is introduced into the product container via a base plate. The coating liquid is sprayed into the fluid bed from above against the air flow (countercurrent) by means of a nozzle. Drying takes place in the air flow as the particles continue to move upwards and subsequently downwards again. Small droplets and a low viscosity of the spray medium ensure that the distribution is uniform. Generally, this method is applicable for solution and suspension coating. The production of spherical granules using the top spray is described in literature, however, this granules exhibit a low rigidity [80].

The bottom fluid bed is the further development of the top spray fluid bed (Figure 10 (b)). The spray nozzle is fitted in the base plate resulting in a spray that is concurrent with the air feed. By using a Wurster cylinder and a base plate with perforations of different diameter, the particles to be coated are accelerated inside the Wurster tube and fed through the spray cone concurrently (bed up region). As the particles continue traveling upwards, they dry and fall back towards the base plate outside the Wurster tube (down bed region). They are guided from the outside back to the inside of the tube where they are once again accelerated. This produces an extremely even film. A layering with this method is possible when solutions or suspensions are used [6].

Using top and bottom spray fluid beds, variations of the dry coating process have been performed. Obara et al. [101] remodeled a fluidized bed (top spray) by installing a separate powder feeder in addition to the liquid spray system. Furthermore a fluidized bed with a Wurster insert can also be used to perform polymer powder coating [107, 112]. The powder feeder is used with a conjunction to the coating chamber feeding the powder into the down-bed region whereas the liquid plasticizer is sprayed into the bed-up region. The major disadvantage of the equipment is that the powder is applied by a separate feeding system into the coating chamber, which leads to higher loss of the coating materials.

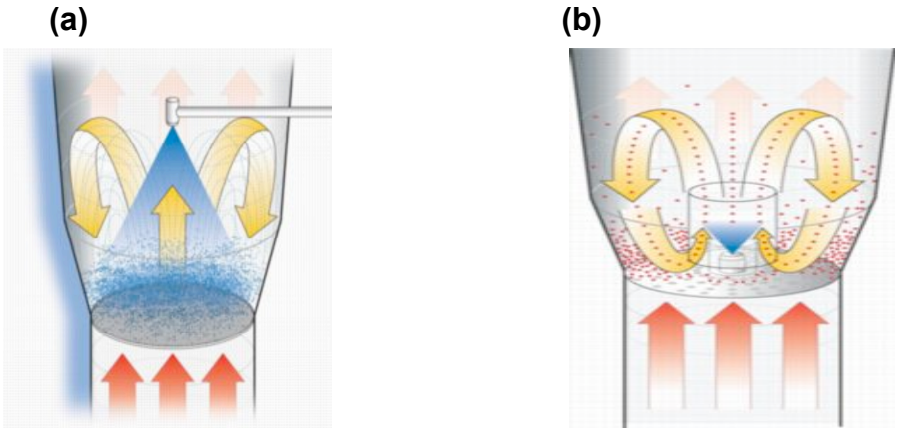

Figure 10: Top spray fluid bed (a) and bottom spray fluid bed (Wurster) (b) [54]

In contrast, using the rotor fluid bed the powder and the liquid can be dosed together into the pellet bed by the three way nozzle. The pellets are set into a spiral motion by means of a rotating base plate, where the air is introduced into the powder bed through the small slit between the rotor plate and the product container. The spray nozzle is arranged tangentially to the rotor disc and also sprays concurrently into the powder bed. Generally, very thick film layers can be applied by means of the rotor method. This is in contrast to the top and the bottom spray fluid bed where the capability is limited by the weight of the spheres, as they need to be accelerated a certain distance. Additionally, in comparison to the bottom spray fluid bed the pellets do not have to pass below the Wurster tube, which is a further limiting parameter for thick film layers.

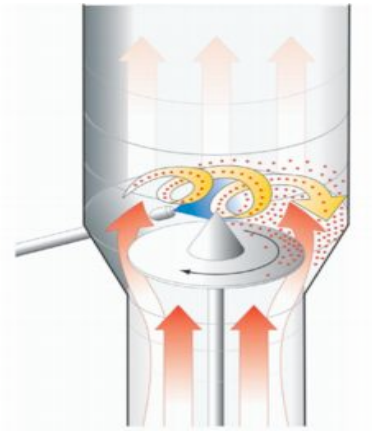

Figure 11: Rotor fluid bed [54]

Due to the optimized process conditions using the rotary fluid bed the pellet bed has a higher density avoiding an excessive loss of polymer powder and preventing pellet agglomeration in comparison to conventional fluid beds with respect to the dry coating process. Since the three way nozzle leads into the dense spiral movement and is covered completely by the pellet bed, the dry powder cannot easily follow the air flow and attach to

the equipment. Additionally, the intense movement enhances the layering of the polymer particles by clinging the coating material tightly to the pellet.

As an alternative Obara et al. used a conventional centrifugal coater (CF – granulator) [101] which is similar to the rotor fluid bed, however, the coater is an open system. Spherical beads were dry coated by dosing the plasticizer and the powder into the cores' bed. Afterwards the coated beads have been cured in an oven. Similar, tablets are coated with polymer powder using a spheronizer. The disadvantage of this method is the pre-step which is needed in order to plasticize the polymer powder by either mixing and sieving [31] or hot melt extrusion [125, 153]. Spheronizers are usually used for breaking extrudates into small cylindrical pieces which are formed into spherical beads due to their spiral motion (Figure 12) [79].

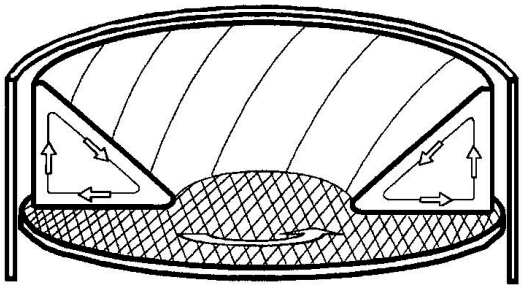

Figure 12: Scheme of a spheronizer [79]

Finally, coating can be performed using a double-structure punch (center punch and outer punch) allowing for dry-coated tablets to be assembled in a single run. A mixture of pellets and filling powder are dry coated by compressing the functional film around the dosage form with the outer punch [2].

Considering the different coating methods it can be assumed that using a rotor fluid bed for the dry coating method a continuous film formation can be achieved on the basis of simultaneously feeding/spraying the dry polymer powder and a plasticizer blend on the pellets using the three way nozzle. Furthermore, the high density of the pellet bed and the spiral movement ensures an efficient layering of the coating material and minimizes the loss of powder.

5 Materials

5.1 Coating materials

5.1.1 Delayed release polymers

Since more than thousand years pills have been coated in order to cover their bad taste. By developing the first synthetic drugs in the 19th century it became of certain interest to protect the stomach against the aggressive substances. Therefore, keratin was used which is digested enzymatically in the ileum in order to achieve enteric resistance. Nowadays, many pharmaceutical dosage forms irritate the stomach due to their chemical properties. Others undergo chemical changes in the acidic gastric environment and through the action of enzymes, becoming less effective. Thus, the need of efficient functional coatings is obvious.

The first functional polymers have been used to coat pharmaceutical solid dosage forms for protective, decorative and functional purposes [9]. Ideal properties for polymers used in film coating include:

- ability to produce films with excellent mechanical properties,
- stability against light, oxygen, hydrolysis,
- low toxicity,
- optimum dissolution in the gastrointestinal tract.

Polymers are macromolecules having a molecular weight range between 10,000 and several million Daltons and consist of a number of repeating units in the structure. They can cause a prolonged drug release in order to extend the intake intervals, or enteric resistance in order to protect the drug against the acidic media in the stomach, or even the stomach against the aggressive drug. Furthermore, polymer blends are designed for pulsatile release [35].

The material groups for enteric resistant coatings can be distinguished into three groups. The smallest and oldest group consists only of shellac, which is of natural origin and has been used almost for hundred years for enteric coatings and taste masking as well as prolonged release [62, 110]. Due to higher coating levels shellac is able to retard the drug release, but these formulations lack of drug release in the gastric environment [111]. Shellac consists mainly of a mixture of polyesters, basically composed of shellolic and alleuritic acid, which are responsible for its gastric resistant properties. However, as a

product of natural origin it is subjected to batch-to-batch variation of the quality in dependence of the purification process and the resulting content of wax, coloring material and other impurities [61, 135].

The second group was developed in the first half of the last century and is based on cellulose. The partial synthetic derivates used for enteric resistant coatings possess different acidic functional groups such as phthalate or acetate [34, 149]. Cellulose acetate phthalate (CAP) was the first semi-synthetic polymer, which gained soon high popularity as a gastric resistant polymer [93]. Other derivate based on cellulose acetate are cellulose acetate trimellitate (CAT) and cellulose acetate succinate (CAS). The later is not used commercially. Additionally, instead of cellulose acetate hydroxypropyl methylcellulose (HPMC) is used as polymer backbone. Polymers with HPMC as backbone are preferred, due to their lower permeability in the gastric fluid and improved stability against hydrolysis [120]. The first representative of this group was HPMCP composed with phthalate as acid resistant functional group. However it was found that this material was not optimal for an aqueous coating system. An alternative material, hydroxypropyl methylcellulose acetate succinate (HPMCAS) was developed subsequently and also derived from HPMC. This material was first approved in 1985 in Japan and is currently being used by several pharmaceutical manufactures as an enteric coating material for digestive enzymes and pH-dependent sustained release formulations. Due to different specifications (HPMCAS – LF, -HF, -MF) it is possible to adjust precisely the demanded pH of disintegration. In this work HPMCAS was used due to its good plasticizer compatibility and its small particle size of 5 µm [99].

Poly(meth)acrylate derivates are the third group used for the first time in 1972 [83]. They are full synthetic copolymers exhibiting an acidic carboxyl group which is responsible for the enteric resistance. The backbone is based on a continuous carbon chain stabilized by methyl groups resulting in poly(methyl methacrylate) (PMMA) which was also used as crystal clear, unbreakable organic glass [82] The enteric resistant polymer is available as Eudragit® L and S. An further full synthetic coating polymer is Kollicoat® MAE which is composed of a methacrylic acid/ethyl acrylate copolymer (1:1). Today the methacrylic acid copolymers Eudragit® L and S and Kollicoat® MAE are widely used polymers for enteric coatings. They contain carboxylic groups and thus are anionic in character releasing the drug at pHs above 5.5 [35]. The major advantage of these polymers is that they are highly stable against hydrolysis.

Furthermore, polyvinyl acetate phthalate (PVAP) has to be named which is used as enteric coating material that disintegrates at a low pH between 4.5 and 5.5 [34].

5.1.2 Hydroxypropyl methylcellulose acetate succinate (HPMCAS, Aqoat®)

The chosen model coating material hydroxypropyl methylcellulose acetate succinate (HPMCAS - MF, Aqoat®) was developed originally for aqueous enteric coating. The first system which was developed by Nagai et al. [99] was a suspension of fine powdered hydroxypropyl methylcellulose phthalate in water containing plasticizers. However, this material was not sufficiently compatible with plasticizers and a new material, HPMCAS, was developed, which shows a good compatibility with plasticizers. The raw material of HPMCAS is highly purified pulp, which is process to hydroxypropyl methylcellulose (HPMC) before acetyl and succinoyl groups are introduced to the HPMC backbone. Due to its succinate moiety which values 10-14% it is stable in the acid stage and dissolves quickly once having passed the pH 6.0 [133].

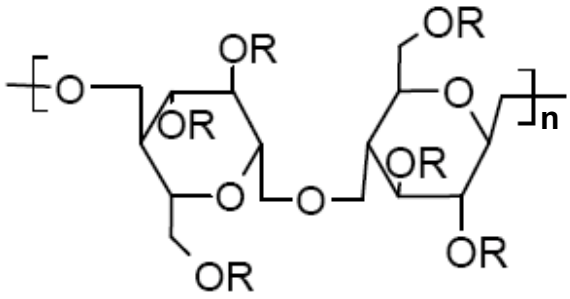

R= **-H** **-CH_3** **-$CH_2CH(CH_3)OH$** **-$COCH_3$** **-$CH_2CH(CH_3)OCOCH_3$** **-$CH_2CH(CH_3)OCOH_2CH_2COOH$** **-$COCH_2CH_2COOH$**

Figure 13: Hydroxypropyl methylcellulose acetate succinate (HPMCAS)

The polymer is available as micronized powder or granules. Generally, the granules are used for solvent based processes whereas the powder is designed for aqueous dispersions. In this study the powder was used as a dry powder. Choosing this way of application its small particle size of 5 µm is crucial as its specific gravity is nearly negligible and consequently a good adhesion facility on larger coating spheres respectively the cohesion of the particles with each other is promoted. Using powders with larger particle sizes and higher weight may lead to a less efficient powder layering and a higher loss of polymer during the process which results in an insufficient functional coating. However, since the dry powder is used the flowability of the coating material plays a certain role. The small particle size of HPMCAS results in a bad flowability which can be increased by the addition of a glidant respectively anti tacking agent to the formulation.

GRADE		ACETYL %	SUCCINOYL %	pH SOLUBILITY	MEAN PARTICLE SIZE
Micronized	AS – LF	8	15	>5.5	5 µm
	AS – MF	9	11	>6.0	
	AS – HF	12	6	>6.8	
Granular	AS – LG	8	15	>5.5	1 mm
	AS – MG	9	11	>6.0	
	AS - HG	12	6	>6.8	

Table 4: Grades of HPMCAS

HPMCAS exhibits brittle properties at room and process temperatures the glass transition temperature lit. ($Tg_{lit.}$) of the pure HPMCAS polymer is 122 °C [133]. To achieve a functional coating with the polymer, the film formation temperature, which is related to the glass transition temperature (Tg), needs to be lowered, since the process temperature is adjusted at lower temperatures. Due to the boiling temperature of the dispersion media (water) coating processes have to be conducted at temperatures below 100 °C. Further, the temperature sensitivity of drugs may dictate a lower process temperature as well as the high costs due to the higher energy demand. A lowering of the temperature can be realized by adding a plasticizer which increases the mobility of the polymer chains by merging in between. This leads to a lower Tg compared to the pure polymer and accordingly to a lower film formation temperature.

5.2 Plasticizers

Many polymers used for pharmaceutical coatings exhibit brittle properties and require the addition of a plasticizing agent in order to obtain a crackless film and an effective coating. The plasticizer has an important function as it has to soften and penetrate into the polymer in order to alter the physical properties of a polymer (i.e. hard or brittle) and to enable the film formation and coalescence of the polymer. It weakens the intramolecular attractions between polymer chains which generally results in a decrease of the Tg [49, 58]. Therefore a good polymer-plasticizer interaction is required which ensures a homogenous decrease of the polymer Tg. It has been theorized that the most effective plasticizer will normally resemble most closely the structure of the polymer they plasticize [138].

Plasticizers are low molecular weight organic solvents with high boiling points. Generally,

there have to be some similar chemical features (i.e. functional groups) between a polymer and its plasticizer. Plasticizers are normally used at concentrations between 15-35% based on the polymer weight. Plasticizers also have a significant influence on the mechanical properties of the film [148]. Specifically, they reduce cohesive intermolecular forces along the polymer chains and enhance flexibility by increasing strain elongation and decreasing tensile strength and elastic modulus of the polymer. Additionally, they influence the permeability characteristics of the film, especially the permeability to water vapor, as well as the glass transition temperature of the polymer to allow a more feasible coating process. Plasticizers may also possess solvent power to insure compatibility with the polymer. Plasticization time (i.e. mixing time of plasticizer with polymer) and plasticizer concentration influence the properties of the polymer films [15]. Three types of plasticizers are commonly used in coating processes: polyols, organic esters and oil respectively glycerides. Polyols are generally miscible with water in contrast to glycerides which are water insoluble. Organic esters often consist of phthalate, citrate or sebacate and can be water soluble or insoluble depending on the combination of functional groups.

PLASTICIZER CLASSIFICATION	PLASTICIZER	MISCIBILITY
Polyols	Glycerol (glycerin)	water miscible
	Propylene glycol (PG)	water miscible
	Polyethylene glycol (PEG 200-6000 grades)	water miscible
Organic esters	Diethyl phthalate (DEP)	water insoluble
	Dibutyl phthalate (DBP)	water insoluble
	Dibutyl sebacate (DBS)	water insoluble
	Triethyl citrate (TEC)	water miscible
	Acetyltriethyl citrate (ATEC)	water insoluble
	Acetyltributyl citrate (ATBC)	water insoluble
	Tributyl citrate (TBC)	water insoluble
	Triacetin (glyceryl triacetate; TA)	water miscible
Oils/glycerides	Castor oil	water insoluble
	Distilled acetylated monoglyceride (AMG)	water insoluble
	Fractionated coconut oil	water insoluble
Water		

Table 5: Plasticizer classification and miscibility with water

By choosing a plasticizer it has to be considered whether the plasticizer is compatible with the polymer. Therefore, the Hildebrand solubility parameters δ can be calculated and compared with each other. Furthermore, compatibility can be checked by mixing plasticizer. In this study TEC and (Myvacet®) AMG was used being miscible with each other.

The manufacturers of acidic coating materials [35, 133] mainly recommend the use of triethyl citrate (Figure 14) as the most efficient plasticizer. Generally, TEC is gaining attention because it is a non-toxic, biocompatible plasticizer that can be used instead of petroleum-based phthalate compounds. It is used as a high boiling liquid and plasticizer for vinyl resins, cellulose acetates and is permitted for application in the field of food additive, food contact material, medical and pharmaceutical products. It is widely used in cosmetics, lacquers and as a fragrance carrier.

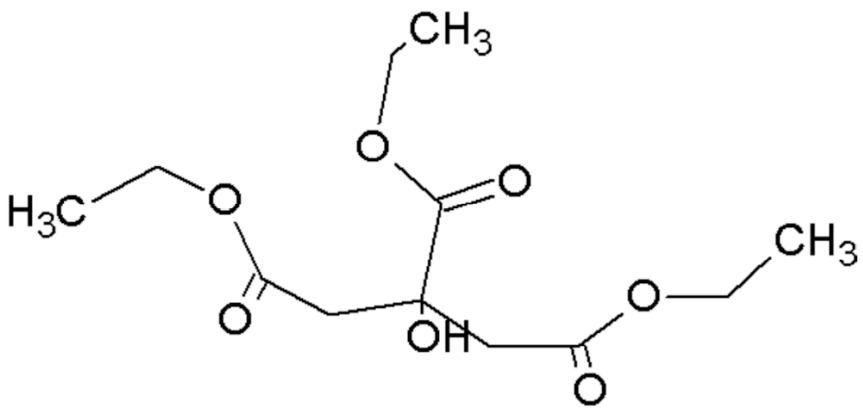

Figure 14: Triethyl citrate (TEC)

After getting in contact with the dissolution media this hydrophilic plasticizer dissolves slowly and the film becomes porous. In the acid stage this disintegration needs a certain time and does not affect the enteric resistance whereas at higher pHs the polymer disintegration overlays this effect [49, 126]. Also in literature TEC is recommended as a plasticizer for HPMCAS [48, 101, 102, 112, 134, 138]. HPMCAS dissolves in anhydrous TEC at room temperature which underlines their excellent compatibility.

Additionally, for the dry coating process the plasticizer has to facilitate the powder layering by increasing the adhesion and cohesion of the particles due to its liquid state. The liquid wets the pellet surface and builds out liquid bridges between the solids exerting capillary forces strongly influence the efficiency of the powder application. Therefore the plasticizer needs to be applied homogeneously and needs to be well distributed onto the pellets and

the polymer particles in the coating chamber. This can be enhanced by adding a wetting agent which increases the spreadability of the liquid on the solid material.

	MOLECULAR WEIGHT	MELTING POINT (°C)	BOILING POINT (°C)	SPECIFIC GRAVITY (at 25 °C)	WATER SOLUBILITY (mg/ml)
TEC	276.3	-55	288	1.14	55.35
Myvacet®		4 – 11	>500	0.94	negligible

Table 6: Properties of TEC and Myvacet®

In order to do so a wetting agent was mixed to the liquid part of the formulation. Obara et al. investigated different plasticizer/wetting blends and figured out that Myvacet® has the highest effect on the coating formulation consisting of HPMCAS and TEC [101]. Myvacet® is an acetylated monoglyceride and is used as solvent, lubricant and plasticizer in the food industry. Besides the good spreadability Myvacet® is playing a role for the reduction of the Tg and for the performance of the film by inhibiting cracking or splitting [47].

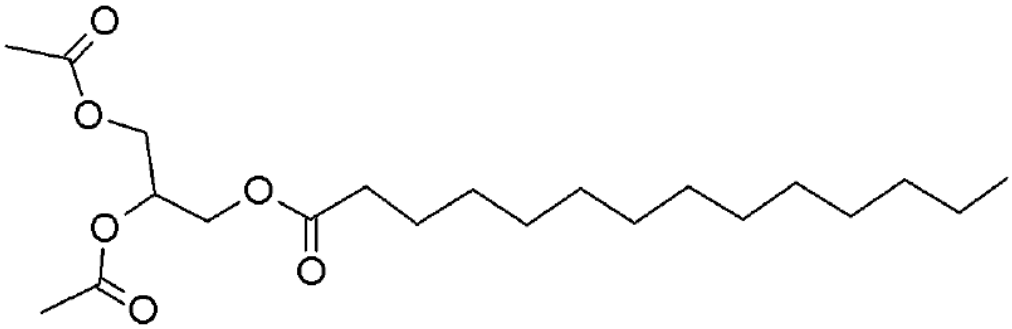

Figure 15: Myvacet® (acetylated Monoglycerid)

5.3 Anti tacking agents

Anti tacking agents are required if the coated dosage forms tend to tack especially during storage. Additionally, anti tacking agents increase the flowability of the micronized polymer powders by mixing the powder with a glidant. Several anti tacking agents are known in literature, for example talc, glycerol monostearate, polyvinylpyrrolidone and silicon dioxide (Aerosil®) [32, 46, 113]. In this work talc and silicon dioxide were used being both silicates with different components and crystal structures.

Talc is a hydrated magnesium silicate which is often used in the pharmaceutical industry due to its inert character and its low price. Talc is a phyllosilicate with 2:1 layers which are

the reason for the glidant facility as the layers are predetermined breaking points because of the weak van der Waals bindings in between. However, the addition of talc holds the disadvantage of possible microbiological contaminations and asbestos impurities which is one of the reasons to renounce talc as additive. As an alternative to talc the anti tacking agent colloidal silicon dioxide can be used as a top powder on top of the coated dosage form inhibiting tacking during storage by acting as spacers between interacting partners [98]. Colloidal silicon dioxide is a tectosilicate with tetrahedral frameworks. Additionally, it increases the roughness of surfaces by adhering on them. Furthermore, colloidal silicon dioxide may function as humidity absorber and gel former [8].

5.4 Active pharmaceutical ingredient

As model drug theophylline was selected known as bronchodilator since introduced by Samson Raphael Hirsch in 1922. Theophylline is first used clinical in asthma treatment in the 1950s. Today it is still used in therapy for respiratory diseases such as COPD or asthma [78]. Due to its narrow therapeutic range it is recommended to take prolonged release theophylline products. Nevertheless Theophylline is used in this study for the characterization of enteric-coated dosage forms due to its physico-chemical properties shown in Table 7.

THEOPHYLLINE		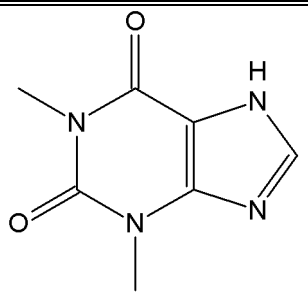
Properties	M_r	180.2
	pK_s values	0.3 and 8.6
	Basal solubility (37 °C)	1.12 g / 100 ml
	Solubility in 0.1N HCl (37 °C)	1.56 g / 100 ml
	Maximum of adsorption in 0.1 N HCl (37 °C)	272 nm

Table 7: Structure and properties of the model drug theophylline

Theophylline is a methylxanthine with low alkalinity (pK_{s1} = 0.3) and low acidity (pK_{s2} = 8.6) [41], causing that theophylline is existent un-dissociated over the complete pH range of the gastrointestinal tract [51]. An advantage of the model drug is that the saturation

concentration is only slightly influenced by the physiological pHs (1.1 - 7.4) as it changes between 1.12 g / 100 ml (pH = 4.41) and 1.60 g / 100 ml (pH = 7.68). Nevertheless, these concentrations are highly above the concentration reached during dissolution of coated dosage forms in the study. Therefore drug release is not impeached in this study. The saturation concentration in the dissolution media (0.1 N HCl) used for approving enteric resistance of the coated dosage forms is 1.6 g / 100 ml at 37 °C.

The drug load of the theophylline pellets donated by Klinge Pharma was 94%. Gelatin and polyvinylpyrrolidone were used as additives. The diameter of the uncoated pellets was between 0.8 mm and 1.25 mm.

6 Methods

6.1 Material characterization

6.1.1 Determination of particle size

The particle size of powders was determined using laser light diffraction. The diffraction of the laser light results from the interaction of monochromatic, coherent light with the particles. With the impact of the laser beam on the particles different phenomena can occur like absorption, refraction, reflection and diffraction. Only the diffracted light is used for characterization, passing a collecting lens and detected by the photo detector. The laser diffraction method of measuring particle size relies on the optical principle which dictates that small particles which are in the wavelength of the incident light scatter the light giving a characteristic, symmetrical pattern. Small particles lead to higher diffraction angles than larger ones. For a single particle, the diffraction pattern shows a typical ring structure. Given a certain pattern of scattered light intensity (as a function of angle to the axis of the incident beam ('flux pattern')) the distribution of particle sizes can be deduced using a mathematical evaluation procedure according to the Fraunhofer theory. A second evaluation procedure accords to the Mie theory using additionally absorbed, reflected and refracted light for characterization. Therefore the refraction index has to be known. This theory was not used for evaluation in this study, as the evaluation according to the Fraunhofer theory is sufficiently precise for determining particles sizes above 1 µm.

The particle size distribution represents the percentage by volume of the individual particle size classes in relation to the total volume. The results are represented by the indication of the 10, 50 and 90 %-quantiles (x_{10}, x_{50} = median, x_{90}). Since the calculation of the particle size is made by assuming a spherical particle shape, the measurement principle is optimally suitable for spherical particles. The more the particle shape differs from a sphere, the higher is the deviation of the measured particle size from the real one. This obtained particle size represents the diameter equivalent to a sphere giving the same diffraction than the measured particle. The sample preparation takes place via wet dispersion using a media wherein the substance is insoluble or via dry dispersion as performed in this work. The substance is desagglomerated by compressed air using a venturi injector and brought into the measuring range, where the size of the single particle will be measured. Following the vacuum generated through expansion of compressed gas applied to the injector, the fine dry particles arrive at low speed in the dispersing line and are subject to immediate acceleration.

6.1.2 Determination of surface tension of the plasticizers

Interactions occur between the molecules of a liquid and those of any liquid or gaseous substance, which is not soluble in the liquid resulting in the formation of an interface. In order to increase the area of this interface, energy is required. The work needed to increase the surface area by one m^2 is known as the interfacial or surface tension.

A tensiometer determines the surface tension with the help of an optimal wettable probe, which is either a ring or a plate suspended from a precision balance. In this work the method following Wilhelmy was carried out. This method utilizes the interaction of a platinum plate with the surface being tested. The calculations for this technique are based on the geometry of a fully wetted plate in contact with, but not submerged in, the liquid. A rough platinum plate was used fulfilling the requirement that the probe must have a very high surface energy. A height adjustable sample carrier is used to bring the liquid to be measured into contact with the probe. A force acts on the balance as soon as the probe touches the surface. Since the length of the plate is known the force measured can be used to calculate the surface tension.

6.2 Coated dosage form

6.2.1 Drug release studies

Generally, the requirement of enteric resistant oral dosage forms is the unimpaired passage through the stomach and the quick disintegration in the upper intestines. Such properties cannot be realized since due to the coating material properties enteric coated dosage forms will never be absolutely enteric resistant. Thus, the pharmacopoeias modified their requirements. The USP XXIX [142] will approve the coated dosage forms according to the drug release of enteric coated articles if less than 10% drug is released in the first 120 minutes in the acid stage (0.1 N HCl). Afterwards the chloric acid is neutralized to pH 6.8 by adding a base (method A) or the media is changed into phosphate buffer (pH 6.8) (method B). In the neutral stage 75% of the drug have to be released within 45 minutes.

The European Pharmacopoeia testing the disintegration in 0.1 N HCl. Disintegration of the dosage form exceptionally parts of the film and cracks which cause drug release must not be macroscopically detectable. Secondly, the dosage form has to disintegrate in phosphate buffer (pH 6.8) within 60 minutes. A recommendation to proof the amount of the API after dissolution in 0.1 N HCl is given but not required [43].

The requirements of the USP XXIX are more strictly in comparison to the European Pharmacopoeia as the drug release in the acid stage is determined quantitatively and not macroscopically merely. Consequently, the dry coated pellets in this work were analyzed with regard to the requirements of the USP XXIX [142]. Additionally, the enteric resistance during storage was investigated which is not an explicitly required of the pharmacopoeias but which is an important aspect for the development of coated dosage forms.

6.2.2 Coating efficiency

The coating efficiency (CE) is one of the major parameters in formulation and process development. It is used to describe the efficiency of the process with regard to the loss of coating material consisting of polymer and plasticizer. The coating efficiency of a film-coating process is commonly evaluated by the weight gain using the following equation (Eq. 17). It is calculated by dividing the actually achieved weight gain wg_m caused by the application of the coating material by the theoretical achievable weight gain wg_t multiplied by 100.

$$CE = \frac{wg_m}{wg_t} \bullet 100\% \qquad \textbf{Eq. 17}$$

In literature the efficiency of a dry coating process often is described as coating level which is the amount of the applied coating material on the solid dosage form calculated on the weight of the uncoated dosage form [31, 53, 107-109, 138, 153]. Using this parameter the amount of coating material needed for functional coatings is defined. However, the total applied amount and loss of powder in order to achieve this coating level is not given and this method is not recommendable.

6.2.3 Sieving system

In general, sieving machines are used for quantitative particle size analysis classifying powder bulks with particle sizes above 40 µm. Therefore sieves of different mesh sizes are connected vertically in series. The sieving tower consists of a bottom tray below the screen inserts with the rest being arranged above in rising mesh size. The weighed sample is fed onto the top screen and after the screening cycle, the oversize on every insert is weighed. In this work sieving was used to determine agglomerates which may occur during storage. The stored sample was sieved using only one mesh sizes which can be passed by a single pellet above the bottom tray and the oversize was measured.

6.2.4 Ring shear tester

The flowability of powders can be measured by using a ring shear tester, a further development of the Jenike – type tester which is a device known in powder technology for some 30 years [70]. In contrast to the Jenike – type tester the ring shear tester allows the removal of the shear cells for time consolidations measurements and measurements of consolidation stresses down to approximately 500 Pa. The ratio of the consolidation stress (σ_c) and the unconfined yield strength (σ_1) is called the flowability (ff_c).

$$ff_c = \frac{\sigma_1}{\sigma_C} \qquad \textbf{Eq. 18}$$

The greater ff_c is, the better a bulk solid will flow. For comparison of the flowability of several bulk solids, a yield locus has to be measured for each powder to determine the individual values of the flowability ff_c [129-131]. The flowability of powders is classified as shown in Table 8.

Flowability ff_c	
$ff_c < 1$	no flowing
$1 < ff_c < 2$	very cohesive
$2 < ff_c < 4$	cohesive
$4 < ff_c < 10$	easy flowing
$10 < ff_c$	free flowing

Table 8: Flowability classification of powders

For the determination of ff_c the Mohr stress cycle is used. The procedure can be explained in the following with a model bulk solid element which undergoes stress. In vertical direction, positive normal stress (σ_v) is exerted on a bulk solid in a cylindrical container. The horizontal stress σ_h results of the vertical stress σ_v and is less than the vertical stress σ_v (Figure 16).

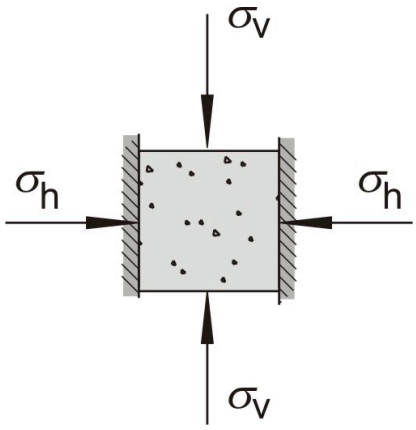

Figure 16: Element of bulk solid and uniaxial compression test [128]

In analogy to solids, different stresses can be found in bulk solid. No shear stresses (τ) are exerted on the top or bottom of the cylindrical model and in the planes the shear stress is nearly 0. Further no shear stress is acting on the lateral walls since it is assumed that they are frictionless. Thus only the normal stresses are acting on the bulk solid from outside. However regarding the bulk solid with angular cross – section cut and using a simple equilibrium of forces, the normal stress (σ_α) and the shear stress (τ_α) acting on a plane inclined by an arbitrary angle can be calculated (Figure 17). After mathematical transformation it follows that:

$$\sigma_\alpha = \frac{\sigma_V + \sigma_h}{2} + \frac{\sigma_V - \sigma_h}{2}\cos(2\alpha) \qquad \textbf{Eq. 19}$$

$$\tau_\alpha = \frac{\sigma_V + \sigma_h}{2}\sin(2\alpha) \qquad \textbf{Eq. 20}$$

The pair of values (σ_α,τ_α), which are to be calculated according to the equations (Eq. 19,Eq. 20) for all possible angles, can be plotted in a σ,τ - diagram. Combining all plotted pairs of values a circle emerges named the Mohr stress cycle. The center of the cycle is located at $\sigma_m = (\sigma_v + \sigma_h)/2$ and $\tau_m = 0$ and the radius is defined by $\sigma_m = (\sigma_v - \sigma_h)/2$.

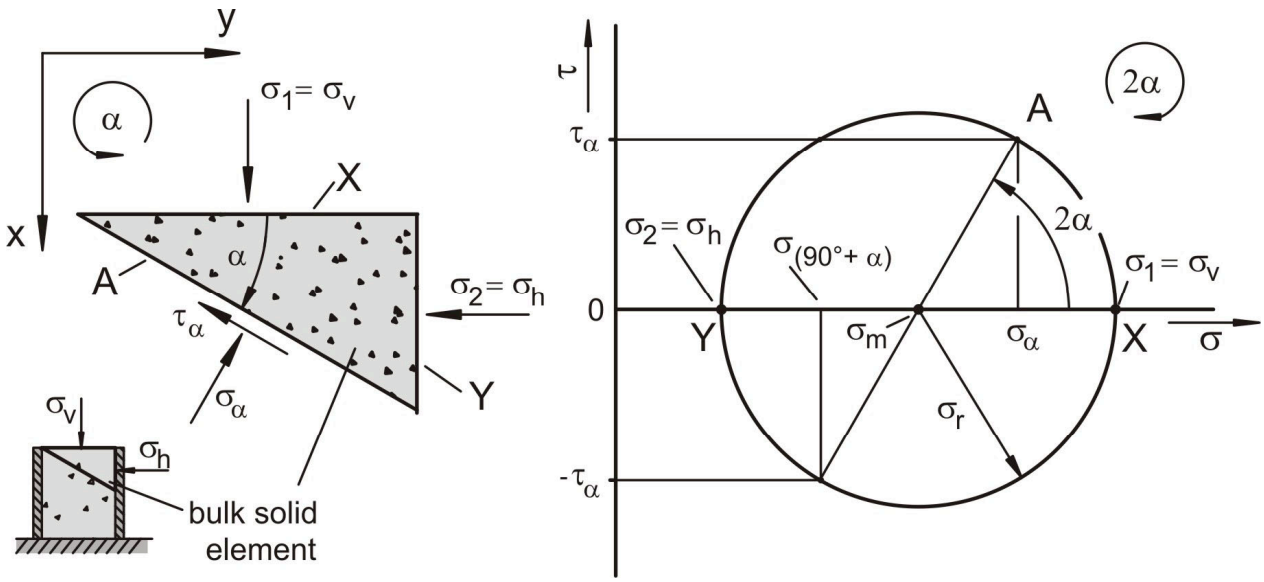

Figure 17: Force equilibrium on a bulk solid element in relation to the Mohr stress cycle [128]

The center of the Mohr stress cycle is located on the σ-axis, each Mohr stress circle has two points of intersection with the σ-axis. The values of intersections are called principal stress. The major principal stress is designed as σ_1 (= σ_v) and the minor one as σ_2 (= σ_h) together defining the Mohr stress cycle.

After having explained the occurring stresses in a solid bulk element the flowability determination can be demonstrated with the uniaxial compression test. Therefore the solid bulk element in the cylindrical container is loaded by the stress σ_1, the consolidation stress, in vertical direction. Afterwards the container is removed and subsequently the consolidated bulk solid is loaded with an increasing vertical compressive stress causing the bulk solid to break or rather fail at a certain stress. The stress causing failure is called comprehensive strength or unconfined yield strength σ_c [131]. In bulk solid technology the failure is named incipient flow since the solid starts to flow under the loaded stress. Conducting this test at different consolidation stresses different pairs of values ($\sigma_c(\sigma_1)$) are determined resulting in the flow functions by plotting these values in a σ_c, σ_1 - diagram.

In practice the bulk solid (in this study coated pellets) is filled in the ring shear cell and the bulk solid is consolidated (called preshear). Subsequently the point of yield limit is measured (called shear to failure). For preshearing the bulk solid is loaded in the vertical direction by a defined normal stress. Then the sample is sheared (Figure 18). At the beginning of preshearing the shear stress τ increases with time. With time the curve of shear stress vs. time becomes flatter, and finally the shear stress remains constant even though the bulk solid is sheared further. The constant shear stress is called τ_{pre}. This type

of flow, attained at preshear, is called steady-state flow. The state of the bulk solid after steady-state flow is called "critically consolidated with respect to the normal stress, σ_{pre}".

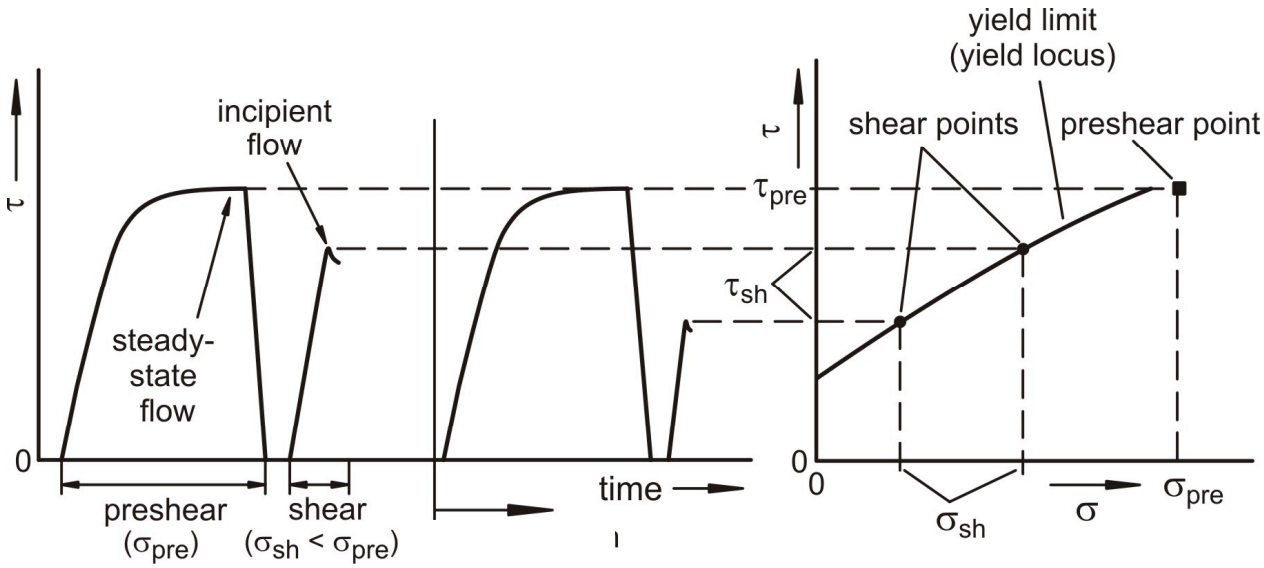

Figure 18: Plot of shear stress vs. time; yield locus [128]

Afterwards the shear to failure is determined. The stress acting on the solid bulk is decreased to a value σ_{sh} which is less than the normal stress at preshear σ_{pre}. If the consolidated solid bulk is sheared under the normal stress $\sigma_{sh} < \sigma_{pre}$, it will start to flow (fail) when a sufficiently large shear stress is attained. The material will start to dilate (decrease in bulk density) and shear resistance and thus shear stress will decrease. The maximum shear stress characterizes incipient flow. The corresponding pair of values (σ_{sh}, τ_{sh}) is a point of the yield locus of the consolidated solid bulk in the σ,τ-diagram called a "point of incipient flow". In order to measure the yield locus, the tests must be performed repeatedly, by consolidating at identical normal stress, σ_{pre} (preshear) first. Then the specimens are sheared (to failure) under different normal stresses, $\sigma_{sh} < \sigma_{pre}$. A straight line through the origin of the σ,τ-diagram, tangent to the greater Mohr stress cycle is the effective yield locus [70].

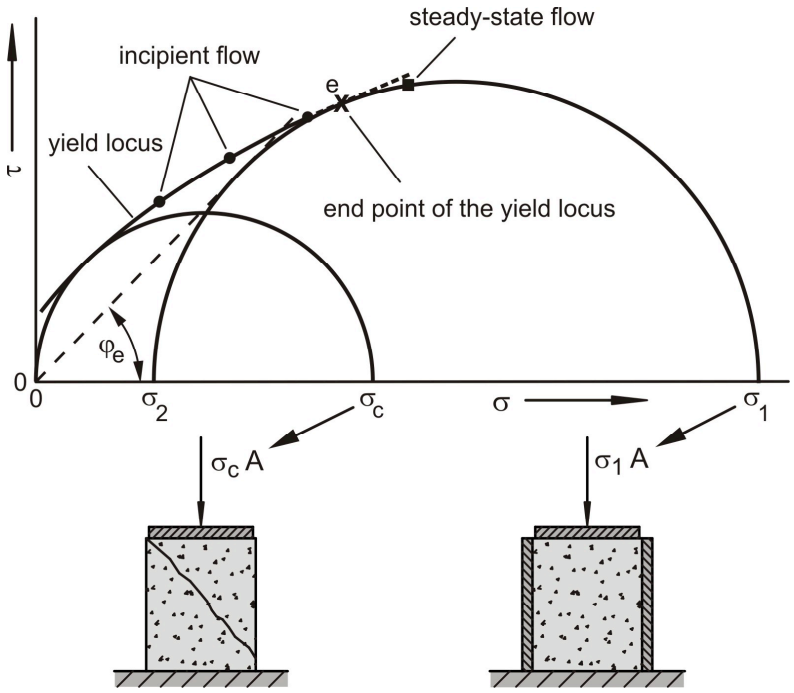

Figure 19: Yield locus in relation to uniaxial compression test [128]

The parameters describing the flow properties of the bulk solid, can be determined using the yield locus (Figure 19). The relevant consolidation stress σ_1 is equal to the major principal stress of the Mohr stress cycle which is tangential to the yield locus and intersects at the point of steady state flow (σ_{pre}, τ_{pre}). This stress cycle represents the stresses in the sample at the end of the consolidation procedure. The unconfined yield strength, σ_c, results from the stress cycle which is tangential to the yield locus and which runs through the origin.

6.3 Coating process

6.3.1 Contact angle determination

The contact angle is used to determine the wetting of a solid by a liquid. Generally, the determination of the contact angle is conducted using the sessile drop method. The liquid is dropped by a micro syringe on the solid and the contact angle between the baseline of the drop and the tangent at the drop boundary is measured. Young formulated a relation between the interfacial tension γ at a point on a 3 phase contact line (Figure 20).

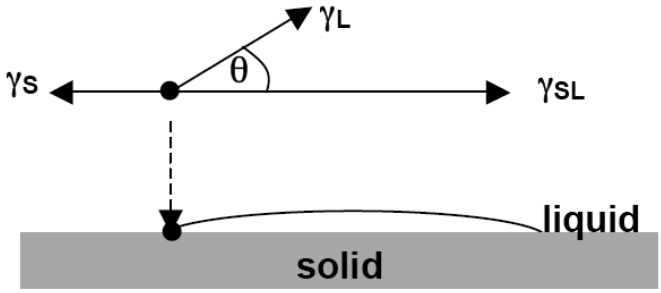

Figure 20: Scheme of the contact angle

The indices 'S' and 'L' stand for solid and liquid, γ_s and γ_L describe the surface tension components of the two phases whereas γ_{SL} represents the interfacial tension between the phases and θ stands for the contact angle corresponding to the angle between vector γ_{SL} and γ_L. Young formulated the relationship between this quantities:

$$\gamma_L \bullet \cos\Theta = \gamma_S - \gamma_{SL} \qquad \textbf{Eq. 21}$$

A certain disadvantage of this method is that smooth surfaces are needed requiring the modification of the investigated polymer particles [104]. Which causes changes of the materials' surface properties. As an alternative the Washburn method (powder contact angle method) has to be mentioned enabling the determination of the average contact angles of powders. The powder is filled in a capillary and the liquid is soaked up. The change of weight is used to calculate the contact angle. However, the results of this method are sensitive, due to the dependence of the determination on the particle size, the bulk density and the geometry of the capillaries [21, 22]. Additionally, as in this study a plasticizer is used which is miscible with the polymer powder, penetration of the plasticizer in the powder will occur during measurement. Thus, this method cannot be used in this

study and the sessile drop method was performed. Buckton et al. examined the value of contact angle measurements on compressed powders. The contact angle was found to be reduced with increased compression force until a constant value was achieved [23]. In this study the powder was compressed to comprimates applying constantly high compress forces in order to achieve a smooth surface and constant values.

6.3.2 Atomic force microscopy

The first steps of atomic force microscopy were performed by Binnig and Rohrer [74] developing the scanning tunnel microscope (STM) [14]. The procedure of the raster tunnel microscopy uses the so-called tunnel effect, which arises, when two electrical conductors are approached within a very small distance to each other (fractions of nanometers). Although no direct contact between sample and probe tip exists, a small tunnel current is measurable in the pico to nano-ampere range, depending on the distance between. If this current is used as input for an automatic control loop, which has to keep the current at a given value also if changes in distance of the tip to the sample occur, topography information of the sample can be obtained from the correcting variables of the automatic control loop. Due to the operational principle an investigations of conductive samples is possible only. The changes of distance and the positioning of the probe are realized by a piezo scanner. In mapping a graphite surface with an insulating stylus a resolution better than 2.5 Å was achieved [13].

The derivative of the scanning tunnel microscope is the atomic force microscope (AFM) or rather scanning probe microscope (SPM) using not electrical, but mechanical effects between sample and tip. The tip is mounted on a flexible carrier, namely the cantilever. The deflection of the cantilever is recorded with the help of a laser beam and permits the evaluation of the forces between tip and sample. This procedure allows also an investigation of non conductive samples and the characterization of surfaces with atomic resolution due to the small tip size at the nanoscale. It is often used to study surface topography of polymers [92] or biological membranes [1, 66]. Specific probes can be used to analyze i.e. lateral variations of frictional, elastic, thermal, electrical and magnetic properties. For AFM measurements a special sample treatment is not necessary. Furthermore, the surface analysis can be performed in liquid or gaseous environment. Additionally, AFM can be used to determine interparticle forces [27].

The experimental setup of the AFM measurement is shown in Figure 21. The substrate is analyzed by a small tip at the top of cantilever (length - 100 µm) that has a diameter between 1 and 200 nm. The laser beam is reflected by the cantilever and gets detected by

the photo detector. Due to the deflection of the cantilever during the measurement the angle of reflection of the laser beam changes which is monitored by the detector. The piezo scanner is movable in all three dimensions ensuring that the substrate can be moved whereas the position of the cantilever is fixed.

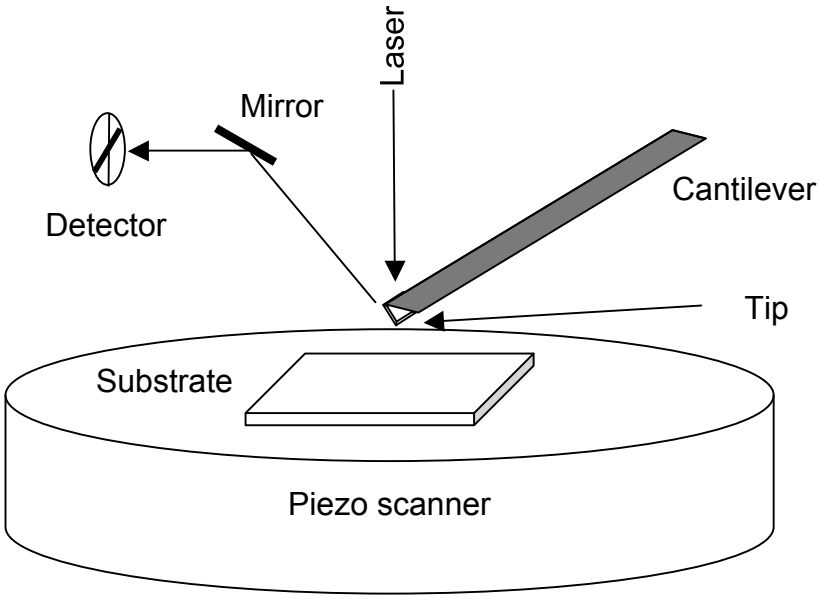

Figure 21: Experimental set up of measurement

The characterization of the surface topography can be conducted with three different methods. Performing the contact mode, a static modus, the tip is in contact with the substrate which is scanned line by line. The deflection of the cantilever is registered by the photo detector which is set in an automatic control loop ensuring the height (z-) adjustment of the piezo scanner. Therefore, the pressing force of the cantilever is kept constant (‘constant force mode’). Alternatively, the height of the cantilever can be adjusted constantly (‘constant height mode’) registering the topography of the surface and the friction of the cantilever tip on the substrate. In both cases the substrate has to be prevented from undergoing changes caused by the friction. The disadvantage of the contact mode is that the speed of scanning is restricted by the response time of the automatic control loop. Additionally, the possible existence of capillary forces imposed by a liquid adsorption layer can decrease the resolution.

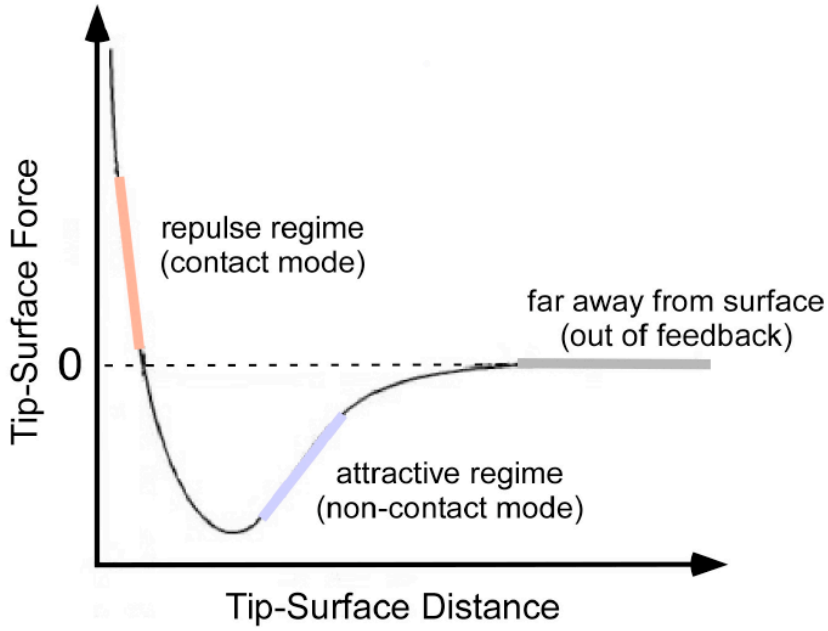

Figure 22: AFM methods and their tip sample distance [151]

Alternatively, the second method namely the non contact mode can be applied where substrate and cantilever tip never get in contact (see Figure 22). Consequently, the tip cannot destroy or damage the sample. Due to the absence of repulsive forces soft samples or even liquids can be imaged. The non contact mode works like an amplitude modulation detection. The amplitude A of the oscillation of the cantilever is changed by the interaction of the tip with the substrate. In order to keep the amplitude constant the movement of the piezo scanner connected with an automatic control loop compensates the changes. The method is called dynamic as the cantilever is in motion. This method was used in this work to characterize the surface topography of the substrate.

Furthermore the tapping mode can be used for sensitive materials and loose powder agglomerates as only slight friction occurs. This method is as well a dynamic mode and combines the characteristics of the contact and non contact mode. The cantilever is oscillating close to its resonance frequency and gets in intermediate contact with the substrate. Similar to the non contact mode the change of the amplitude is monitored and due to the automatic control loop the z –scan of the piezo is readjusted in order to image the surface topography of the substrate. Additionally, when the tip touches the sample's surface it experiences not only repulsive but also attractive capillary and other forces that cause a certain temporary adhesion. So interactions of the tip with the substrate surface result not only in frequency changes but also in phase shift as well. Phase imaging gives material specific information about the visco-elastic properties or the adhesion forces between the substrate and the tip.

Conducting adhesion forces measurements using AFM the experimental design has to be set as shown in Figure 21. The determination of adhesion forces on material surfaces can be measured with the tip of the cantilever itself or in order to determine interparticle forces with a fixed particle at the tip [73]. The piezo scanner moves the substrate on which the adhesion force of the tip or the fixed particle is measured in vertical direction. Due to the deflection of the cantilever in relation to the movement of the piezo the adhesion force can be measured.

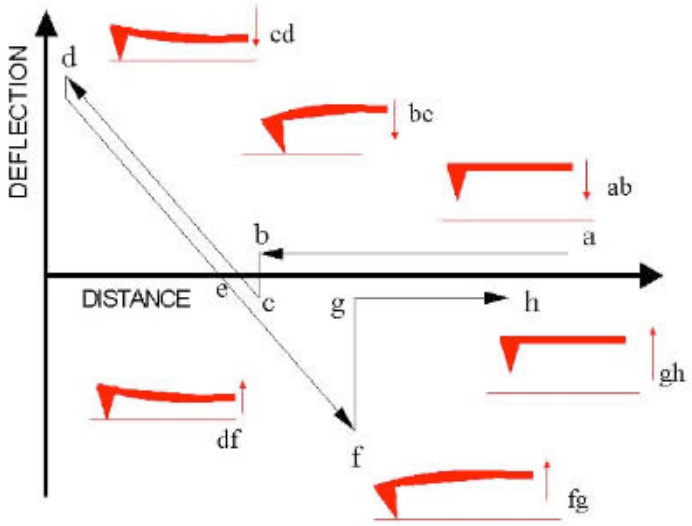

Figure 23: Standard force distance curve [18]

Figure 23 shows a standard force distance curve. The cyclic process of cantilever, approach and retraction, starts on the right of the drawing in (a). Here, the cantilever and the sample are at rest. Because of the large distance between tip and sample, no interaction takes place and the cantilever is not deflected. Even when the sample approaches the tip there is a whole interval of no interaction (zero force region, (ab)). When the separation distance decreases further, the tip gets into the range of attraction and the cantilever is deflected (bc). In Figure 23 a total attractive force is assumed and the tip may "jump" onto the sample. This happens when the attractive forces exceed the sum of the elastic force of the cantilever and the repulsive forces. If the sample is moved further in direction of the cantilever, the deflection of the cantilever decreases first and than increases in opposite direction as the displacement of the sample (constant compliance region, (cd)). Finally, the sample is retracted from the contact position (de). During this process the tip may stick to the surface due to adhesion forces (ef), and at the end it suddenly snaps away from the surface (fg) moving back to the starting position.

The calculation of the force, F, is based on a simple relationship (Hooke's Law) between the force and the cantilever deflection:

$$F = -k \bullet \delta_C \qquad \text{Eq. 22}$$

where k is the spring constant and δ_c the deflection of the cantilever.

Drucker et al. [38] and Butt [26] performed the so-called Colloid Probe Technique. By attaching a particle with defined geometry at the tip interparticle forces between the particle and the substrate can be investigated [73]. Adhesion force measurements are performed in literature in order to investigate the influence of the surface roughness or rather the contact area between the tip's particle and the substrate [63, 64]. Alternatively, API particles can be attached to the tip and the interparticle forces between the API and the substrate can be determined [12, 44]. A common field in pharmaceutical science is the investigation of interparticle forces between API and carrier of dry powder inhaler [10-12, 89, 150]. In this study the interparticle forces between the coating materials were investigated. A particle of the coating polymer is attached to the cantilever's tip and the interparticle forces were measure between the particle and different substrates consisting of differently modified coating materials.

6.3.3 Thermal analysis

Thermal analysis includes a group of methods by which the physical and chemical properties of a substance, a mixture and/or reaction mixtures are determined as a function of temperature or time, while the sample is subjected to a controlled temperature program. The program may involve heating or cooling (dynamic), or holding the temperature constant (isothermal), or any combination of these. With different methods it is possible to determine on the one hand properties of crystalline substances as melting – respectively solidification or boiling – respectively dew point, called first order transitions. On the other hand properties of amorphous substances can be detected like the glass transition temperature known as second order transition. With these methods information from the dry coating materials as well as dry coated films can be obtained and they are used as an important tool to analyze the dry coating process.

6.3.3.1 Differential scanning calorimetry

Differential Scanning Calorimetry (DSC) is a technique for measuring the energy necessary to establish a nearly zero temperature difference between a substance and an inert reference material, as the two specimens are subjected to identical temperatures regimes in an environment heated or cooled at a controlled rate. The melting respectively solidification point and the boiling respectively dew point as well as the recrystallization or modification of substances can be determined. There are two types of DSC in use. In power–compensation DSC the temperatures of the sample and the reference are controlled independently using separate identical furnaces. The temperature of sample and reference are kept identical by varying the power input to the two furnaces. The energy required to do this is a measure of the enthalpy or heat capacity changes in the sample relative to the reference.

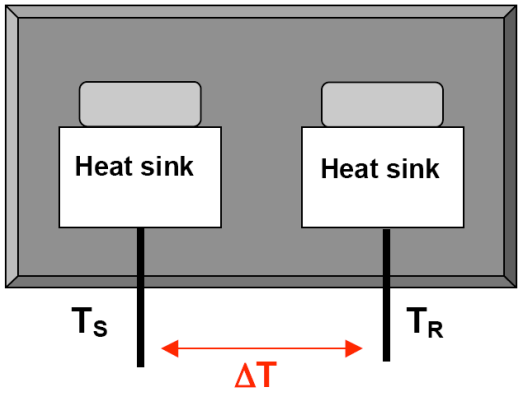

Figure 24: Principle of heat flux DSC

In this work heat-flux DSC was used. Sample and reference are connected by a low resistance heat flow (metal disc). The assembly is enclosed in a single furnace. As the thermal resistance of the samples' environment is known the enthalpy or heat capacity can be determined by the temperature difference (ΔT) (Figure 24). If no transition occurs the temperature of the sample (T_S) and the temperature of the reference (T_R) will differ constantly the same amount due to their different heat capacity in contrast to the point of transition where the difference will increase. The temperature of the sample will not follow the programmed heating or cooling rate as long as the transition takes place. The difference is recorded and transformed into enthalpy changes in the sample using calibration experiments. Plotting the heat flow versus the temperature a DSC thermogram is designed (Figure 25). Detecting a positive heat flow the sample is accepting more heat than the reference indicating i. e. a melting transition (endothermic). Contrarily, observing a negative heat flow the sample releases heat that occurs during crystallisation processes

(exothermic). The resulting peak areas can be integrated and the change of the sample's enthalpy can be calculated. For characterization it is recommended to analyze the heating curve since there is a certain risk that the sample undergoes undercooled melt instead of a thermodynamically stable state during the cooling interval. Using the cooling curve may lead to incorrect transition determinations.

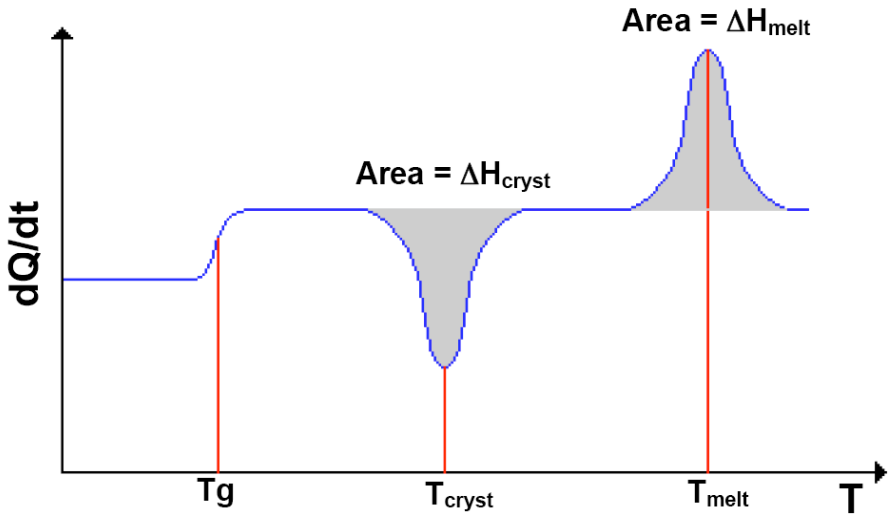

Figure 25: Scheme of thermal transitions

6.3.3.2 Thermo mechanical analysis

The aim of the thermo mechanical analysis (TMA) is to measure the deformation of a sample (expansion method) or the penetration of a tip into a sample (penetration method) under a non-oscillating load with time or variation in temperature. Properties which can be determined using TMA are the coefficient of thermal extension α and the glass transition temperature (Tg). Because of the sensitivity TMA is often used to measure Tgs that are difficult to obtain using DSC. In this study, the Tgs used for the characterization was determined solely by TMA as no Tg was observable performing DSC measurements. Performing the expansion method the sensor above the sample is adjusted being in contact with the sample by a minimum load before the temperature program is started. The expansion is measured by the sensor's lift. The expansion of the free volume allows greater chain mobility of the polymer corresponds to the Tg, which can be calculated from the coefficient of expansion.

In this work the penetration method was used (Figure 26) in order to determine the softening temperature (Ts) of the sample, which is characteristic for the method and is

closely to the Tg [52, 55, 106]. However, studies of comparison by Riesen et al. demonstrate that the Tg determined by using TMA equals the Tg measured by DSC [122]. In contrast, Okhamafe et al. distinguishes between Ts and Tg [105]. Passing the Ts the mobility of the polymer chains is high and the interparticle bindings are getting weak promoting the penetration of the TMA sensor. Due to the diameter of the TMA sensor a defined area has to have a certain mobility of the polymer chains for the penetration resulting in a softening temperature (Ts) which may be slightly higher than the glass transition temperature (Tg). With regard to the literature this difference is classified marginally. A critical point of TMA measurements is the sample preparation as it is crucial that the sample is dense and smooth. Matthée et al. compared the Tgs obtained using films to the Tgs of powder comprimates prepared with a torque hand press. Different pressures were adjusted for the preparation of the comprimates. The Tg was determined after preparation and after storage. It was demonstrated that the comprimate Tgs irrespectively of the pressure equal the film's Tgs and that this method is suitable to determine the Tg as well the decomposition temperature (Tg_2) [95].

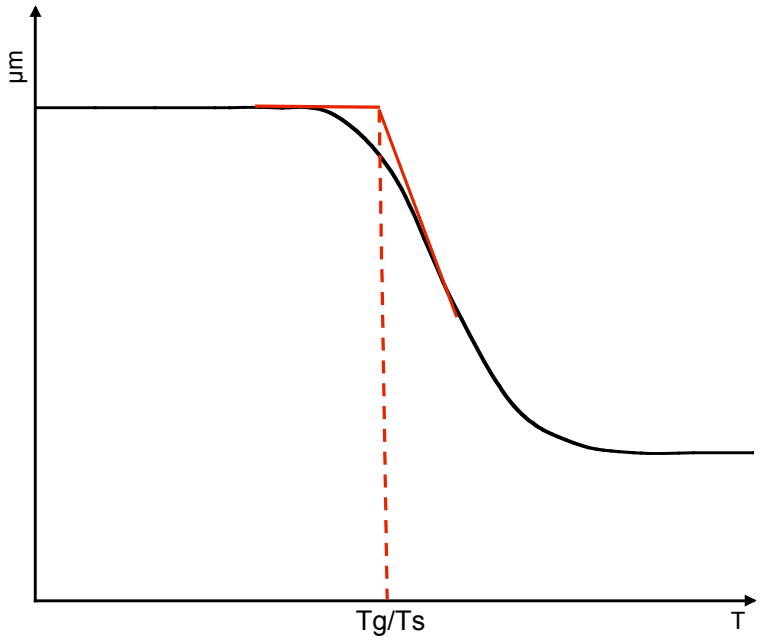

Figure 26: Scheme of a TMA measurement (penetration method)

Experimentally, a TMA consists of an analytical sensor that allows precise measurements of positions and can be calibrated against known standards. A temperature control system of a furnace, heat sink and temperature measuring device surrounds the sample. The plate on which the sample is fixed and the sensor are normally made of quartz because of its low coefficient of expansion. After having adjusted the sample the temperature program

is started and the Tg respectively Ts is measured by determining the distance the sensor penetrates into the sample.

6.3.4 Scanning electron microscopy

The scanning electron microscope (SEM) images surfaces by scanning the surface with an electron beam. The electrons impinge on the surface and generate secondary electrons which are detected by a detector forming images of the sample displayed on a cathode ray tube screen. The high energy incident electrons interact with the loosely-bound secondary electrons of the gold sputtered sample. The amount of energy given to these secondary electrons as a result of the interactions is small, and so they cannot penetrate deep into the sample very well (a few nm). Because of this, only those secondary electrons, that are produced close to the surface of the sample, are able to escape from the sample [123]. The detection mode boasts high resolution topographical images, films and stains as thin as 20 nm and produce adequately contrast images. Materials are viewed at useful magnifications up to 300.000 x without the need for extensive sample preparation except for sputtering thinly by gold.

B AIM OF THE STUDY

Coating of solid oral dosage forms especially pellets is a essential technology since drugs have to be protected against the environment respectively gastrointestinal juices or rather the gastric mucosa against the drug. Generally, coating is performed using coating material solutions or dispersions which is a time consuming processes as the solvent respectively dispersion media has to be evaporated. Hence, dry coating without the use of these vehicles is an innovative and promising alternative.

The aim of the study is the development of a robust dry coating process using the rotary fluid bed equipment (GPCG 1.1, Glatt GmbH, D - Binzen) and to compose stable, enteric resistant formulations using the enteric resistant polymer **h**ydroxy**p**ropyl **m**ethyl**c**ellulose **a**cetate **s**uccinate (HPMCAS).

Another important objective is the characterization of the process with respect to material application and film formation. The material application depends on interparticle forces, which are investigated by AFM. As the plasticizer facilitates an efficient layering of the polymer, the spreadability is investigated by contact angle measurements. By increasing the spreadability and the interparticle forces the application can be optimized with regard to the coating efficiency. Since the film formation of the dry coating process differs considerably from conventional coating methods, a parameter like the minimum film formation temperature (MFT) of aqueous dispersion based processes is defined. As film formation is supposed to take place during the curing step, parameters influencing the curing process namely curing temperature and time have to be especially considered. Additionally, the influence of the process parameters are determined and their settings are optimized in order to increase the coating efficiency and the enteric resistance.

Finally, the transfer of the process on a larger scale using the rotary fluid bed equipment GPCG 5 is performed in order to demonstrate the suitability of the dry coating process for coating larger batch sizes.

C RESULTS AND DISCUSSION

1 Development of the coating process

Water-insoluble polymers for pharmaceutical, functional coatings are generally applied using either organic polymer solutions or aqueous dispersions [33]. However, both technologies hold several disadvantages giving rise to continuous development of new coating technologies finally leading to the preparation of films using polymer powder formulations. This dry coating technology, where the dry polymer powder is applied separately but simultaneously with the plasticizer to the core, is an innovative and promising alternative to liquid-borne coatings.

1.1 Process equipment

Conducting the dry coating process the conventional coating equipment has to be modified. As the dry powder has to be delivered separately from the liquid plasticizer to the pellets, two feeders are needed. Using the fluidized bed with a rotor insert it is possible to apply the coating materials by a three way nozzle aligned tangentially to the fluid bed which ensures that the materials are applied simultaneously. The modified equipment is illustrated in Figure 27 showing a scheme of a GPCG 1.1 (Glatt GmbH) with the additionally connected twin screw powder feeder (K-Tron Soder K-CL-24-KT20). Due to the poor flowability of the coating polymer powder a special powder feeder was chosen which doses the powder gravimetrically by a twin screw to the three way nozzle.

The feeder feeds the powder to the three way nozzle by letting it fall down into the attached funnel which is connected with the outer pipe of the nozzle. The powder gets into the coating chamber by suction due to the low pressure in the coating chamber. The inner pipes of the nozzle are transporting the liquid plasticizer and the atomizing air (Figure 28). Since the amount of liquid is very small in comparison to conventional coatings, a double reciprocating pump (504 U, Watson & Marlow Bredel Inc.) was used to spray the plasticizer ensuring a homogeneous application. This pump is equipped with a Coriolis system controlling exactly the applied amount.

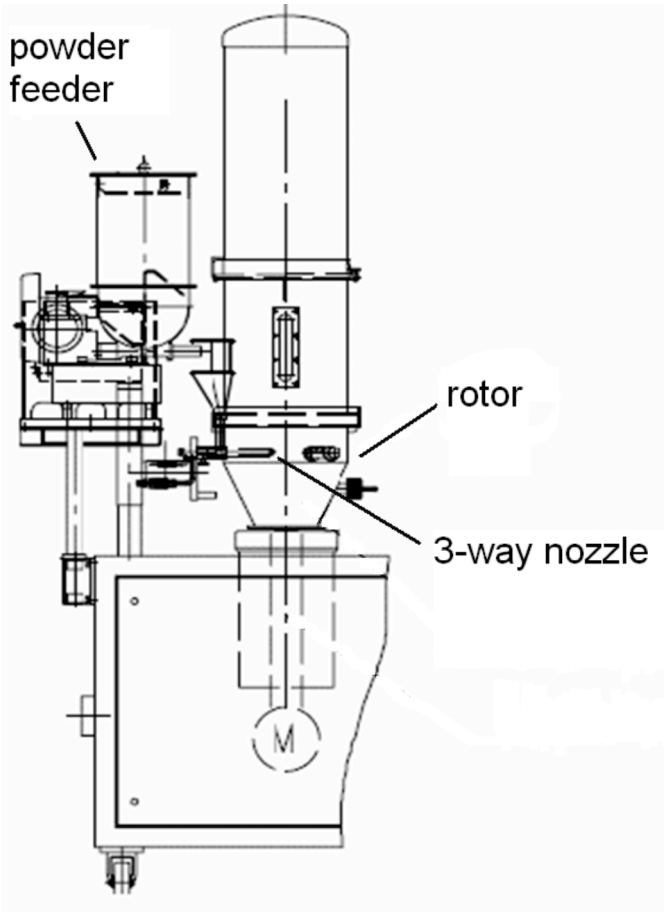

Figure 27: Scheme of the GPCG 1.1 with the gravimetrically powder feeder

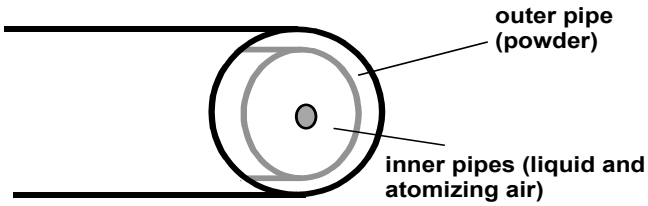

Figure 28: Scheme of a 3-way nozzle

The nozzle is aligned tangentially to the pellet bed which covers its tip completely. This technology ensures a simultaneous application of the coating components and an intimate contact of the coating materials with the pellets. Additionally, the use of the rotor fluid bed is advantageously with regard to the coating material application. The pellet bed in the rotor features a high density leading to less material loss in comparison to other fluid bed equipments where the pellet bed is enlarged with a very low density. The spiral bed movement ensures the mixing of the pellets and the periodical passing of the nozzle. Combining the advantages of the different equipments an optimal application is achieved, thereby minimizing the loss of coating material.

1.2 Process performance

The dry coating process is divided in two phases, the coating and the curing phase (Figure 29). During the coating phase polymer powder and liquid plasticizer are added to the pellets and adhere on their surface. At the beginning the plasticizer is sprayed 30 seconds before the feeding of the dry polymer is started. This ensures the wetting of the pellets' surface facilitating the adhesion of the polymer to the surface of the pellets. Further during the application the plasticizer promotes the cohesion of the polymer particles due to its liquid state resulting in a layering of the particles on the pellets. Additionally, as the plasticizer penetrates into the polymer particles they get softened and sticky enhancing the cohesion with each other. After 23 minutes the application of the coating material is completed and the following curing step is induced (Figure 29). During the curing phase of 45 minutes the film formation is achieved by an increase in temperature.

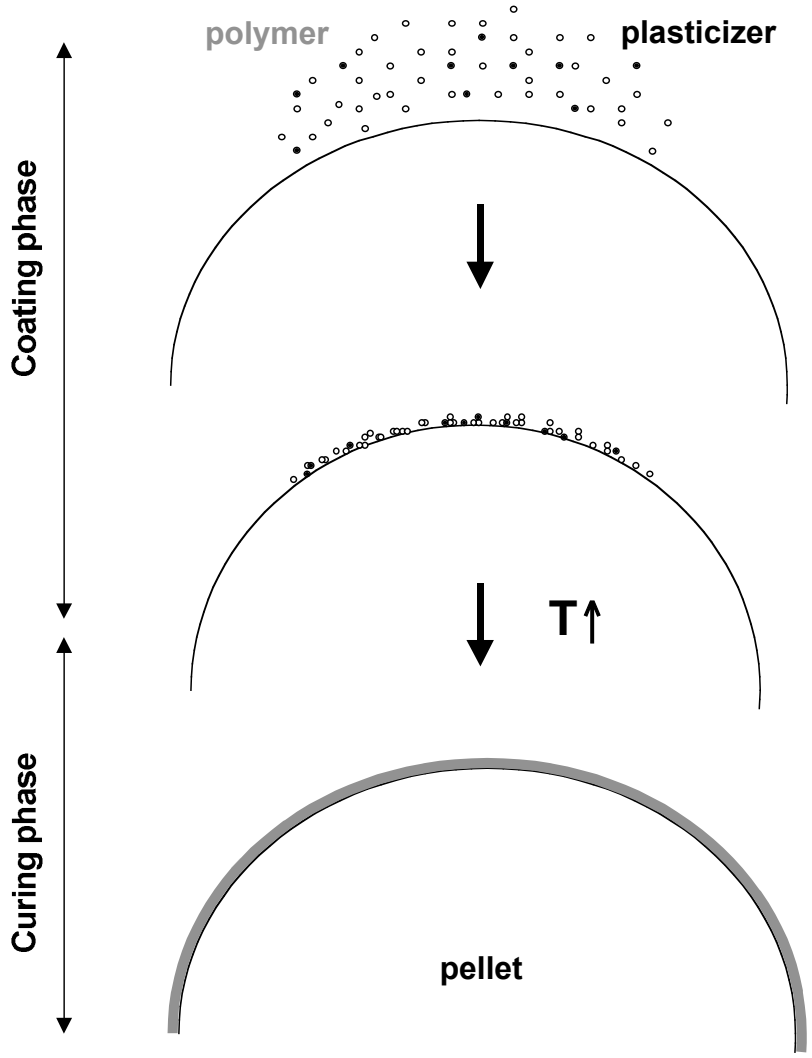

Figure 29: **Principle of the dry coating process**

The operation conditions of the process are shown in Table 9. The batch size is approximately 1 kg and the rotation speed of the rotor is 230 rpm. The pellets are preheated in the fluid bed up to a temperature of 40 °C. This is below the Tg of the coating material but high enough to obtain a certain stickiness of it and, hence, facilitating the adhesion of the polymer particles on the cores and the cohesion of the polymer particles with each other. It thereby minimizes the loss of coating powder. Furthermore, the low airflow rate of 70 m^3/h keeps the loss of coating material low. Otherwise the polymer powder might be carried along with the airflow due to its small particle size. Coating at temperatures above the Tg on the one hand could reduce the loss of coating material as well but on the other hand could lead to agglomeration of the pellets in the coating chamber due to the polymer's stickiness. After the application of the coating material has been completed the curing phase is performed at a product temperature of 55 °C which is above the Tg inducing film formation. At temperatures above the Tg, polymer particles coalesce and a homogenous film is formed. During this phase the airflow has to be increased to 120 m^3/h in order to prevent pellet agglomeration since the stickiness is enhanced at temperatures above the Tg in the rubbery state [39].

PROCESS PARAMETERS	COATING PHASE	CURING PHASE
Rotor speed (rpm)	230	230
Inlet air temperature (°C)	43	60
Product temperature (°C)	40	55
Outlet air temperature (°C)	40	55
Air flow rate (m^3/h)	70	120
Atomizing air pressure (bar)	1.5	-
Spray nozzle diameter (mm)	1.2	-
Spray rate (g/min)	3.5	-
Powder feed rate (g/min)	11	-
Time (min)	23	45

Table 9: Process parameters of the dry coating process during the coating and the curing phase

1.3 Formulation development and composition

The aims of the formulation development are to achieve a high coating efficiency and, a negligible loss of coating material, as well as to obtain a formulation with a high enteric resistance since an enteric resistant polymer was used. Additionally, the formulation has to have a good storage stability and no agglomeration tendency during storage.

As dry coating powder **h**ydroxy**p**ropyl **m**ethyl**c**ellulose **a**cetate **s**uccinate (HPMCAS, Aqoat®) was used which originally has been developed for aqueous enteric coating. Due to its succinate moiety which values 10-14% it is stable in the acid stage and dissolves quickly at pH values above 5.5 [133]. Conducting the dry coating process its small particle size of 5.4 µm is crucial as its specific gravity is lower in comparison to its van der Waals forces and consequently a good adhesion on larger coating spheres is guaranteed as well as the cohesion of the particles with each other is facilitated leading to a high coating efficiency. HPMCAS exhibits brittle properties at room and process temperatures as the Tg of the pure HPMCAS polymer is 122 °C. Consequently, the treatment of HPMCAS demands the addition of plasticizer in order to achieve film formation.

The plasticizer weakens the intramolecular attractions between polymer chains which generally results in a decrease of the Tg [49, 58] enabling film formation and coalescence of the polymer. Therefore a good polymer-plasticizer interaction is required. In the literature as well as by the suppliers of HPMCAS [35, 133] the use of triethyl citrate is recommended as the most efficient plasticizer [101, 102, 112, 134, 138] inhibiting cracking or splitting of the film [47]. HPMCAS is soluble in anhydrous TEC at room temperature which demonstrates compatibility.

Additionally, the plasticizer has to facilitate the powder layering during the coating phase increasing the adhesion and cohesion of the particles. On the one hand the liquid wets the pellet surface and builds up liquid bridges between the solids exerting capillary forces prior to penetration that strongly influence the efficiency of the powder application. On the other hand, adhesion and cohesion is enhanced after the penetration of the plasticizer into the polymer powders due to its softening properties. Nevertheless, the plasticizer distribution may be insufficient. Due to the high compatibility of the plasticizer and the polymer the plasticizer will penetrate immediately into the polymer after getting in contact without spreading on the surface. Thus, the liquid is not well distributed and due to its liquid state acts very shortly as attachment enhancer exerting capillary forces. Moreover, this phenomenon may lead to a higher loss of coating material.

In order to promote a homogeneous distribution of the plasticizer Myvacet® an acetylated monoglyceride was used as further plasticizer and wetting agent enhancing the spreading of the plasticizer. Obara et al. investigated the wettability of different plasticizer blends with wetting agents by contact angle measurements and figured out that the blend of TEC and Myvacet® has a better spreadability than merely TEC [101]. Besides this, Myvacet® is playing a role for the reduction of the polymer's Tg and for the performance of the film. However, the interaction between the polymer HPMCAS and Myvacet® and consequently the plasticizing effect is not high enough to achieve functional coatings and to perform the process without an addition of plasticizer (see C 3.2.2).

In order to inhibit the agglomeration tendency of the coated pellets anti tacking agents were added to the formulations. The additives talc and colloidal silicon dioxide were compared regarding their efficiency to inhibit the tacking of the coated pellets. Talc was applied during the coating phase together with the coating polymer. As an alternative to talc, colloidal silicon dioxide was added at the end of the curing phase as a top powder. Generally, the use of talc seems to be disadvantageous due to its possible microbiological loading.

The dry coating process was conducted by using different compositions consisting of the above mentioned coating material and additives as shown in Table 10. First, a formulation composed of HPMCAS and talc as anti-tacking agent and glidant (formulation A), promoted by Obara et al. [101], was used. In order to relinquish of talc and to simplify the formulation, pure HPMCAS as coating powder (formulation B-E) instead of a mixture consisting of HPMCAS and talc was applied afterwards. The amount of talc was substituted by HPMCAS. Since a certain stickiness of the pellets coated with pure HPMCAS (formulation B) was expected colloidal silicon dioxide was added as a top powder in formulation C with the purpose of inhibiting pellet agglomeration. In order to analyze the influence of the plasticizer and the wetting agent the use of the mixture of TEC and Myvacet® (formulation A – C) was compared with the single application of TEC or rather Myvacet® (formulation D and E).

	FORMULATION	A	B	C	D	E
Powders	HPMCAS	47%	75%	75%	75%	75%
	Talc	28%	-	-	-	-
	Aerosil®	-	-	1%	-	-
Plasti-cizers	Triethyl citrate (TEC)	17.5%	17.5%	17.5%	25%	-
	Myvacet®	7.5%	7.5%	7.5%	-	25%
	Total	100%	100%	101%	100%	100%

Table 10: Compositions of the formulations used for dry coating

All formulations were analyzed and characterized with a special focus on coating efficiency, enteric resistance and agglomeration tendency (see C 2).

1.4 Summary

In this study the dry coating process is carried out applying different formulations in the rotary fluid bed equipment with a three way nozzle aligned to the direction of the fluid bed movement. Optimized equipment is assembled using a rotary fluid bed with a three way nozzle and a gravimetrical powder feeder achieving optimum coating materials' application during the first phase of the process, namely the coating phase, which takes 23 minutes. The polymer is dosed as dry powder via the powder feeder to the three way nozzle which is able to apply separately but closely together the plasticizer composition and the dry powder into the pellet bed. This method enables a homogeneous application of the coating material onto the pellets. Due to the optimized process equipment using the rotary fluid bed the pellet bed has a higher density in comparison to conventional fluid beds avoiding an excessive loss of polymer powder. In contrast to the conventional fluid beds the intensity of pellet movement is higher preventing pellet agglomeration. During the second phase of the process, which lasts further 45 minutes film formation occurs due to an increase in temperature. Pellet agglomeration, which may occur due to the arising stickiness of the polymer at elevated temperatures, is prevented by increasing the air flow rate.

As material hydroxypropyl methylcellulose acetate succinate (HPMCAS) is used which has characteristically good gastric resistance and dissolves quickly over a wide range of pH

once the acid stage is overstepped and shows a good compatibility with plasticizers [99]. The coating process was performed with triethyl citrate as plasticizer and Myvacet® as wetting agent, both playing a critical role with respect to the reduction of the Tg and the integrity of the film [47]. As anti-tacking additives talc and colloidal silicon dioxide were used.

2 Characterization of coated dosage forms and stability testing

The dry coating process is an emerging coating technology. However, up to now, there is only little knowledge on the coating process itself and the properties of the products available. In order to strengthen this process as an alternative to conventional coating procedures and in order to compare it with them the pellets coated with different formulations (see C 1.3) were characterized.

The coating efficiency was determined as an important parameter generally monitored during formulation, process and scale-up development. Also the drug release and the agglomeration tendency were investigated directly after preparation and storage according to the ICH guidelines [67].

2.1 Coating efficiency

Generally, it has to be admitted that lower coating efficiencies are obtained by performing the dry coating process in comparison to conventional coating methods where coating efficiencies ≤ 93% are achievable [91]. This might be the reason why this parameter is rarely reported in literature [53, 71, 101]. However, in this study it is used on the one hand to have a tool in order to compare the process with conventional coating processes and on the other hand to show that additives especially wetting additives are influencing this parameter. They can increase the coating efficiency due to their good spreadablilty and, consequently, increase the adhesion and cohesion of the polymer particles (Table 11).

FORMULATION	A	B/C	D	E
Coating efficiency	80.7% ± 3.6%	84.0% ± 0.6%	72.5% ± 0.4%	87.3% ± 1.0%

Table 11: Coating efficiencies of the coating formulations, n=3, mean ± CI (95%)

Formulation A that contains talc as anti-tacking agent has a coating efficiency of 80.7% ± 3.6%. Formulations B and C which merely differ by the addition of silicon dioxide as top powder at the end of the curing phase exhibit a higher coating efficiency of 84.0% ± 0.6%.

Comparing the coating efficiencies of formulation B/C with formulations D and E the influence of a wetting agent is demonstrated. Formulation D does not contain Myvacet® resulting in a lower coating efficiency of 72.5%. Since TEC is highly compatible with HPMCAS as mentioned above, it penetrates into the polymer before it is distributed homogeneously persisting only shortly on the polymer's surface. Due to penetration the polymer surface will be softened which leads to a locally good cohesion between particles treated with plasticizer and an insufficient cohesion between untreated particles. Additionally, the property of the liquid to exert capillary forces between the particles is limited due to the immediate penetration resulting in a low coating efficiency. Furthermore, the distribution of the TEC is insufficient that leads to a lower enteric resistance described more detailed in section C 2.2.2. By adding the wetting agent Myvacet® the adhesion and cohesion and, consequently, the coating efficiency is enhanced (84.0%). Myvacet is less compatible with HPMCAS inhibiting that the liquid mixture is soaked up immediately into the polymer. This leads to a longer residence time on the surface and consequently persisting capillary forces. Besides, the liquid spreads on the surface resulting in a better distribution. This hypothesis can be confirmed regarding the coating efficiency of formulation E. By using solely Myvacet® as liquid the highest coating efficiency is achieved with 87.3%.

Additionally, the amount of polymer (mg) per cm^2 was calculated since this parameter is used for comparison between aqueous dispersion based films. Usually, the applied amount of polymer of dispersion based films is between 0.5 mg/cm^2 and 10 mg/cm^2 depending on the coating material [139]. Thus, with respect to the amount of polymer the dry coated films are comparable with the conventional films being between 2.3 mg/cm^2 and 3.6 mg/cm^2 (Table 12). For the calculation the pellet size distribution was considered since it differs between 0.8 mm and 1.25 mm. According to the coating efficiencies the amount of polymer increases by achieving higher coating efficiencies.

FORMULATION	**A**	**B/C**	**D**	**E**
Film (mg/cm^2)	3.3 – 4.4	3.5 – 4.4	3.0 – 4.0	4.1 – 4.8
Polymer (mg/cm^2)	2.6 – 3.3	2.7 – 3.3	2.3 – 3.0	2.8 – 3.6

Table 12: Amount of coating material and polymer per cm^2

Considering the coating efficiencies it can be assumed, that even though a wetting agent was added, lower coating efficiencies were obtained in comparison to conventional coating processes. Further investigations about the coating efficiency and its influencing

parameters are performed in section 3.1 with respect to the spreadablilty on and the interparticle forces between the polymer particles.

However, the functionality of the film is the key parameter for the development of a new coating technology and for the efficiency of the process. Since HPMCAS as enteric coating material was used the functionality of the film was characterized by determining the enteric resistance.

2.2 Enteric resistance

The claim of enteric resistant dosage forms is a quick disintegration in the upper intestines after an unimpaired passage through the stomach. Therefore the drug release was investigated according to the USP XXIX [142]. All investigations were conducted with one batch of each formulation in order to ensure that all samples got the same treatment prior to characterization. The division of the batches for sample storing is depicted in section E1.4.

2.2.1 Pellet core

Theophylline pellets with a drug content of 94% have been chosen as cores. Drug release profiles of the uncoated theophylline pellets in 0.1 N HCl show a complete disintegration of the drug within 5 minutes (Figure 30), indicating a high drug release of uncoated pellets in the acid media.

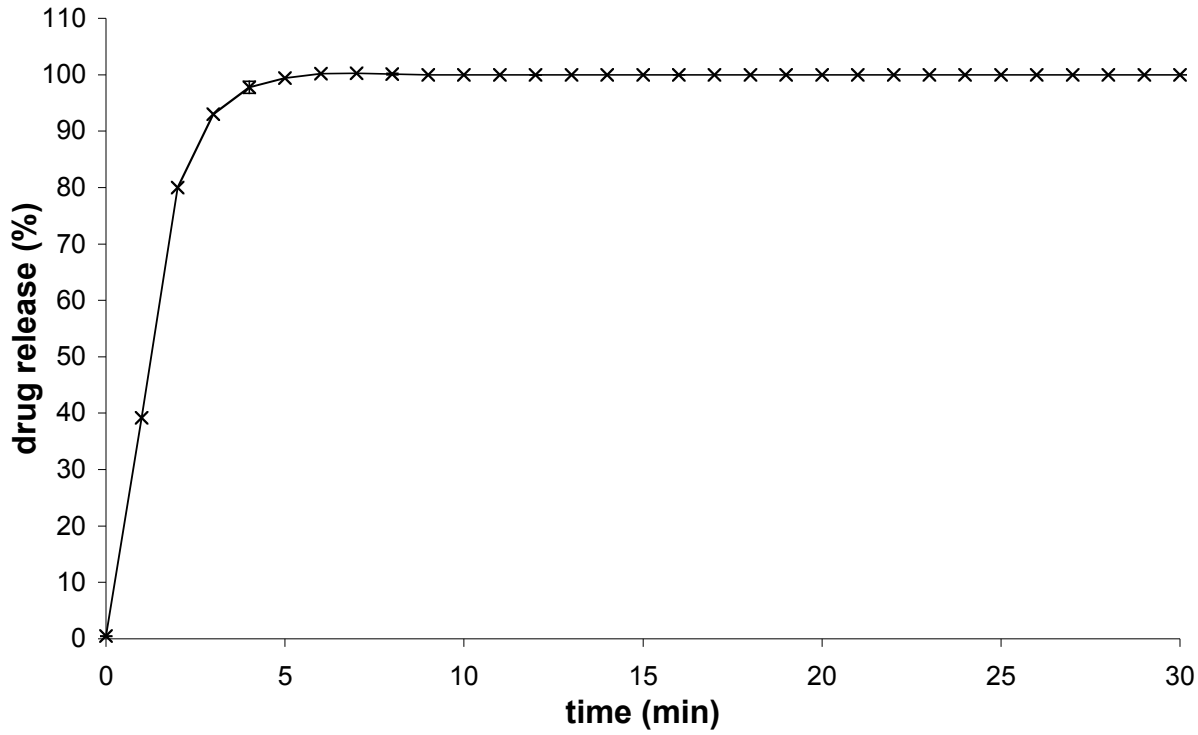

Figure 30: Dissolution of uncoated Theophylline pellets in 750 ml 0.1 N HCl, n = 6, mean ± CI (95%)

2.2.2 Coated pellets

In order to evaluate the formulations with regard to the enteric resistance the drug release of pellets coated with formulation A - E was determined according to the requirements of the USP XXIX [142]. Dissolution studies were carried out at the acid stage using 750 ml 0.1 N HCl (pH 1) within the first 120 minutes and after addition of 250 ml $Na_3PO_4 \cdot 12\ H_2O$ solution at the buffer stage (pH 6.8) [126, 133].

Regarding the graph which shows the drug release after preparation (Figure 31) it can be seen that all formulations containing TEC (formulation A – D) meet the requirements of the USP XXIX method enteric coated articles at the acid stage (drug release ≤ 10%) [142]. Drug releases vary between 2.2% ± 0.4% and 5.5% ± 1.0%.

Formulation A consisting of HPMCAS as polymer powder, talc as glidant and a mixture of TEC and Myvacet® as plasticizer respectively wetting agent has a drug release of 3.4% ± 0,3% during the first two hours of the acid stage. However the insolubility of talc in the dissolution media causes a slower disintegration of the film in the neutral stage of the dissolution. In contrast to this the drug release of the formulation B and C with HPMCAS,

TEC and Myvacet® amounted 3.5% ± 0.9% (B) and 2.2% ± 0.4% (C). Both formulations disintegrate immediately after the pH change. The difference between the drug releases of formulation B and C is not significantly.

The highest drug release with 5.5% is determined for the formulation D with HPMCAS and TEC. Probably the high drug release is caused by the low coating efficiency of the formulation (see C 2.1). Due to the lower amount of coating material on the pellet the film is thinner compared to the other formulations increasing the permeability of the film. The amount of TEC in this formulation is higher compared with the other formulations, however, the quality of the film and, consequently, the enteric resistance is not increased. Although the polymer's Tg is lowered more by the higher amount of TEC compared to the other formulations, film formation seems be less efficient leading to a reduced film quality. Due to the missing wetting agent and the good compatibility with HPMCAS, TEC may penetrate immediately into the polymer without being distributed on the polymer's surface effecting domains in the polymer layering with high amounts of plasticizer besides domains with less amount of plasticizer. This causes on the one hand a partly worse film formation with a higher drug release and on the other hand a lower coating efficiency and thus a lower film. Furthermore, this phenomenon was observed by preparing plasticized powders of HPMCAS and TEC where agglomerates of polymer with high amounts of TEC in the plasticized powders were detected (see C 3.1.4). The formulation also has the highest confidence interval demonstrating an inhomogeneous film formation due to the missing wetting agent and insufficient distribution of the plasticizer.

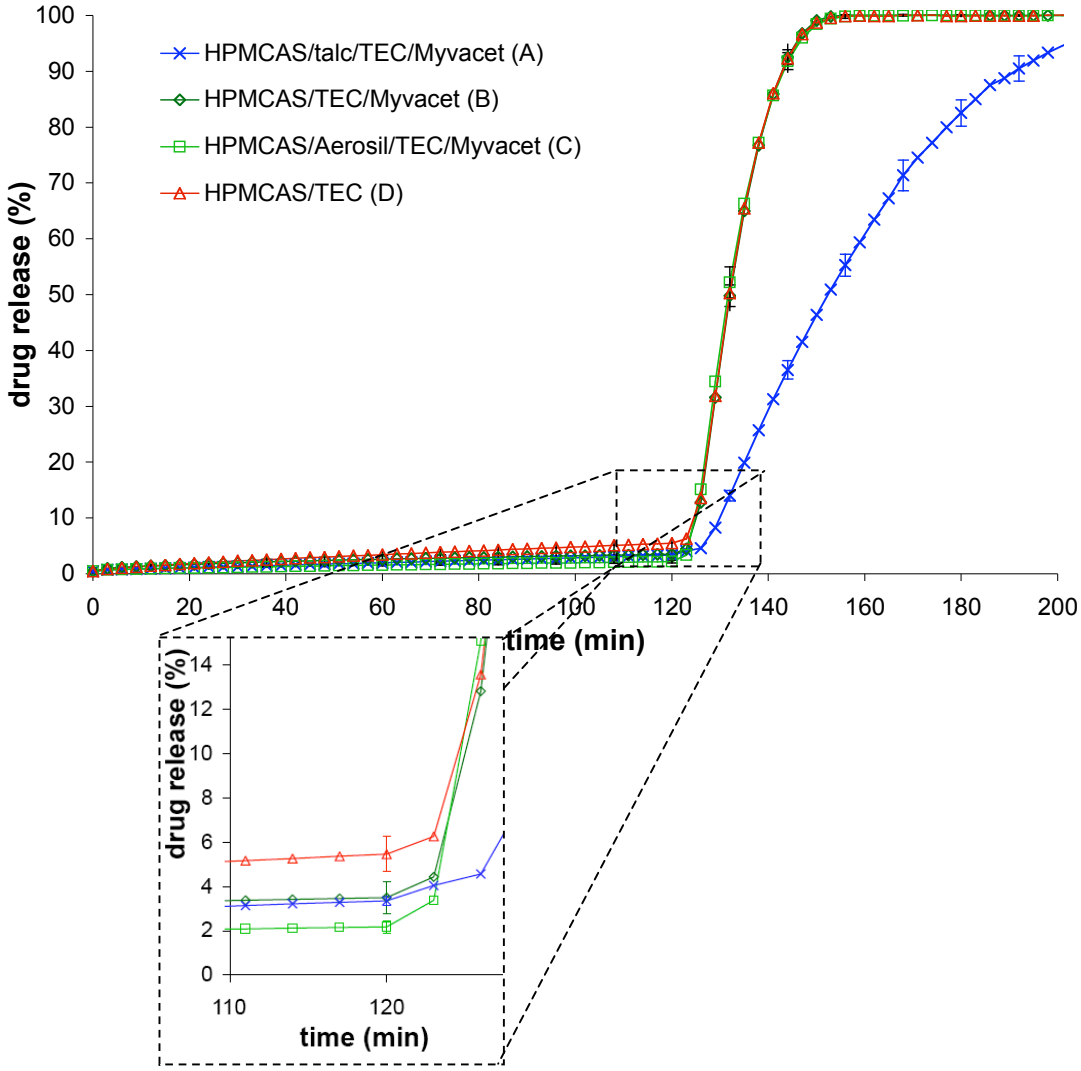

Figure 31: Drug release of theophylline pellets coated with formulation A - D in 750 ml of 0.1 N-HCl (pH 1) for 120 minutes and after addition of 250 ml of $Na_3PO_4 \cdot 12\ H_2O$ solution (65 g/l) (pH 6.8) further 80 minutes, n = 6, mean ± CI (95%)

On the contrary, the film consisting of HPMCAS and Myvacet® (Formulation E) is not enteric resistant showing a fast drug release in the acid stage (Figure 32). After 6 minutes already 10% of the drug has been released and after 120 minutes almost 90%. In contrast to TEC the plasticizing effect of Myvacet® is supposed to be insufficient and, consequently, functional coating at the chosen process conditions is not achieved. As shown in chapter C3, the Tg of the coating material which stands in relation to the film formation of dry coated films is too high to achieve film formation during the curing phase of the process. Thus, enteric resistance is not obtained.

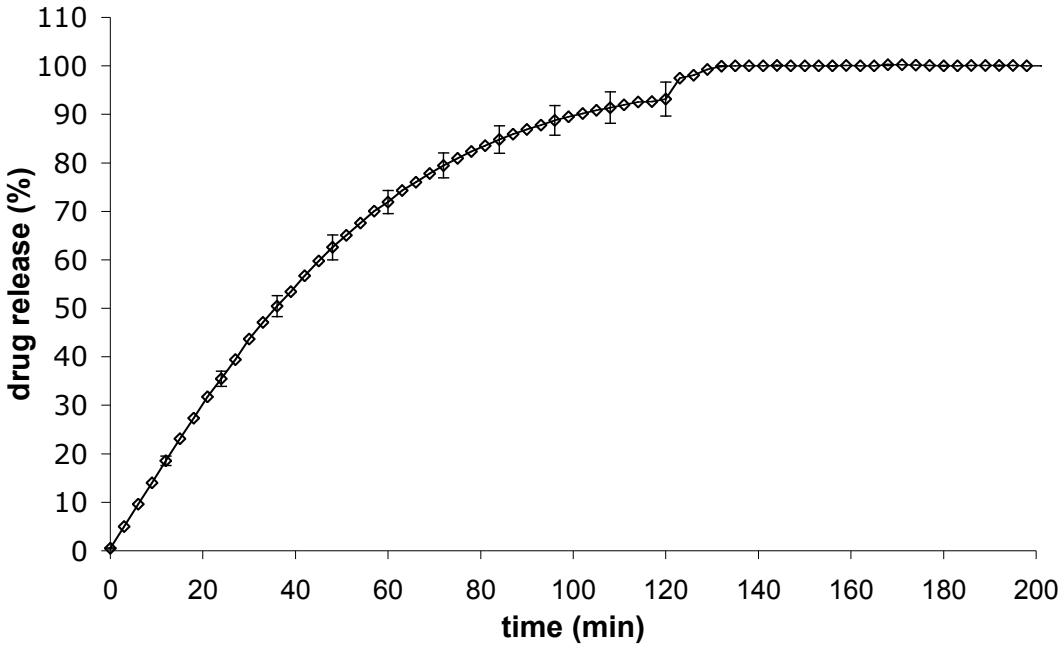

Figure 32: Drug release of theophylline pellets coated with formulation E in 750 ml of 0.1 N-HCl (pH 1) for 120 minutes and after addition of 250 ml of $Na_3PO_4 \cdot 12\ H_2O$ solution (65 g/l) (pH 6.8) for further 80 minutes, n = 18, mean ± CI (95%)

(A) Formulation B/C **(B) Formulation E**

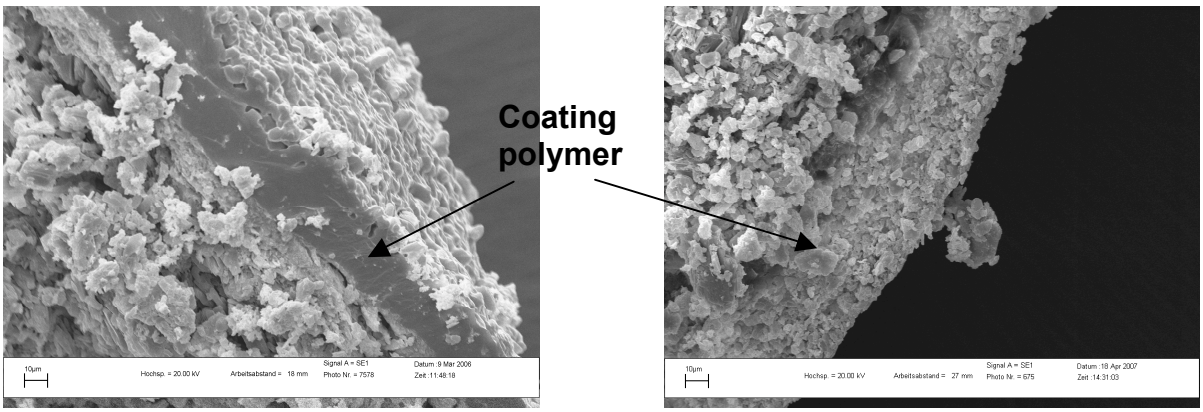

Figure 33: Scanning electron micrographs of pellets coated and cured with formulation B/C (A) and E (B) (magnification 500)

Additionally, scanning electron micrographs (SEM) of pellets coated and cured with formulation B/C and E were compared demonstrating the need of TEC in order to achieve enteric resistance respectively a functional film (Figure 33). The cross section of the pellets coated and cured with formulation B/C shows a polymer film in contrast to the cross section of the pellet coated with solely Myvacet® where the polymer particles are layered on the pellets but no film is observable.

After having determined the required ingredients of a formulation needed to achieve an enteric resistant film the required coating level was evaluated. Formulations B/C described before were coated with 25% coating powder based on the weight of uncoated pellets. The pellets coated with 20% HPMCAS, TEC and Myvacet® released 11.2% ± 5.1% drug within the first 120 minutes at the acid stage not fulfilling the requirements for enteric coated articles according to the USP XXIX (Figure 34) [142]. Therefore the necessary coating level at 84% coating efficiency lies between 20% and 25% (see C 2.1, A6.2.2).

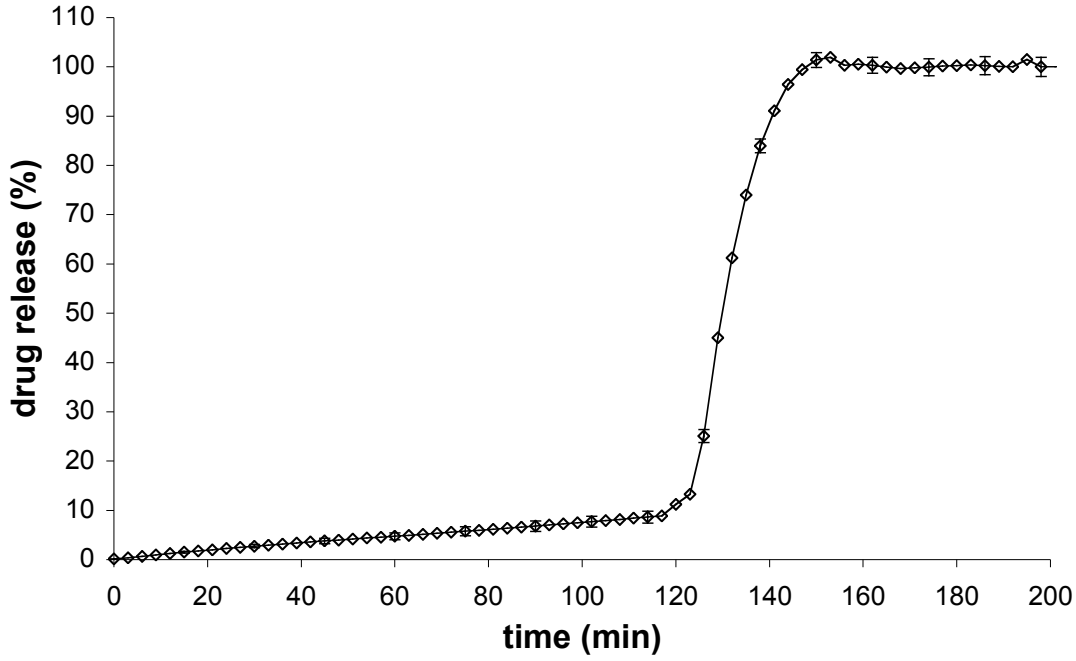

Figure 34: Drug release in 750 ml of 0.1 N-HCl (pH 1) from theophylline pellets of 20% coating level coated with HPMCAS, TEC and Myvacet® at the acid stage, n = 12, mean ± CI (95%)

Regarding the obtained results it can be summarized that all formulations containing TEC (formulation A – D) are enteric resistant meeting the requirements of the USP XXIX [142] at 25% coating level.

2.2.3 Stability of coated pellets

The drug release profiles of pellets coated with formulations A - D which were enteric resistant after preparation, were investigated with regard to storage stability. Therefore they were stored according to the ICH guidelines of long term and accelerated conditions [67] and, additionally, at silica gel conditions (10% RH ± 5% RH) (Table 13) in order to investigate the influence of humidity. Every 3 months samples were withdrawn for drug release studies according to the requirements of the USP XXIX [142].

STUDY	STORAGE CONDITION	SAMPLING POINT
Long term	25 °C ± 2 °C / 60% RH ± 5% RH	0 – 3 – 6 – 9 - 12 months
Long term	25 °C ± 2 °C / 10% RH ± 5% RH	0 – 3 – 6 – 9 - 12 months
Accelerated	40 °C ± 2 °C / 75% RH ± 5% RH	0 – 3 - 6 months

Table 13: Storage conditions and time periods for stability testing

After three months storage the samples stored at accelerated conditions (40 °C ± 2°C / 75% RH ± 5% RH) were stuck together possibly due to further film formation. Thus, the increased film stickiness caused that the needed amount from the stored sample could not be withdrawn without damaging obviously the film which would lead to increased and incorrect drug releases. Therefore the stability testing and dissolution studies were not performed any further.

Regarding Figure 35 the drug release after 120 minutes at the acid stage is plotted against the storage intervals of formulation A (a) respectively B (b). After 3 months storage at 10% RH ± 5% RH formulation A has a marginal decrease in drug release from 3.4 % ± 0.3% to 2.5% ± 0.3% remaining on this level over the remaining storage interval (Figure 35 a). The samples stored at 60% RH ± 5% RH reveal a decrease in the drug release to 1.9% ± 0.3% after 3 months also not changing after further storage time. The changes compared to the drug releases after preparation indicate that film formation continues during storage. Especially at increased humidity further film formation is observed due to the plasticizing effect of water, which results in enhanced enteric resistance. Nevertheless, film formation during storage, named aging [58], occurs only between preparation and 3 months storage indicating a complete cured film after short storage intervals.

(a) Formulation A

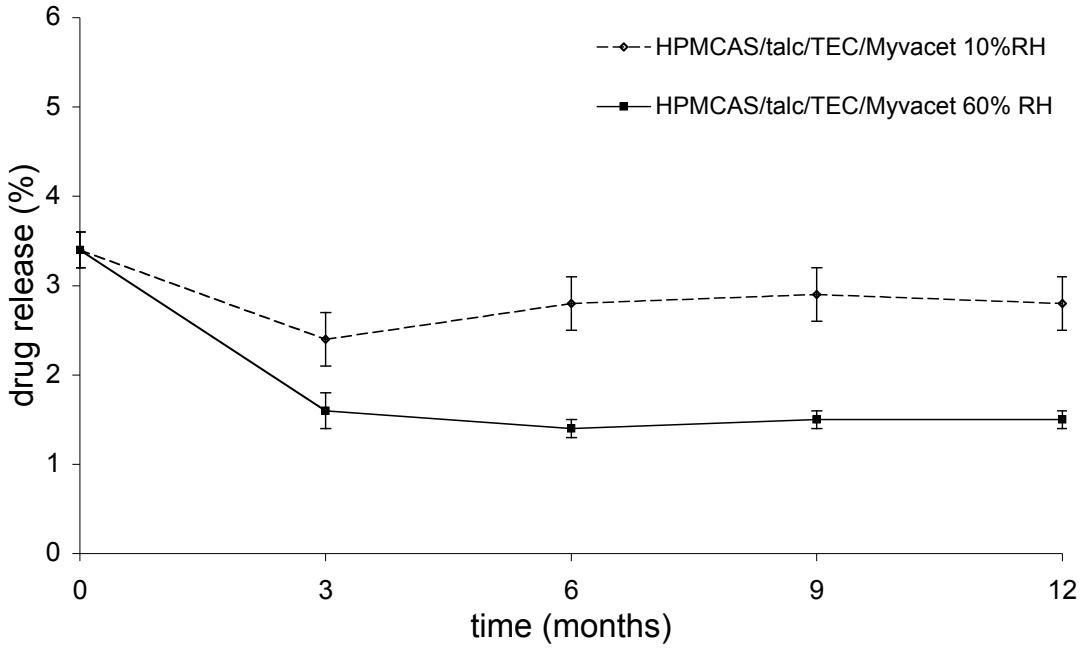

(b) Formulation B

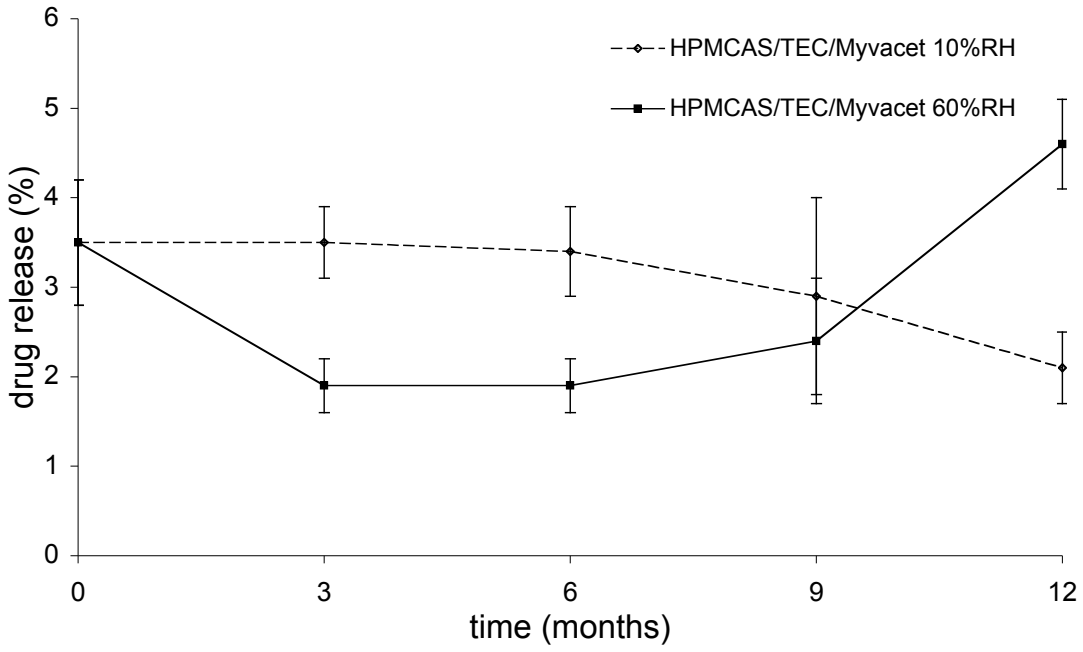

Figure 35: Drug release of theophylline pellets coated with formulation A (a) and B (b) after 120 minutes at the acid stage (0.1 N HCl) after preparation and storage for 3, 6, 9 and 12 months, n = 6, mean ± CI (95%)

Formulation B shows drug releases between 3.5% ± 0.9% and 2.9% ± 1.1% at 10% RH ± 5% RH after preparation and 9 months storage (Figure 35 b). After 12 months storage only a minor change compared to the drug release after preparation can be

observed determining a drug release of 2.1% ± 0.4% possibly caused by aging. In contrast, increasing the humidity to 60% RH ± 5% RH significant changes are found revealing a drug release of 1.9% ± 0.3% after 3 and 2.4% ± 0.7% after 6 months storage. However, after storing formulation B at 60% RH ± 5% RH for 12 months the drug release is enhanced due to the stickiness of the film which might have lead to film damage during sample preparation prior to dissolution. The increased stickiness is caused by the plasticizing effect of water which lowers the Tg of the film giving rise to a softening of its surface.

The plot of formulation C displays only marginal changes indicating that during storage at 10% RH ± 5% RH and 60% RH ± 5% RH further film formation plays a minor role (Figure 36 a). The drug release of 3.4% ± 0.3% after preparation is reduced to 2.3% ± 0.3% after storage at 10% RH ± 5% RH. In contrast the drug release after 3 months storage at 60% RH ± 5% RH is decreased to 1.5% ± 0.1% intrinsically indicating aging. However, after 3 months further storage the drug release is again slightly increased to 2.1% ± 0.1%. Obviously by chance the drug release after 3 months storage is lower than the drug release after 6 months storage as it is not caused by film's damage since the increase is not excessively and still below the drug release after preparation. The drug release of the samples stored for 9 and 12 months confirms this suspicion having the same value. Since formulation B and C differ only by the absence or presence of silicon dioxide as a top powder at the end of the process it can be assumed that the silicon dioxide sorbs the water inhibiting further plasticization of formulation C thereby inhibiting the increase of stickiness. Nevertheless, it has to be mentioned that the addition of colloidal silicon dioxide does not eliminate the phenomenon of aging with regard to formulation B.

(a) Formulation C

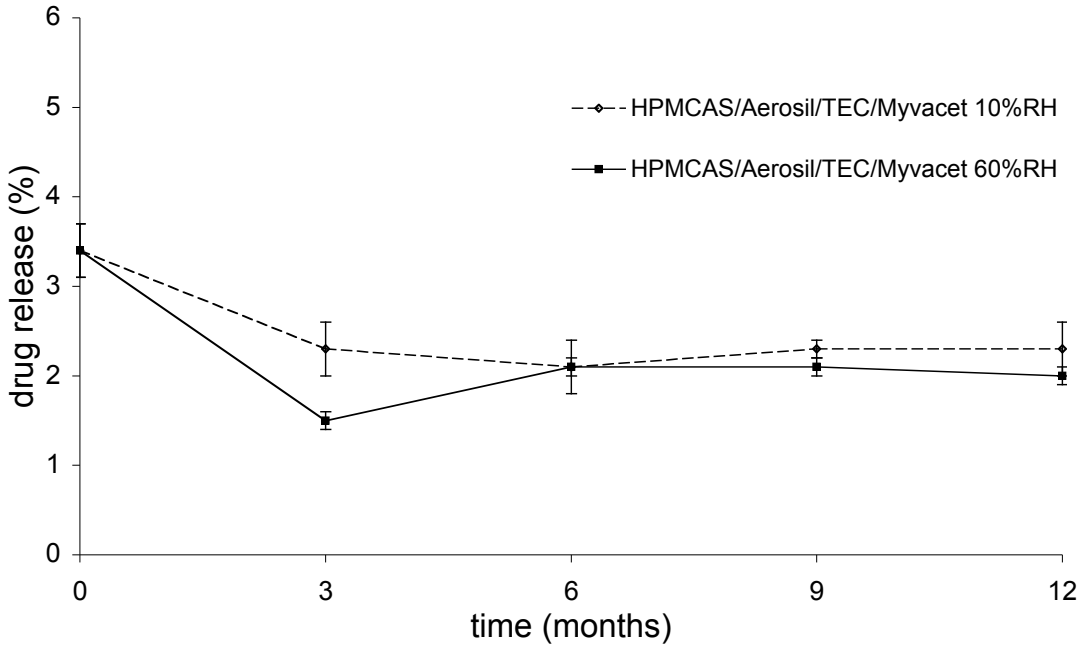

(b) Formulation D

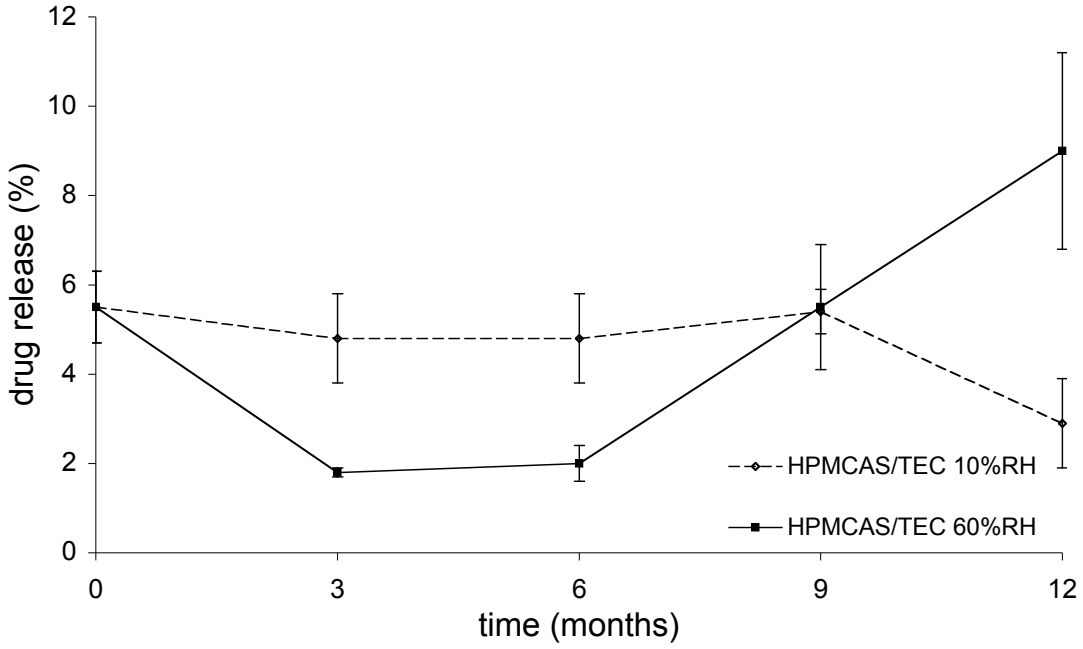

Figure 36: Drug release of theophylline pellets coated with formulation C and D after 120 minutes at the acid stage (0.1 N HCl) after preparation and storage for 3, 6, 9 and 12 months, n = 6, mean ± CI (95%)

Regarding the drug release for formulation D no changes can be observed at 10% RH ± 5% RH revealing a drug release between 5.5% ± 1.0% after preparation and 4.8% ± 0.1% after 6 months (Figure 36 b). Exceptionally, the drug release after 12 months

storage exert a decreased drug release of 2.9% ± 0.5% in comparison to 9 months, but no significant differences in comparison to 3 and 6 months. However this reduced drug release is of minor importance in contrast to the samples stored at 60% RH ± 5% RH where further film formation occurs which is caused by the phenomenon aging. The drug release is reduced to 1.8% ± 0.1% after 3 months storage differing significantly from the drug release determined after preparation. Nevertheless, after further storage time the drug release is increased to 5.5% ± 1.4% after 9 months storage and further up to 9.0% ± 2.2% after 12 months storage. As mentioned above, the formulation contains a higher amount of TEC compared to the other formulation (see C 1.3). This higher amount of plasticizer causes an increased stickiness of the coated pellets since the film's Tg is lower compared to the Tgs of the other formulations and closer to the storage temperature (see C 3.2). This enhances the risk of films' damage during sample preparation prior to the dissolution leading to an increased drug release. The increased drug release of 9.0% ± 2.2% might be explained by the synergism of the effects of the higher amount of TEC and the increased water content in the air.

Considering the results only minor changes are detectable after storing at 10% RH ± 5% RH in contrast to samples stored at 60% RH ± 5% RH where major changes are observed caused by the phenomenon aging. All formulations reveal a decreased drug release differing significantly from the drug release determined after preparation. This demonstrates that by an increase of humidity film formation continues triggered by the plasticizing effect of water leading to enhanced enteric resistance.

Nevertheless, it could be shown that formulations A and C have storage stability with regard to the enteric resistance although aging could not be prevented, generally a phenomenon which known from aqueous coated dosage forms during storage [58]. Formulation B and especially D consisting only of HPMCAS and TEC shows arbitrary drug release due to the arising stickiness during storage at elevated humidity leading to film's damage during sample preparation. It can be assumed that with regard to formulation D the influence of the water on the film's performance is more distinctive since the Tg of this film is lower compared to the other formulations caused by the higher amount of TEC. Therefore, the given formulations were investigated in order to determine the influence of humidity during storage with regard to the agglomeration tendency.

2.3 Agglomeration tendency during storage

Formulations without an anti-tacking agent tend to agglomerate during storage and, accordingly, tacking preventing additives were tested in this study. To reduce the agglomeration effect during storage colloidal silicon dioxide was added to the pellets as a top powder at the end of the curing phase using a concentration of 1% calculated on the amount of coating material. On the contrary, talc was mixed with the coating polymer in advance to the powder application in the ratio 10:6 (see C 1.3.). The investigations were performed using the same batches investigated in section 2.2.

2.3.1 Sieving

The formulations A – D were analyzed with regard to agglomeration tendency by sieving after a defined storage time at 25 °C ± 2 °C and 10% RH ± 5% RH respectively 60% RH ± 5% RH (Table 14) according to the ICH guidelines used for the stability testing [67] (see C 2.2). Prior to analysis all samples were stored in vials of a defined geometry each vial containing 15 g of the pellets. This was in order to ensure that the force of gravity by which the pellets were pulled together was equal for all samples. In order to analyze the agglomeration tendency the amount of residue on the sieve was determined. As after preparation none of the formulations showed agglomeration tendency and passed the sieve completely the data are not shown.

STUDY	STORAGE CONDITION	SAMPLING POINT
Agglomeration tendency	25 °C ± 2 °C / 60% RH ± 5% RH	3 – 6 - 12 months
	25 °C ± 2 °C / 10% RH ± 5% RH	3 – 6 - 12 months

Table 14: Storage conditions and time periods for agglomeration tendency testing

In Figure 37 the residues of the pellets remaining on the sieve are plotted against the sieving time. The graph show the results after a three months storage time at 10% RH (Figure 37 a). All formulations exhibit no agglomeration tendency passing the sieve almost completely after one minute. It can be assumed that due to the low humidity during storage the surface of the film is unchanged and no stickiness occurs.

(a) Agglomeration tendency, 3 months storage at 25 °C ± 2 °C and 10% RH ± 5% RH

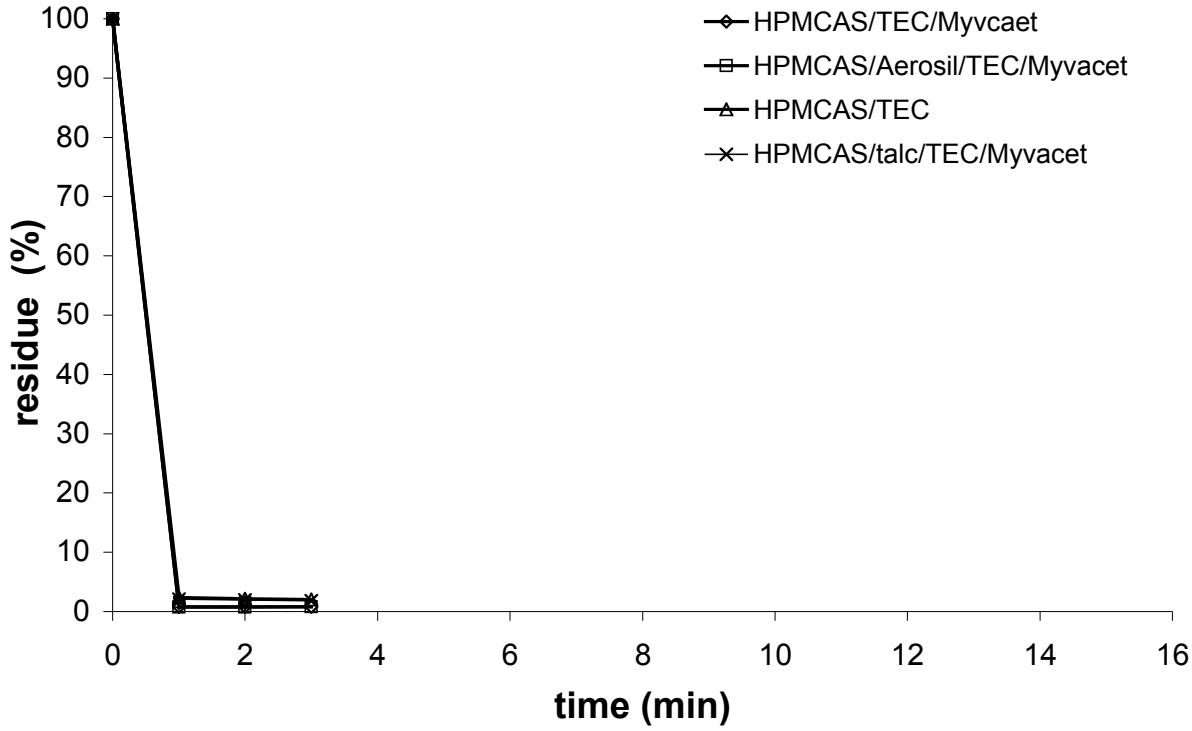

(b) Agglomeration tendency, 3 months storage at 25 °C ± 2 °C and 60% RH ± 5% RH

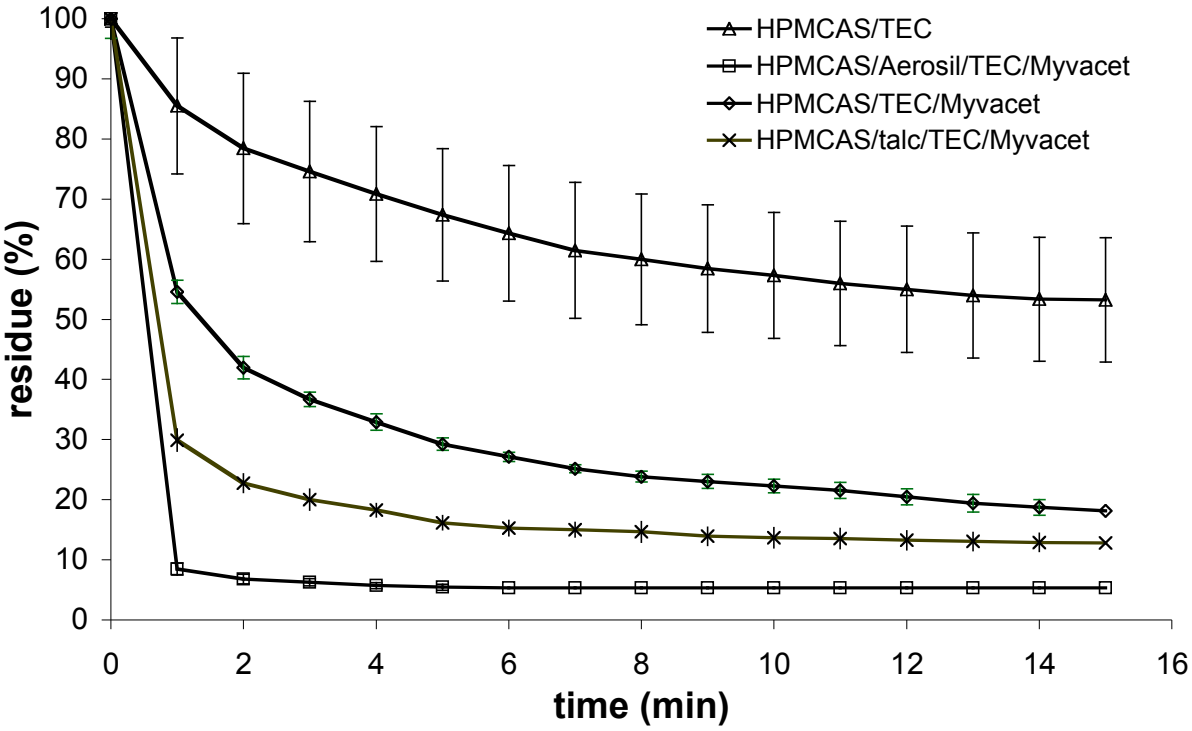

Figure 37: Residue (%) of formulations A - D after 3 months storage, n = 4, mean ± CI (95%)

Storing the samples at 60% RH ± 5% RH agglomeration of the coated pellets is observed (Figure 37 b). The lowest amount of agglomerates is determined for formulation C passing the sieve almost after 3 minutes with a residue of 5.3%. Using silicon dioxide as a top powder after the curing, tacking is reduced on the one hand due to the increased roughness of the pellet's surface by adhering silicon dioxide onto it and on the other hand due to the ability of silicon dioxide to sorb water from the air avoiding further plasticization and, accordingly, avoiding an increase of the polymer's stickiness. The residual agglomerates of formulation A and B are with 12.8% (A) and 18.2% (B) higher. Both formulations do not contain silicon dioxide as a top powder which may cause less roughness of the pellet's surface and an increase in tackiness. Nevertheless, the residue of formulation A is lower compared to formulation B based on the addition of the glidant talc to the polymer. The highest amount of residues was determined for formulation D with 53.2% which is more than the half of the sample. This extreme tackiness can be explained by the higher amount of the plasticizer TEC in formulation D, that in addition with the water in the air results in an increased stickiness of the pellets surface and tackiness of the pellets in the bulk. Contemplating the obtained results, the formulation without the additive talc and instead of with colloidal silicon dioxide exhibits a lower agglomeration tendency after three months storage.

The residues determined after 6 months storage time do not show major changes. The samples stored at 10% RH do not agglomerate having 0.4% - 0.8% residues after three minutes sieving (Figure 38 a). After storing at 60% RH the amount of residual agglomerates is increased compared to the one after three months storage demonstrating that time plays a certain role for the agglomeration tendency (Figure 38 b). Due to the longer exposure to the increased humidity the plasticizing effect of the water is extended leading to further softening of the coat and to further tackiness.

(a) Agglomeration tendency, 6 months storage at 25 °C ± 2 °C and 10% RH ± 5% RH

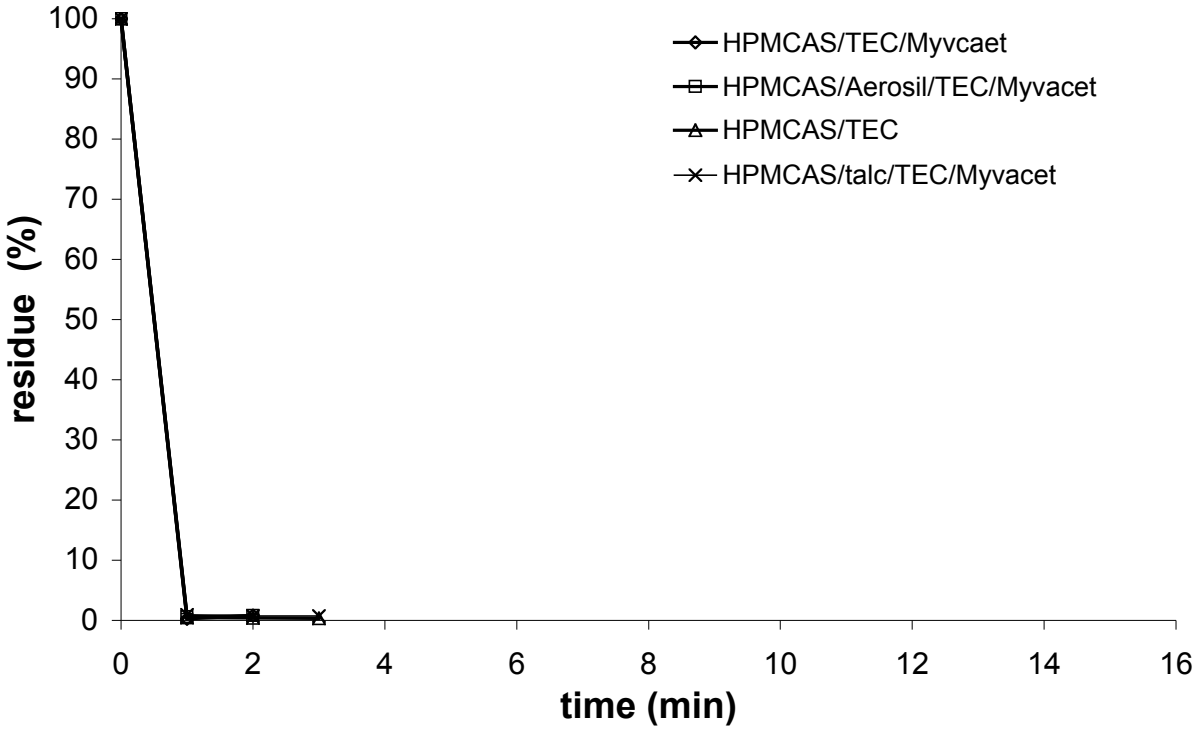

(b) Agglomeration tendency, 6 months storage at 25 °C ± 2 °C and 60% RH ± 5% RH

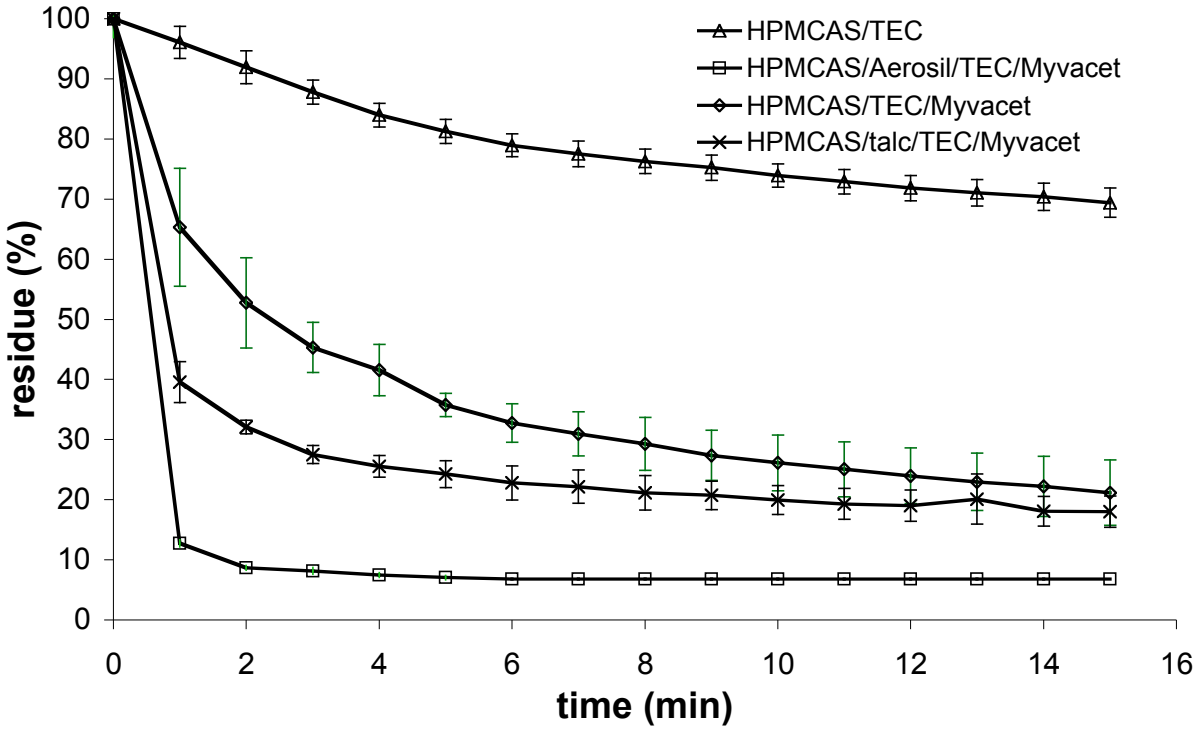

Figure 38: Residue (%) of formulations A - D after 6 months storage, n = 4, mean ± CI (95%)

After extending the storage interval to 12 months the samples stored at 10% RH do still not show any agglomeration tendency demonstrating that the absence of water in the air inhibiting nearly any alteration of the film (Figure 39 a). In contrast the residues of the samples stored at elevated humidity (60% RH) are further increased (Figure 39 b). However, the sample containing talc as glidant (formulation A) shows the lowest agglomeration tendency with 16.8% residue in contrast to previous determinations after 3 and 6 months storage, where formulation C had the lowest agglomeration tendency. Due to the increase in the residues to 40.1% of formulation C the capacity of silicon dioxide to sorb water is assumed to be depleted resulting in an increase of tackiness. Formulation B and D have the highest agglomeration tendency with 87.0% (B) and 98.9% (D). The missing anti tacking agent may cause these extremely increased residues. Considering again the higher amount of plasticizer TEC in formulation D, it can be presumed, that in synergism with the water the film alters and increases in stickiness even more in comparison to formulation B.

(a) Agglomeration tendency, 12 months storage at 25 °C ± 2 °C and 10% RH ± 5% RH

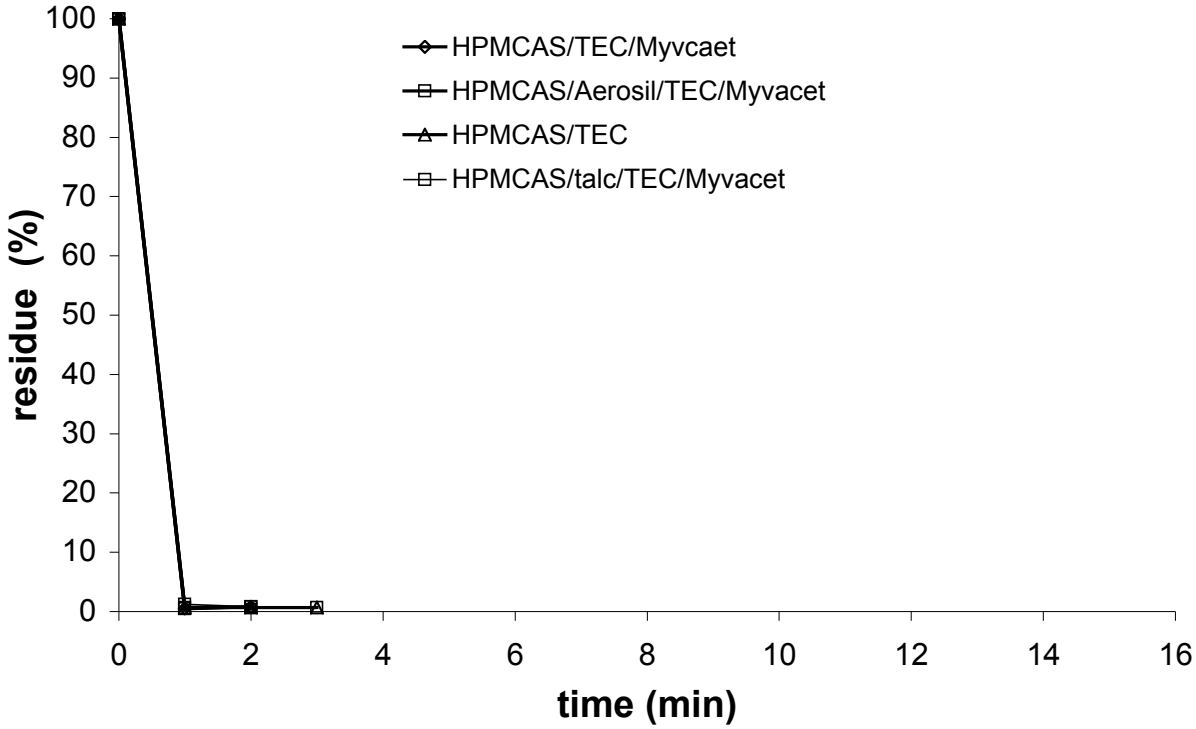

(b) Agglomeration tendency, 12 months storage at 25 °C ± 2 °C and 60% RH ± 5% RH

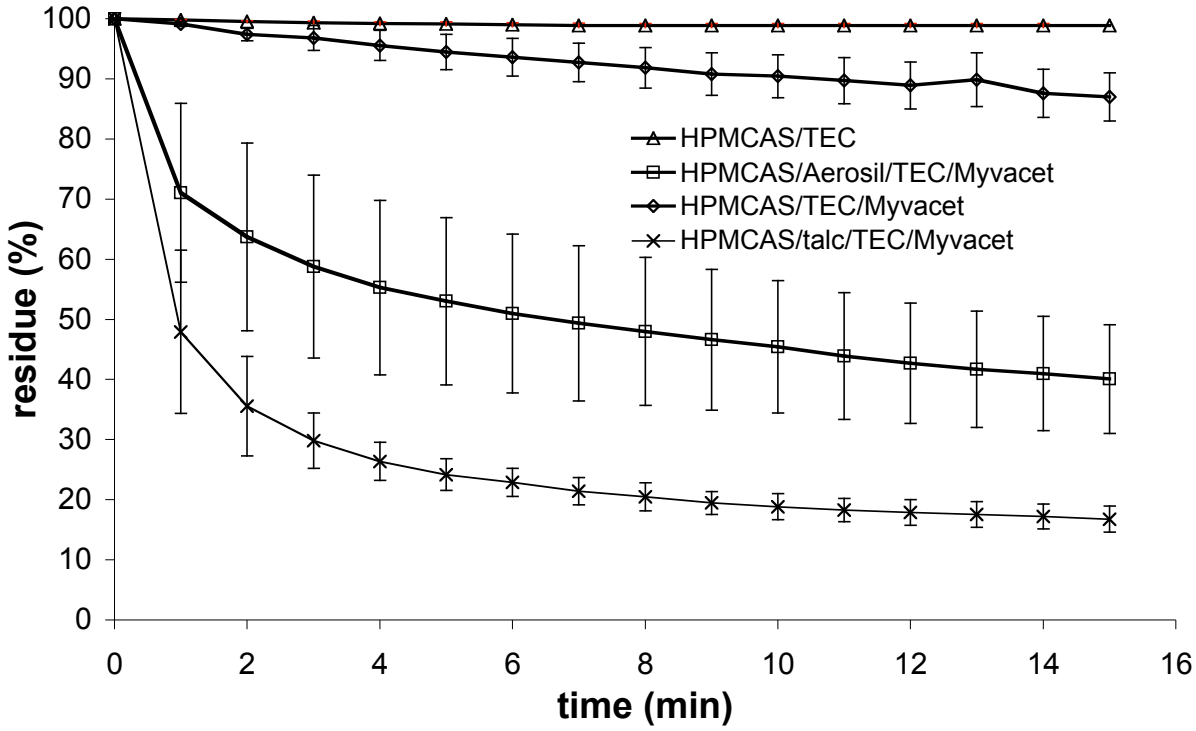

Figure 39: Residue (%) of formulations A - D after 12 months storage, n = 4, mean ± CI (95%)

2.3.2 Ring shear tester

Since no agglomeration tendency of the formulations A – D could be observed by sieving immediately after the process, the flowability of all formulations was investigated after the process using a ring shear tester in order to give a prognosis of the agglomeration tendency during storage. Therefore the yield locus of all formulations was determined after 24 h storage at 60%RH ± 5% RH and 25 °C ± 2 °C ensuring standardized conditions. In literature bulk material is called free flowing with a yield locus above 10 [128].

All results show a ff_c above 10 confirming that all formulations are free flowing after preparation. However, differences between the determined ff_c can be observed (Table 15). The highest flowability of 43.7 ± 7.3 is shown by formulation A with talc as additive mixed to the polymer which confirms the results obtained after 12 months storing. Furthermore formulation C has the second highest ff_c of 25.5 ± 1.7, followed by formulation B with 19.2 ± 0.5 and formulation D with 12.6 ± 2.4. Regarding the results a similarity to the results after 12 months storage obtained by sieving is obvious and it can be assumed that flowability measurements with a ring shear tester are appropriate for predicting the tendency of dry coated pellets to agglomerate.

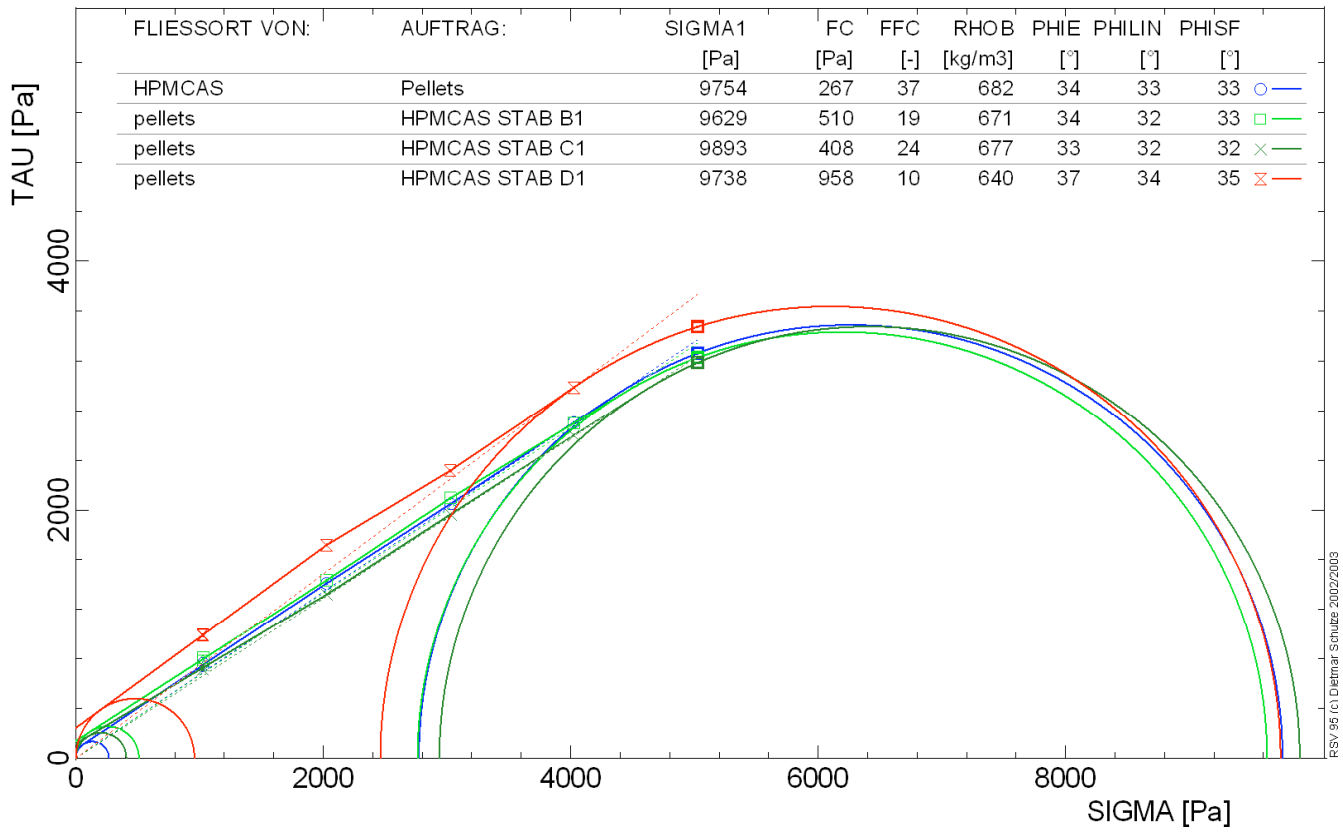

Figure 40: Flowability (ff_c) of formulation A-D

Nevertheless, it has to be considered that compared with shorter storage times the results differ from each other. With the ring shear tester the temporarily efficient anti tacking agent silicon dioxide cannot be considered. During the measurement the pellets undergo a certain load and are pushed together. This may effect that the surfaces' roughness due to the silicon dioxide is decreased and its anti tacking ability becomes negligible. Consequently, the flowability of the pellets of formulation C is sampled out lower compared to formulation A. Here the anti tacking agent is well distributed in the polymer powder and cannot get influenced during the measurement. Thus, this method can be applied for predicting agglomeration tendencies after long term storage, however, for comparison the effect of the method on the additives has to be considered.

FORMULATION	ff_C
A (HPMCAS/talc/TEC/Myvacet®)	43.7 ± 7.3
B (HPMCAS/TEC/Myvacet®)	19.2 ± 0.5
C (HPMCAS/Aerosil®/TEC/Myvacet®)	25.5 ±1.7
D (HPMCAS/TEC)	12.6 ± 2.4

Table 15: Yield locus of formulation A – D after 24 h storage at 25 °C ± 2 °C and 60% RH ± 5% RH, mean ± CI (95%)

2.4 Summary

Dry coated pellets were characterized by investigating after preparation the enteric resistance, the coating efficiency and the agglomeration tendency. Additionally, the storage stability was analyzed focusing on the enteric resistance and the agglomeration tendency. Considering the results it can be summarized that formulations A – D are appropriate for the dry coating process with regard to the enteric resistance after preparation and after storage meeting the requirements of the enteric coated articles USP XXIX [142]. In contrast, formulation E is not enteric resistant due to insufficient film formation which is caused by the missing TEC. Consequently, formulation E was not tested on stability, although, the highest coating efficiency was achieved. The formulation with high coating efficiency and high enteric resistance is formulation B/C followed closely by formulation A. Formulation D is outstanding as it exerted a low coating efficiency and a low enteric resistance even though meeting the requirements of the USP XXIX [142]. Additionally, formulation D has the highest agglomeration tendency caused by the higher amount of TEC in the formulation, which decreases the Tg of the polymer to a lower value,

compared to the other formulations. Thus, the stickiness of the film is increased and agglomeration arises. Formulation B also tends to agglomerate, as no anti tacking agent is included in the formulation. Formulation A and C show low agglomeration tendency, however, after 12 months storage at 60% RH ± 5% RH formulation C starts to agglomerate due to the exhausted capacity of the silicon dioxide top powder. Nevertheless, considering the high coating efficiency and enteric resistance and the intention to simplify the formulation for dry coating, formulation C is favorable and is used for further studies focusing on the mechanical view of the coating material application and film formation.

3 Mechanical view of coating material application and film formation

In the following chapter the dry coating process will be characterized with respect to the material application and the film formation. As the dry coating process is divided into two phases, the coating and the curing phase, the next sections are arranged chronologically. After the material application, which takes place during the coating phase, the film formation, which mainly occurs during the curing phase, is elucidated. Since film formation occurs during the curing phase, the curing temperature and time are investigated. Furthermore, parameters influencing the material application and the film formation are determined.

3.1 Coating material application

The film formation of aqueous dispersion coating processes occurs already during the coating material application. In contrast to liquid borne coatings coating material application and film formation of the dry coating process are divided into two phases, the coating phase where dry powder and plasticizer are applied to the pellets, and the curing phase where film formation takes place (see C 1.2). During the application it has to be ensured that in the beginning the coating material gets attached on the cores and afterwards starts to layer on it in order to achieve a certain thickness. Thus, the coating materials have to adhere and cohere during this phase without any dispersion media in contrast to the conventional coatings. Nevertheless, the liquid plasticizer acts as an attachment enhancer since it wets the polymer and builds up liquid bridges between the particles. Furthermore, due to the penetration of the plasticizer into the particle temporary capillary forces are exerted. After the plasticizer is penetrated completely into the particles the capillary forces disappear and van der Waals forces and electrostatic forces become important. Additionally, it has to be considered that the plasticizer softens the polymer's surface, which will influence the adhesion and cohesion of the particles as well.

In order to investigate the parameters influencing the material application during the coating phase, contact angle measurements were performed determining the spreadability of different plasticizer compositions with and without a wetting agent. Liquids with a good spreadability build up strong capillary forces [4], which enhance the adhesion and cohesion being of certain interest for the material application. Additionally, atomic force microscopy was conducted analyzing the adhesive forces between the coating materials comparing again the influence of the different liquid additives.

A measure of the efficiency of material application's gives the coating efficiency (CE), however, it has to be kept in mind that the CE is determined after the curing phase and consequently after the complete process. Therefore the possible loss during this second phase is discarded (see C 2.1). Nevertheless, the results obtained by contact angle measurements and atomic force microscopy were related to the coating efficiency of the formulations described in chapter C 2 in order to have a measure to evaluate the material application since the parameters of the curing phase were kept constant.

3.1.1 Application process of the coating material and consideration about the interparticle forces influencing the material application

The polymer and the plasticizer were applied to the cores at constant feeding and spraying rates. As the plasticizer has been sprayed 30 seconds before the feeding of the dry polymer was started, wetting of the pellets' surface is ensured facilitating the adhesion of the polymer powder to the surface of the substrate. Thus, at the beginning of the coating phase, the ratio of plasticizer and polymer powder is higher than the named ratio of 25/75 and will approach this ratio once the application of the powder has started. Especially in the beginning the adhesion will be promoted mainly by capillary forces due to the high amount of liquid and will increase as the penetration of the liquid into the polymer proceeds. Once the liquid is penetrated completely into the particles van der Walls forces and electrostatic forces will be responsible for the cohesion of the particles.

Regarding the scanning electron micrographs (SEM) (Figure 41) a continuous layering can be detected after a certain lag time. After the first 5 minutes when almost a quarter of the material has been applied only a thin layer of polymer particles is detectable, in contrast to the SEM after 10 minutes where a pronounced increase can be observed (Figure 41 A - B). A steady growing of the layering is visible after further application (Figure 41 C – E). This is promoted by mechanical interlocking with polymer particles already attached to the pellets surface and certain softness of the polymer particle caused by penetration of the plasticizer. In contrast, during the first 5 minutes of material application only a small part of the polymer powder adheres on the pellets' surface due to the missing softness of the particles and no ability to interlock mechanically. According to this, it can be assumed that the time needed to achieve a first complete layer of the polymer is an important factor of material application. Thus, in the beginning instead to adhere on the pellet's surface the polymer particles partly stay in the air flow above the fluid bed in the relaxation zone of the rotor and partly attach at the chamber wall and the filter.

(A) 5 minutes coating

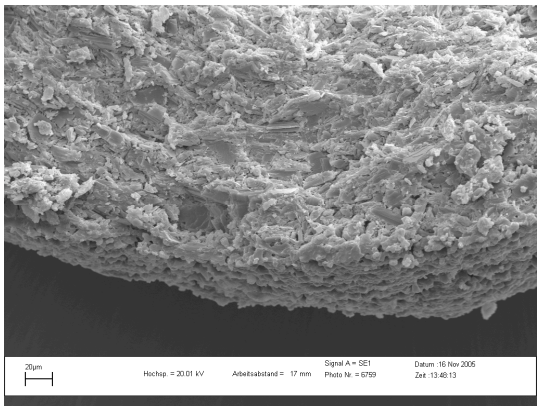

(B) 10 minutes coating

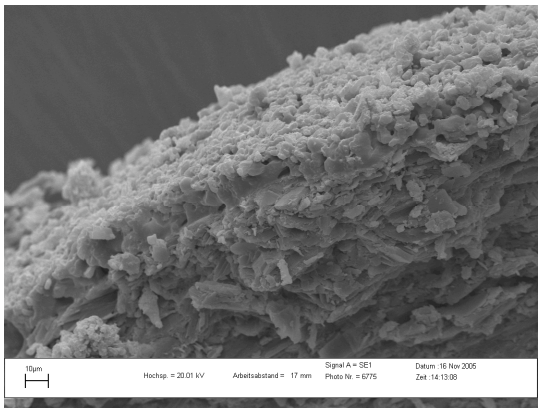

(C) 15 minutes coating

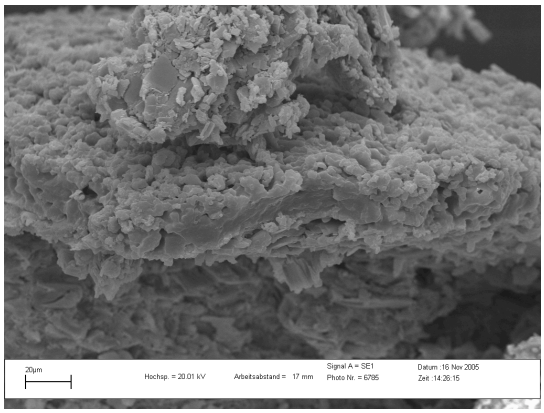

(D) 20 minutes coating

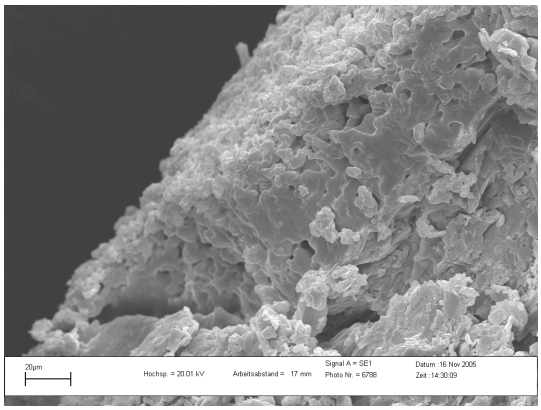

(E) 23 minutes coating

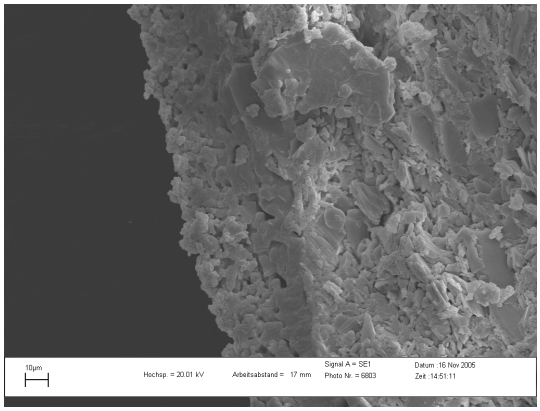

Figure 41: Scanning electron micrographs of pellets after different coating times

However, due to the rocking of the filter and the pressurization between the coating chamber and the chamber above the filter, after each filter rocking these particles can detach from the filter and chamber wall, whenever the filter rocking function is actuated, falling down on the pellets bed.

In order to optimize the application the loss of powder has to be kept as small as possible which can be achieved by efficient wetting of the pellets' surface and the polymer particles ensuring the formation of capillary forces and enhancing adhesion and cohesion.

3.1.2 Influence of wetting agents on the spreadability

Contact angle measurements were performed, in order to analyze, whether the spreadability of the liquid on the solid is enhanced by the wetting agent. The measurements were carried out according to the sessile drop method where one single drop is dropped down on the surface of the material. After 25 seconds resting time of the drop on the solid the angle between the liquid and the solid was determined by circle fitting. The results were related to the coating efficiencies of the corresponding formulations.

The plasticizers TEC, Myvacet® and a mixture of both were used, composed of 70% (w/w) TEC and 30% (w/w) Myvacet® corresponding to the mixture used in section C 1.3. The solid substrate consisted of HPMCAS and of a mixture with HPMCAS and talc (10:6).

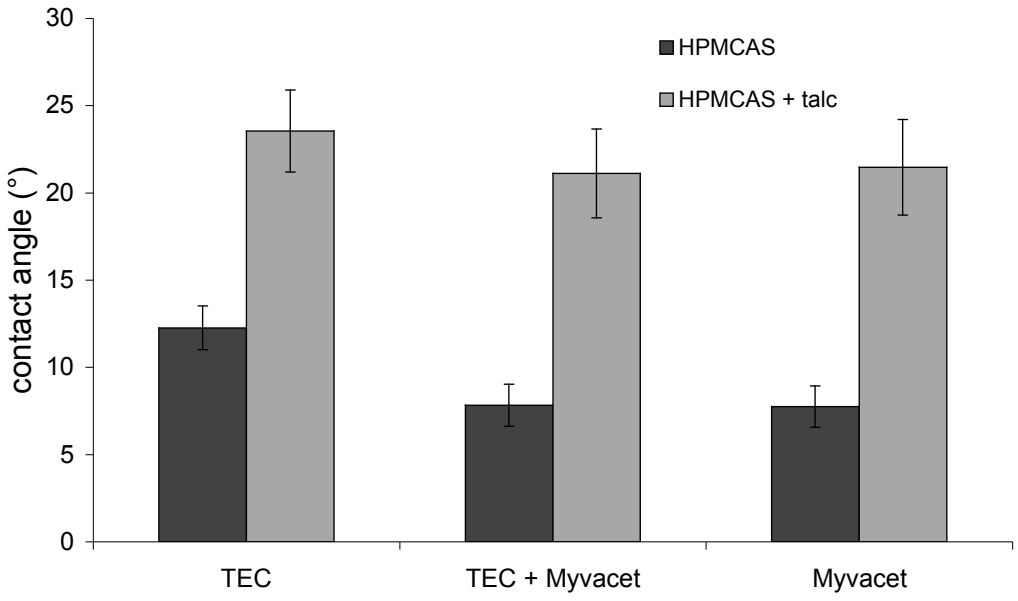

Figure 42: contact angles (°) of plasticizers on HPMCAS and HPMCAS + talc (10:6), n = 8, mean ± CI (95%)

The contact angles of the liquids on comprimates of HPMCAS and talc are approximately two times higher than the contact angles on pure HPMCAS comprimates. The difference of the contact angles of the liquids on HPMCAS and talc as substrate is not significant determining contact angles between 23.5° ± 2.4° and 21.1° ± 2.5°. These results do not

correspond to the results determined by Obara et al. who measured significantly lower contact angles by adding Myvacet® to the plasticizer. However, the mixture consisted of TEC and Myvacet® in a ratio of 5:2 and the ratio of HPMCAS and talc (10:3) differed as well [101], which might here cause the deviation of the measurements.

Nevertheless, as mentioned above the contact angles of the liquids on HPMCAS and talc in this study are two times higher than the ones of HPMCAS comprimates. When mixing HPMCAS and talc together, the surface of the comprimates is not perfectly homogeneous but is composed of compressed talc and HPMCAS particles. HPMCAS has a hydrophilic character in contrast to talc, which is hydrophobic, resulting in a certain heterogeneity of the surface. The used plasticizer TEC is hydrophilic. When the hydrophilic liquid spreads on the surface, the three-phase line, where liquid, solid and air meets in one point, advances on the substrate continuously. By spreading the droplet will in some point come into contact with a hydrophobic area. If the kinetic energy is not high enough to overcome this point, the three-phase line will “jump” immediately in a position, where the value of the contact angle becomes locally 90° at the three-phase point. The effect is called line pinning. Transferring this phenomenon on the HPMCAS/talc with regard to the lower contact angles of the HPMCAS comprimate the higher contact angles may caused by the heterogeneity and higher hydrophobicity of the HPMCAS/talc comprimate. In contrast, the HPMCAs comprimates are homogeneous hydrophilic which inhibits line pinning.

The contact angles of the liquids on pure HPMCAS comprimates show significantly different contact angles. TEC has a contact angle of 12.2° ± 1.3° being higher than the contact angles of the mixture with Myvacet® and pure Myvacet®. Between the later ones no difference can be observed determining a contact angle of 7.8° ± 1.2° for pure Myvacet® and 7.9° ± 1.2° for the mixture of TEC and Myvacet®. Remembering the results of the coating efficiency in section C 2.1 the coating efficiency of the formulation with TEC as liquid was the lowest being 72.5%. This result corresponds to the high contact angle of TEC resulting in weak capillary forces. By mixing Myvacet® to the liquid the coating efficiency was increased to 84.0%. Even higher was the coating efficiency of the formulation using solely Myvacet® with 87.3%. The increase in the coating efficiency cannot be explained by the spreadability of Myvacet® as no difference exists between the contact angles. However, it has to be kept in mind that the interfacial tension γ_{SL} between the solid and the liquid is not considered as it is one of the parameters influencing the contact angle cos θ, as well as the roughness of the surfaces. In order to clarify this phenomenon the surface tension of all three liquids was determined.

PLASTICIZER	SURFACE TENSION
TEC	34.44 N/m ± 0.05 N/m
TEC/Myvacet® (70/30)	33.18 N/m ± 0.04 N/m
Myvacet®	32.66 N/m ± 0.05 N/m

Table 16: Surface tension of plasticizers, mean ± CI (95%)

Nevertheless, the highest surface tension of 34.44 N/m ± 0.05 N/m is determined for TEC followed by the mixture with 33.18 N/m ± 0.04 N/m. The lowest surface tension is obtained for Myvacet® being 32.66 N/m ± 0.05 N/m.

3.1.3 Determination of interparticle forces emerging during the application

Generally, interparticle forces influencing the dry coating process are an addition of several interparticle forces. First of all, capillary forces emerging from the plasticizer prior to its uptake into the polymer particles play a role. Capillary forces are the strongest interparticle forces acting over a range of 10^{-4} cm. Nevertheless, these forces are temporarily and will become negligible after penetration into the polymer. Once the plasticizer has been penetrated into the particle Van der Waals forces and electrostatic forces will ensure the adhesion and cohesion of the polymer. Van der Waals forces have a short acting range which is negligible at a distance of 10^{-5} cm. In contrast to electrostatic forces that may act up to a range of 10^{-1} cm. Furthermore, during coating mechanical interlocking between the particles occurs also being responsible for the cohesion of the particles.

In order to determine the strength of the forces responsible for the adhesion and cohesion between the particles atomic force microscopy was performed. However, with this method it is not possible to distinguish between the different interparticle forces. The purpose of the investigation was to analyze the influence of the used formulation additives on the interparticle forces with regard to the influence on the coating efficiency. It is expected that a high adhesion between the particles will lead to a high coating efficiency.

3.1.3.1 Influence of surface topography

Prior to the investigation of the interparticle forces the preparation of the substrate and the tip has to be considered due to its influence on the surface area getting in contact with. However, the particles used in this study have a rough surface with a certain curvature,

which is disadvantageous since the contact area between two surfaces influences strongly the interparticle force (see Figure 43).

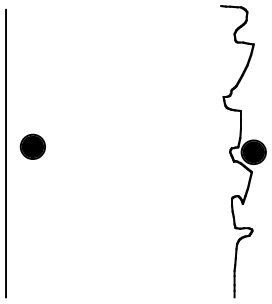

Figure 43: Scheme of the influence on the adhesion forces of surface roughness

If using rough surfaces the contact area will change whenever the position of the substrate is changed in contrast to even surfaces where each contact point will exhibit the same contact area. For the elimination of the surface roughness, the coating material was modified in order to smooth the surface. Comprimates of the particles were prepared and the surface topography was analyzed prior to the adhesive force measurement. Regarding the AFM surface scan (Figure 44 (A)) the comprimate's surface is still rough. Thus, the samples were subject to a second preparation step. The comprimates were cured for 24 h above their Tg ensuring coalescence of the compressed particles and obtaining smooth films. Alternatives for the preparation of smooth surfaces are described in literature [10, 88].

(A) uncured HPMCAS comprimate **(B) cured HPMCAS comprimate (film)**

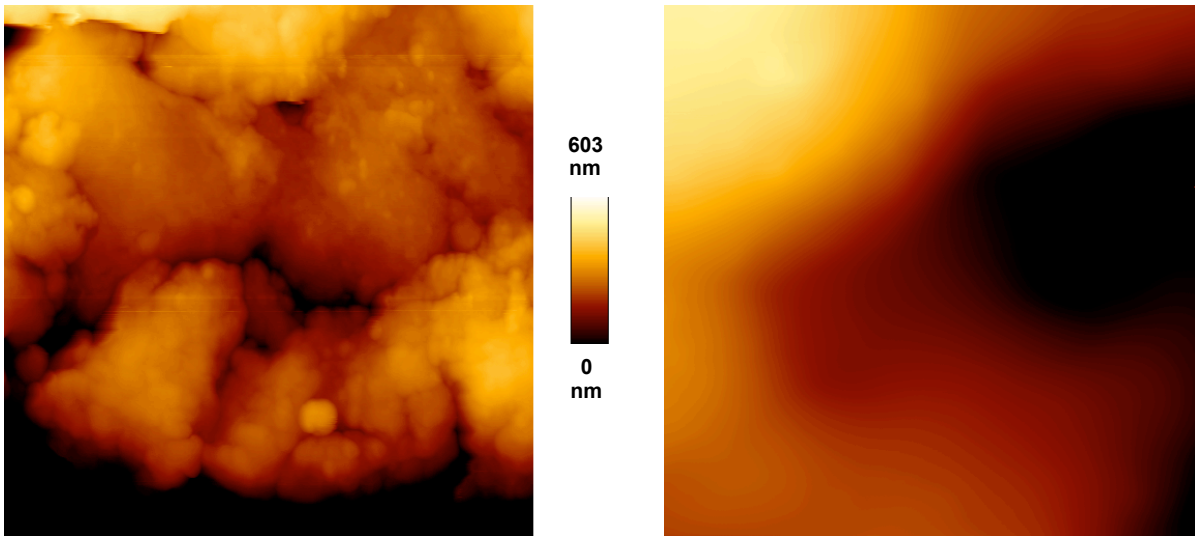

Figure 44: AFM Surface scans of uncured (A) and cured (B) HPMCAS comprimates, A= 5 x 5 µm

Regarding the surface topography scans obtained by AFM (Figure 44) the difference between the surfaces before and after the curing step is visible. The surface of the uncured comprimate (A) is rough with an extreme curvature. Single particles in the comprimate are still observable. Contrarily, the surface of the cured comprimate is smooth with less curvature. The remaining curvature is not constricting the measurement as in the area of the force measurements (1 x 1 µm) exhibit a certain planarity.

Additionally, the particles attached to the cantilever tips were modified. Usually, they get attached to the cantilever tip with glue accepting the risk that the adhesion force of the glue may be determined instead of the particle's, in case the particle is completely covered by the glue. Hence, in order to avoid this circumstance the particles were attached by heating them above the Tg ensuring sintering of the material at the tip and resulting in a strong attachment to. Furthermore, due to the applied heat the shape of the particle becomes droplet like and the particle surface becomes smoother also ensuring a defined contact area with the plane and smooth substrate's surface. A top view of a cantilever tip is shown in order to give an impression of the particle and its position at the tip.

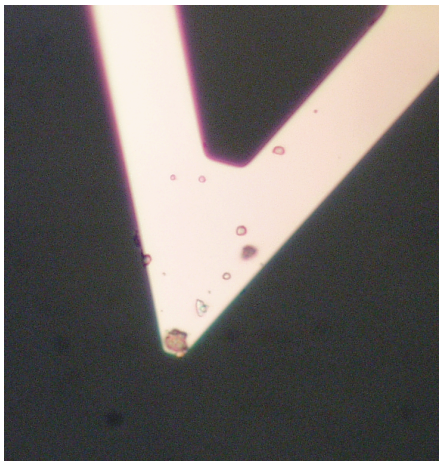

Figure 45: Top view of a cantilever tip after sintering

In literature cantilever tips illustrations are made by scanning electron microscopy [88] which may modify the polymers' surface. In order not change the surface quality photographs of the cantilevers were taken using a digital camera adjusted on a microscope using a magnification of 1:50.

The presumption that instead of the particle the cantilever itself respectively other particles attached behind on the tip are getting in contact has to be considered. However, since the cantilever is adjusted angular to the substrate this risk is minimized.

3.1.3.2 Influence of the liquid additives on the interparticle interactions

In order to determine the influence of plasticizers on the interparticle force, different substrates were prepared as described in section C 3.1.4. With respect to the formulations used in section C 1.3 it would have been reasonable to investigate the plasticized powders of the formulation D (75% (w/w) HPMCAS and 25% (w/w) TEC), formulation B/C (75% (w/w) HPMCAS and 25% (w/w) TEC/Myvacet®) and formulation E (75% (w/w) HPMCAS and 25% (w/w) Myvacet®). However, the plasticized powder of formulation D could not be used for AFM measurements due to the fact that this mixture is a liquid at room temperature. Therefore, the investigation was based on formulation B/C preparing the plasticized powders of this formulation and two plasticized powders containing solely one liquid, either TEC or Myvacet®, in the same ratio (see Table 17). The preparation of the powders is described in the following section. They were compressed, cured and stored above silica gel.

SAMPLE	HPMCAS	TEC	MYVACET®
a	100 parts	-	-
b	75 parts	17.5 parts	-
c	75 parts	17.5 parts	7.5 parts
d	75 parts	-	7.5 parts

Table 17: Formulations of plasticized powders and pure HMCAS

Single plasticized particles were not used as particle at the tip because sintering did not lead to a sufficient attachment of the material. Also, the particles were not stuck to the tip due to the risk to cover the particle completely with glue. The particle, sintered to the cantilever tip, consisted of HPMCAS and the comparison between the plasticizers was evaluated by varying merely the substrate. In order to keep the contact area constant, the same particle on the cantilever tip was used for measurements on every single substrate. However, due to the fact that this particle is getting in contact with different substrates a blank measurement was performed between the functional substrates in order to check whether an alteration of the particle might have taken place. The inert substrate used as blank measurement was MICA, a silicate, which is outstanding for its excellent smoothness on the molecular level [143].

In Figure 46 the adhesion forces of HPMCAS against HPMCAS and plasticized HPMCAS is displayed. The median of 8 measured squares of 1 x 1 µm, each consisting of 1024 single measurements is shown (CI = 95%). Before and after each measurement a blank measurement was performed. In comparison the values of the sample measurements the

blank values are 3 – 4 times higher. The high cohesion force of the blank measurements can be explained by the absolute smoothness of MICA. Due to this smoothness the contact area is maximized and the cohesion force is high.

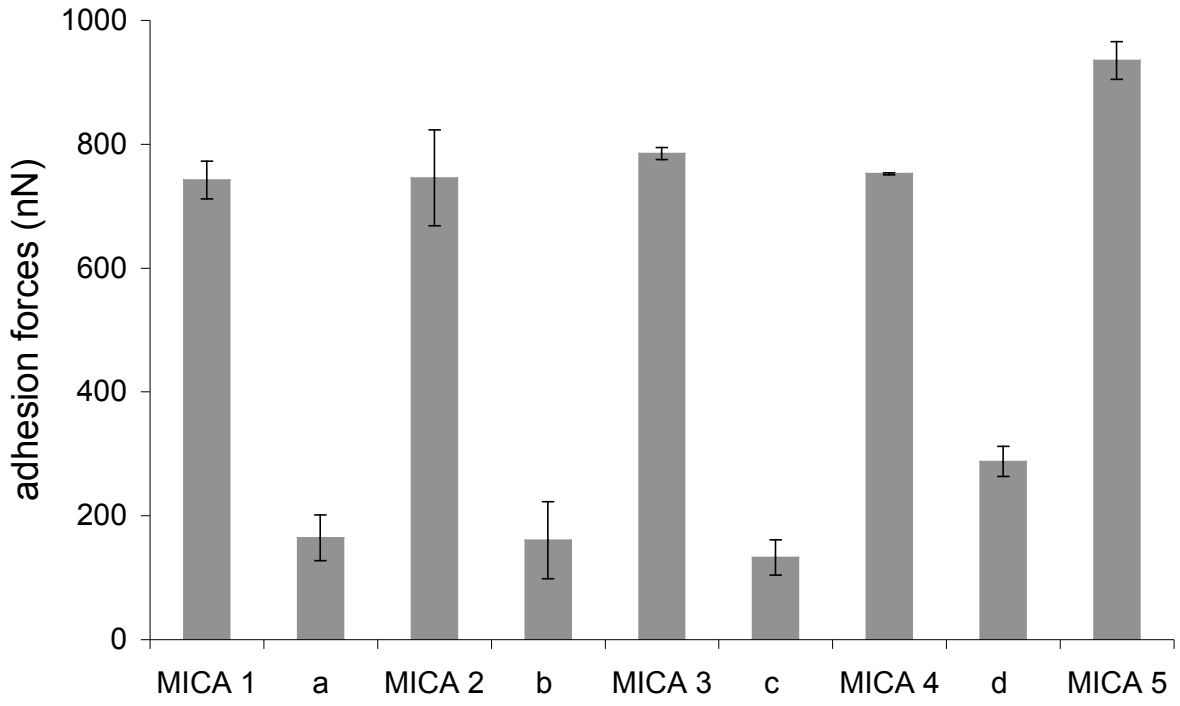

Figure 46: Measurements of HPMCAS at the tip against HPMCAS (a), HPMCAS and TEC (b). HPMCAS, TEC and Myvacet® (c) and HPMCAS, Myvacet® (d) as substrate controlled alternately with MICA measurements, n = 8 x 1024, mean ± CI (95%)

Regarding the interpretation of cohesion forces no significant differences can be observed between the samples consisting of pure HPMCAS, HPMCAS and TEC and, HPMCAS with the plasticizer blend of TEC and Myvacet®. In contrast, the last substrate, containing solely Myvacet® as liquid, show increased cohesion forces. Generally, it might be expected that the adhesion of HPMCAS on pure HPMCAS is lower compared to the cohesion between HPMCAS and plasticized HPMCAS. Indeed, the plasticizer lowers the polymers Tg and leads to an increase in stickiness at elevated temperatures during the process. However the stickiness of the polymers plasticized with different plasticizers is very similar at room temperature, well below the Tg. Remembering the investigation of the agglomeration tendency of pellets during storage (see C 2.3.1) it was demonstrated that all samples of pellets coated with different formulations did not tack to each other after storing at 25 °C and 10% RH. In contrast to the samples stored at 60% RH where water acts as volatile plasticizer leading to further plasticization and enhanced stickiness of the polymer even at

room temperature. As the samples were stored above silica gel prior to the AFM measurement conditions were adjusted which inhibit further plasticization giving an explanation why the adhesion forces of pure and plasticized HPMCAS are similar.

The adhesion forces between the substrate containing solely Myvacet® and HPMCAS on the cantilever is two third higher than the other determined forces. It can be assumed that Myvacet® has a high influence on the adhesion forces. Furthermore, it was observed that Myvacet® does not penetrate into the polymer and remains on its surface. The substrate was laid on blooding paper and dark spots were detected after a few minutes as though Myvacet® does not penetrate into the polymer and stays on the surface. Nevertheless, no increased adhesion force was determined for the sample containing HPMCAS, TEC and Myvacet® which indicates that the phenomenon of the increased adhesion force only appears when using Myvacet® without TEC. Further it can be presumed that TEC acts as a trigger for Myvacet® and transports it into the polymer particle.

Regarding the adhesion forces of the blank measurements with MICA, determined before and between the samples, no change of the adhesion force is determined. Accordingly, the particle at the cantilevers' tip does not undergo any alteration between the measurements. However, after performing the measurement of the substrate containing HPMCAS and Myvacet® the blank measurement with MICA is increased as well. After the particle has been in contact with the liquid Myvacet® a liquid film seems to stay on the surface on the particle resulting in higher cohesion forces of the blank measurement. Due to the liquid, capillary forces are exerted between the blank substrate MICA and the particle attached to the cantilever.

The intention of the AFM measurements was to find a relation between the interparticle forces and the coating efficiency. As a reminder the obtained coating efficiencies (see C 2) are shown in Table 18. Furthermore, it has to be remembered that instead of plasticized powders of formulation D and E containing each 25 parts TEC respectively Myvacet® and 75 parts HPMCAS, plasticized powders containing 17.5 parts TEC respectively 7.5 parts Myvacet® were investigated.

FORMULATION	B/C	D	E
Coating efficiency	84.0% ± 0.6%	72.5% ± 0.4%	87.3% ± 1.0%

Table 18: Coating efficiency of formulations B – D

It can be observed that the highest coating efficiency is obtained with formulation E containing HPMCAS and Myvacet®. In comparison, the highest cohesion forces were observed by using the plasticized powder consisting of HPMCAS and Myvacet®. This indicates that Myvacet® has the ability to exert capillary forces between HPMCAS particles and does not penetrate into the polymer. According to this hypothesis, the lower coating efficiency and cohesion force of formulation B/C are caused by the missing capillary forces since Myvacet® is incorporated in the polymer, triggered by TEC. The low coating efficiency of the formulation D consisting of HPMCAS and TEC cannot be explained by AFM measurements. The cohesion forces of the plasticized powder containing 17.5 parts TEC instead of 25 parts TEC in formulation D were equal with the forces of formulation B/C giving the expectation of a similar coating efficiency. Nevertheless, it has to be kept in mind that the experimental design differs form the dry coating process by using coalesced polymer films instead of loose powders due to the roughness of the surfaces (see C 3.1.3.1). The study explains why high coating efficiencies are achieved using solely Myvacet® as liquid and gives the presumption that using a liquid that stays on the surface and exerts capillary forces is advantageous. As Myvacet® seems to remain on the polymer surface, a worse compatibility with HPMCAS in comparison to TEC may be assumed. Although the coating efficiency of the mixture of TEC ad Myvacet® is higher in comparison to the coating efficiency using TEC alone an increased adhesion force was not observed by AFM. However, the time needed for the penetration of the mixture may be extended since TEC seems to trigger the penetration into the polymer leading to an extension of the effect of capillary forces. In order to elucidate this presumption plasticized powders were prepared and characterized with regard to the plasticizing effect of the liquids and the amount of free plasticizer responsible for the formation of capillary forces.

3.1.4 Preparation of plasticized powders for analyzing the application during the dry coating process using the GPCG 1.1

In the following section the production of plasticized powders is introduced as a new method for preparing isolated films like cast films obtained from aqueous dispersions. The glass transition temperature of the powders was determined and compared on the one hand with the Tg of cast films and on the other hand with the Tg of films obtained from dry coated pellets in order to ensure conformity. Additionally, the approved plasticized powders were used further for investigations of the interparticle forces in section C 3.1.3 and for the determination of the free amount of plasticizer in section 3.1.4.3.

3.1.4.1 Preparation of plasticized powders

In literature often studies were performed for characterization of coating processes and formulations using cast films. Usually, films are cast by spreading out a dispersion on a MFT bench and evaporating the dispersion media in order to remain a functional, isolated film [7]. Conducting the dry coating process, no isolated film can be produced with this technique due to the missing dispersion media [71]. Nevertheless, it is of certain interest to prepare isolated films in order to characterize the coating material of the dry coating process.

During this study different alternatives were developed in order to obtain isolated dry coated films. The simplest way by mixing the powder with the plasticizer using mortar and pestle was insufficient, detecting agglomerates with high amounts of plasticizer in contrast to areas without any plasticizer due to the small amount of liquid of only 25% (w/w) and the high amount of 75% (w/w) micronized polymer exhibiting a large volume. As an alternative inert large spheres, namely ping pong balls, were dry coated in the rotary fluid bed and the films were to peeled off. The advantage of this method is that exactly the same process with the same process conditions is used for the production of the isolated films. The Tg of the isolated films consisting of 75% (w/w) HPMCAS and 25% (w/w) plasticizer (sample 3 in Table 19) was determined to be 42.5 °C ± 0.6 °C. However, since the film consisting of 75% (w/w) HPMCAS and 25% (w/w) plasticizer - obtained from a cast organic solution of the coating components - exhibits a Tg of 51.7 °C ± 3.3 °C, it can be assumed that the dry coated isolated film differs in the ratio of polymer and plasticizer.

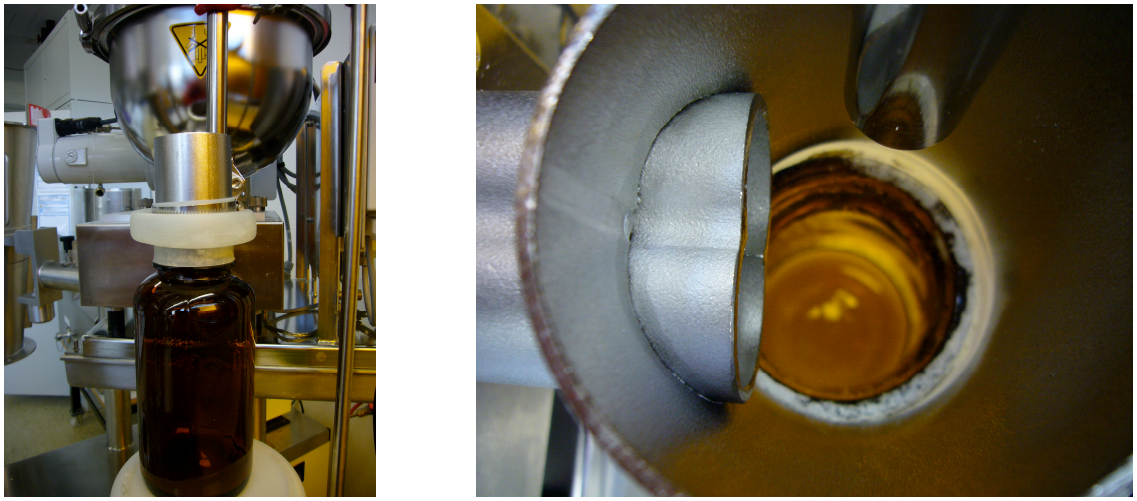

Figure 47: Preparation of plasticized powders front view and top view

The third method was also conducted using the fluid bed equipment. Mixtures of powder and plasticizer were prepared by mounting the spray nozzle together with the powder

feeder on a vial (Figure 47). An advantage of this method is that the plasticizer is sprayed under conditions similar to the process conditions. The powder and the plasticizer are fed in the same ratio as applied during the process and are collected in the vial. Afterwards the Tg was determined to be 57.0 °C ± 1.3 °C of the mixture consisting of 75% (w/w) HPMCAS and 25% (w/w) plasticizer demonstrating that the plasticized powder mixture is similar to the organic cast films.

Using this technology plasticized powders were prepared containing HPMCAS as polymer and TEC (sample 1, 2) as well as a mixture of TEC and Myvacet (sample 3) and Myvacet (sample 4,5) in different concentrations (Table 19). The same ratios as used for the formulation development are used.

SAMPLE	HPMCAS	TEC	MYVACET®
1	75 parts	25 parts	-
2	75 parts	17.5 parts	-
3	75 parts	17.5 parts	7.5 parts
4	75 parts	-	7.5 parts
5	75 parts	-	25 parts

Table 19: Formulations of plasticized powders prepared with the extern nozzle, feeder position above a vial

3.1.4.2 Characterization of plasticized powders focusing the Tg

The Tgs of the plasticized powders were investigated using TMA. In order to ensure that the distribution of the plasticizer is homogeneous all samples were heated twice and the second heating was used for the determination. However, preparing plasticized powders containing HPMCAS and TEC, domains consisting predominantly of HPMCAS with high amounts of TEC beside fine HPMCAS powder were detected. Therefore, prior to characterization the samples were heated above the Tg and afterwards levigated using mortar and pestle in order to obtain a homogeneous mixture. The sample 1 consisting of 25 parts TEC was not investigated as the mixture was liquid at room temperature. Therefore it could not be used for further studies.

Regarding the Tgs of the plasticized powders 2 and 3 (Table 20) it can be shown that the mixture containing 17.5 parts TEC reveals a Tg of 55.7 °C ± 2.7 °C being close to the Tg of 57.0 °C ± 1.3 °C obtained from plasticized powder 3 that consists of the same amount TEC and additionally 7.5 parts Myvacet®. Due to this similarity, it can be assumed that

TEC has the major role of plasticization in contrast to Myvacet® which apparently does have minor influence on the Tg. The plasticized powder 4 containing only Myvacet® has a high Tg of 93.4 °C ± 0.4 °C confirming the hypothesis that Myvacet® has a minor role in plasticization of the polymer. This is underlined by the fact that the Tg decreases marginally by increasing the amount of Myvacet® up to 25 parts (plasticized powder 5). The Tg is reduced to 88.5 °C ± 2.1 °C. Furthermore, the result explains the missing functionality of pellets dry coated with HPMCAS and Myvacet® (see section C 2.2.2). The formulation conforming to the plasticized powder 5 did not show enteric resistance. After 6 minutes in the acid stage almost 10% drug was released. In contrast, pellets coated with formulations containing TEC were enteric resistant according to the USP XXIX [142].

SAMPLE	Tg
1	-
2	55.7 °C ± 2.7 °C
3	57.0 °C ± 1.3 °C
4	93.4 °C ± 0.4 °C
5	88.5 °C ± 2.1 °C

Table 20: Glass transition temperatures of plasticized powders

In order to ensure that the lowering of the Tg by the plasticizer is related linearly to the amount of plasticizer, organic solutions of HPMCAS and the plasticizer mixture of 70% (w/w) TEC and 30% (w/w) Myvacet® were cast in different ratios shown in Table 21. The solutions were poured in PTFE Petri dishes and the solvent was evaporated. The cast films were peeled off prior to the determination of the Tg using TMA. The amount of plasticizer was increased in 10% steps starting form 0% up to 50%. Additionally, the Tgs of the mixtures containing 25% (w/w) plasticizer and 35% (w/w) plasticizer were determined.

HPMCAS (%)	PLASTICIZER MIXTURE (%)
100	0
90	10
80	20
75	25
70	30
65	35
60	40
50	50

Table 21: Mixtures of polymer and plasticizer used to cast organic films

Figure 48 shows the linear relation between the Tg and the amount of plasticizer. Regarding the results it can be observed, that by increasing the amount of plasticizer the film's Tg decreases. The Tg of the organic cast films with 75% (w/w) HPMCAS and 25% (w/w) plasticizer is 51.7 °C ± 3.7 °C being close to the Tg of the plasticized powder with the identical ratio having a Tg of 57.0 °C ± 1.3 °C. This similarity indicates that the ratio between polymer and plasticizer of the organic film is comparable to the plasticized powders of the same ratio. The Tg of the organic film with 70% (w/w) HPMCAS and 30% (w/w) plasticizer is lower with 46.7 °C ± 0.9 °C in contrast to the Tg of the film consisting of 80% (w/w) HPMCAS and 20% (w/w) plasticizer, which is significantly higher being 67.3 °C ± 0.5 °C.

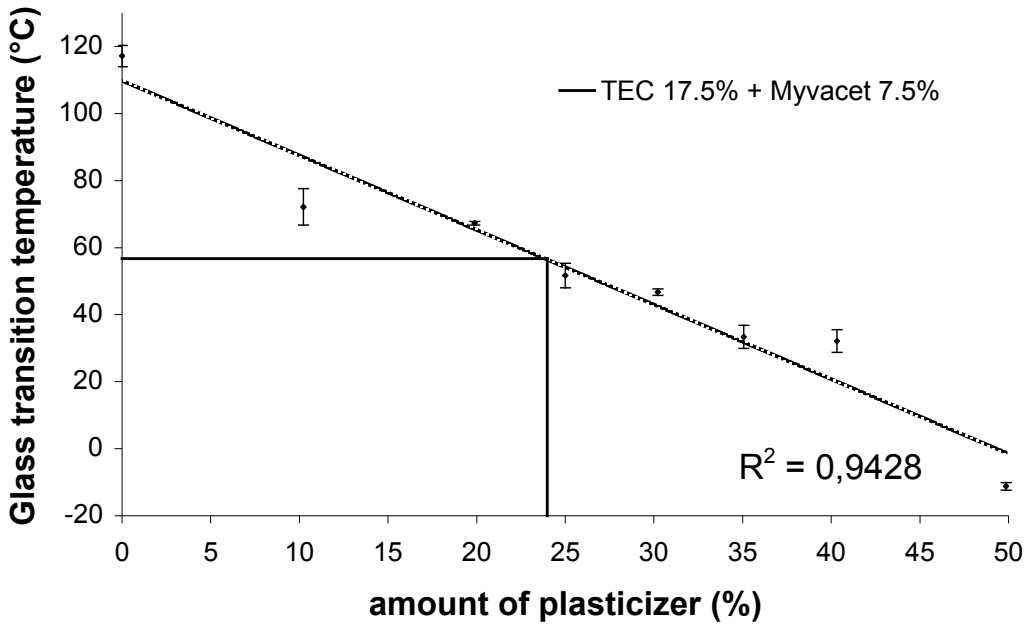

Figure 48: Tgs of plasticized powder containing a mixture of TEC (17.5%) and Myvacet® (7.5%) in relation to organic cast films of different compositions of HPMCAS and plasticizer (70% (w/w) TEC and 30% (w/w) Myvacet®), n = 3, mean ± CI (95%)

Generally, when observing the linear relation between the Tg and the amount of plasticizers, it will be verified if the materials follow the equation of Gordon and Taylor [56]. The equation enables (Eq. 23) to calculate exactly the ratio between the polymer and the plasticizer mixture after determining the Tg, respectively to predict the Tg of the chosen ratio between the polymer and the plasticizer.

$$T_g = \frac{w_1 T_{g1} + k w_2 T_{g2}}{w_1 + k w_2} \qquad \textbf{Eq. 23}$$

However, remembering the phenomenon that Myvacet® does not lower the Tg (Figure 48), the relation of Gordon & Taylor is not applicable since this relation is only valid when the components are miscible.

Nevertheless, the Tgs of organic cast films can be used to check the polymer/plasticizer ratio of films of dry coated pellets (see C 3.2.4). The Tg of dry coated films of formulation B/C was determined to be 49.8 °C ± 3.2 °C which is similar to organic cast films (51.7 °C ± 3.3 °C) and plasticizer powders (57.0 °C ± 1.3 °C). Additionally, the Tgs show that the loss of polymer is marginally during the process respectively that the loss of

plasticizer is equal to the loss of polymer. Considering the results it can be summarized that a linear relation between the amount of plasticizer and the Tg is given. Further, the preparation of plasticized powders can be used for the characterization of the dry coating process.

3.1.4.3 Determination of the free amount of plasticizer in the formulation

Considering the cohesion forces of the formulation containing only Myvacet® as liquid in comparison to the cohesion forces of all other formulations obtained by AFM (see C 3.1.3.2) it can be assumed that Myvacet® is not penetrating into the polymer. Additionally, in chapter C 2 a high coating efficiency (see C 2.1) was observed reflecting the strong adhesion forces (see C 3.1.3.2). In order to approve this phenomenon the amount of free plasticizer in the plasticized powders was investigated by differential scanning calorimetry. If plasticizers are miscible with a polymer, they will be incorporated between the polymer chains increasing their flexibility and mobility. With regard to the DSC this leads to the disappearance of the melting peak of the liquid and a lowering of the polymer's Tg.

The different plasticized powders containing TEC and Myvacet (sample 3 - 5, Table 17) were frozen down to –60 °C and kept at this temperature for 30 minutes ensuring a complete solidification of the materials. Afterwards the samples were heated up to 50 °C increasing the temperature 2 °C per minute. Regarding the different curves it can be shown that no melting peaks of the samples containing TEC and the mixture of TEC and Myvacet® are found (Figure 49). The sample containing Myvacet® and no TEC shows a freezing peak between 5 °C and -5 °C which is only slightly below the melting temperature interval of 4 °C – 12 °C indicated by the supplier [76] (Figure 50). This slight deviation between melting interval and freezing interval may be caused by supercooling of the liquid. Hence, free Myvacet® is detected in the plasticized powder and the hypothesis that Myvacet® does not penetrate into the polymer is confirmed. Furthermore, the hypothesis that Myvacet® builds up capillary forces between the polymer particles is supported and explains why the cohesion forces are increased in comparison to the other mixtures.

(a)

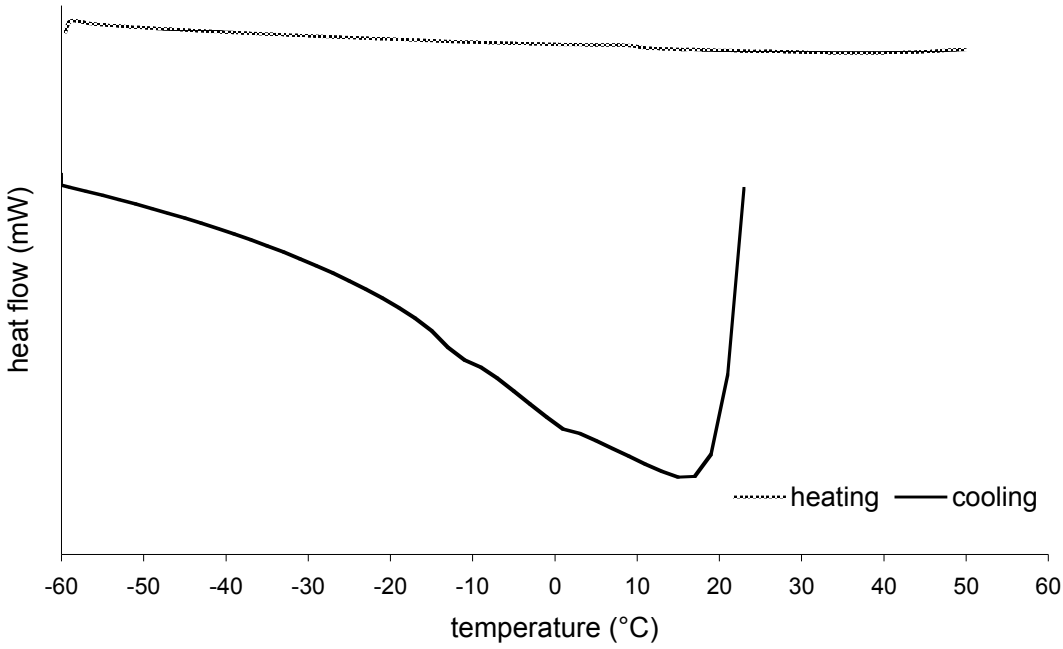

(b)

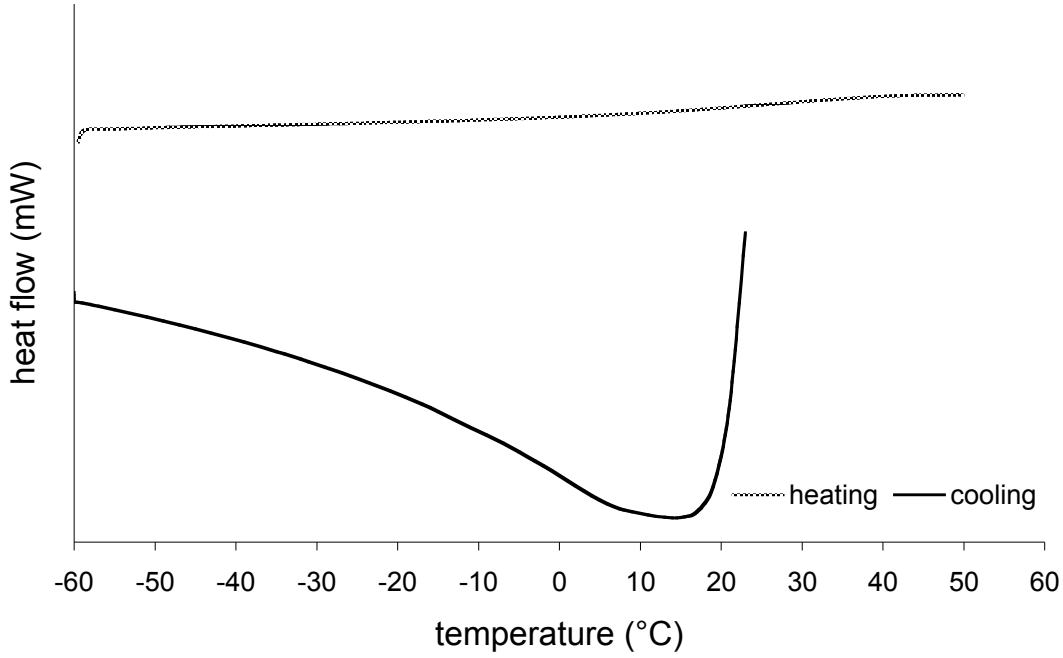

Figure 49: DSC curves of plasticized powder containing HPMCAS and TEC (a) and HPMCAS, TEC and Myvacet® (b)

(a)

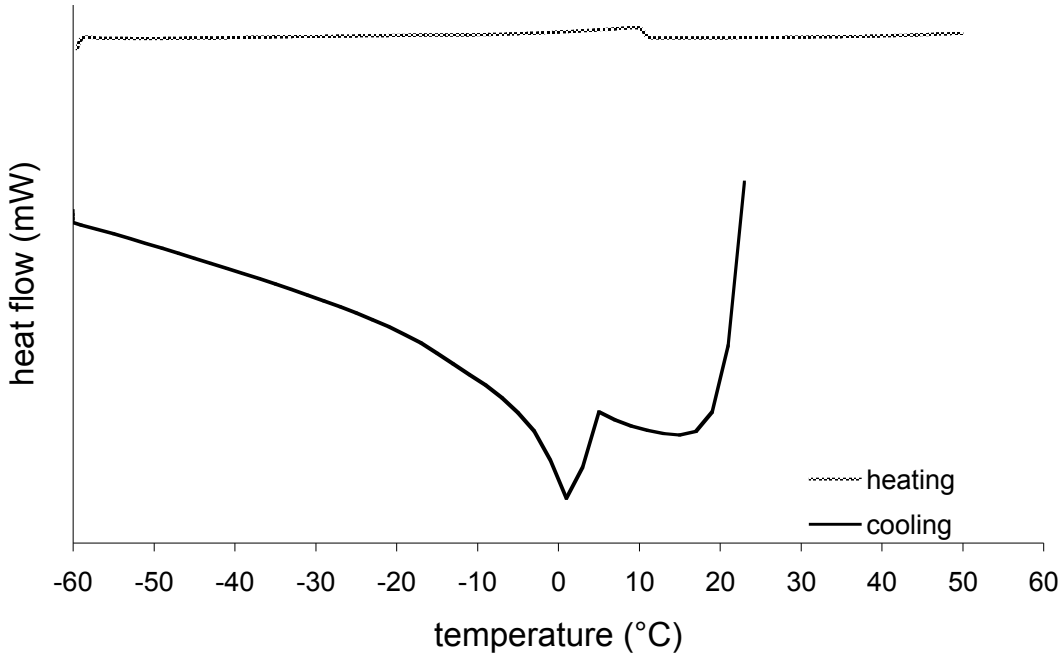

(b)

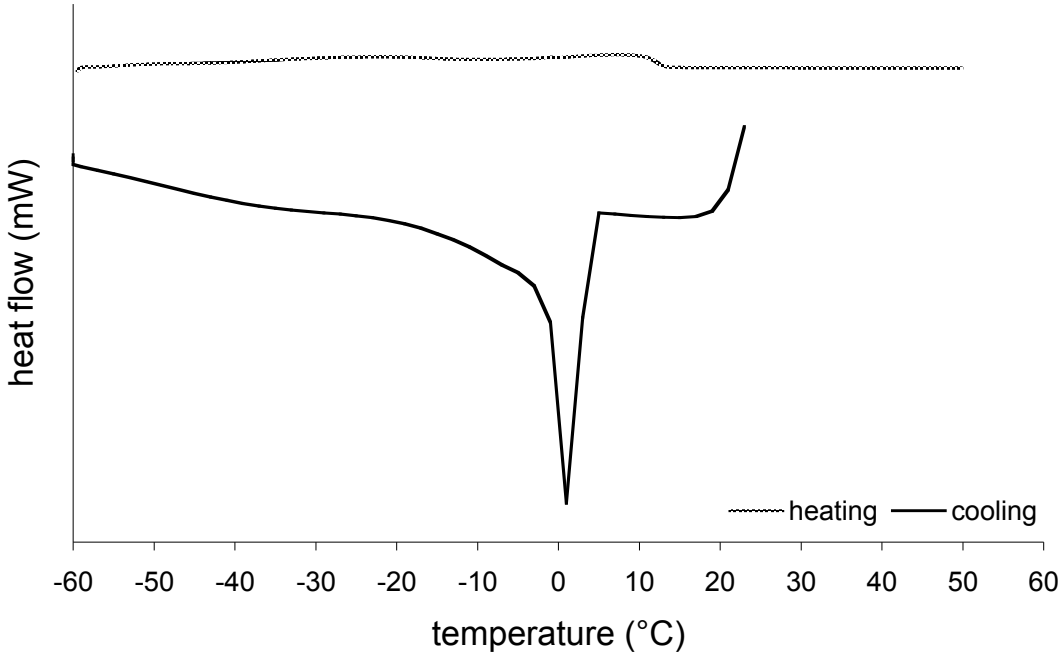

Figure 50: DSC curve of plasticized powder containing HPMCAS and Myvacet® (a) and pure Myvacet® (b)

Although free Myvacet® is observed by DSC, it has to be considered that Myvacet® could have been condensated in capillaries of the polymer particle instead of staying on the particle surface. Thus, the liquid would not be able to build up capillary forces between the particles. However, condensed liquids material melt at lower temperatures as the bulk

liquid [94] due to interactions with the capillary wall. If capillary condensation occurs a second peak of the condensed Myvacet® should have been observable. Having a closer look to the DSC curves this phenomenon can be excluded. No second peak is observable in the thermogram of the plasticized powder consisting of HPMCAS and Myvacet®. Additionally, the melting peak of the mixture was compared to the DSC curve of pure Myvacet® performed with the same settings (Figure 50). No second peak is observed demonstrating that Myvacet® in the plasticized powder is not condensated in capillaries.

However, free Myvacet® cannot be detected in the mixture with TEC supposing that TEC triggers the penetration of Myvacet® into the polymer (see Figure 49). Further, since the liquids are miscible, it can be assumed that the liquids acts as solvents for each other. In the case that Myvacet® is a solvent for TEC a freezing point depression of the liquid has to be observed. Therefore DSC measurements were performed with pure TEC and a mixture of TEC and Myvacet® and compared with the thermogram of Myvacet®. The thermogram shows the heating curves of Myvacet®, TEC and a mixture of both in the known ration (70% (w/w) / 30% (w/w)) (Figure 51). In contrast to the melting point of pure Myvacet® which is 7.5 °C ± 0.2 °C the melting point of Myvacet® in the mixture is lowered being –1.5 °C ± 0.1 °C. The shape of the curves is similar differing solely in the intensity, which indicates that no material alteration occurs. The heating curve of pure TEC does not show any melting peak.

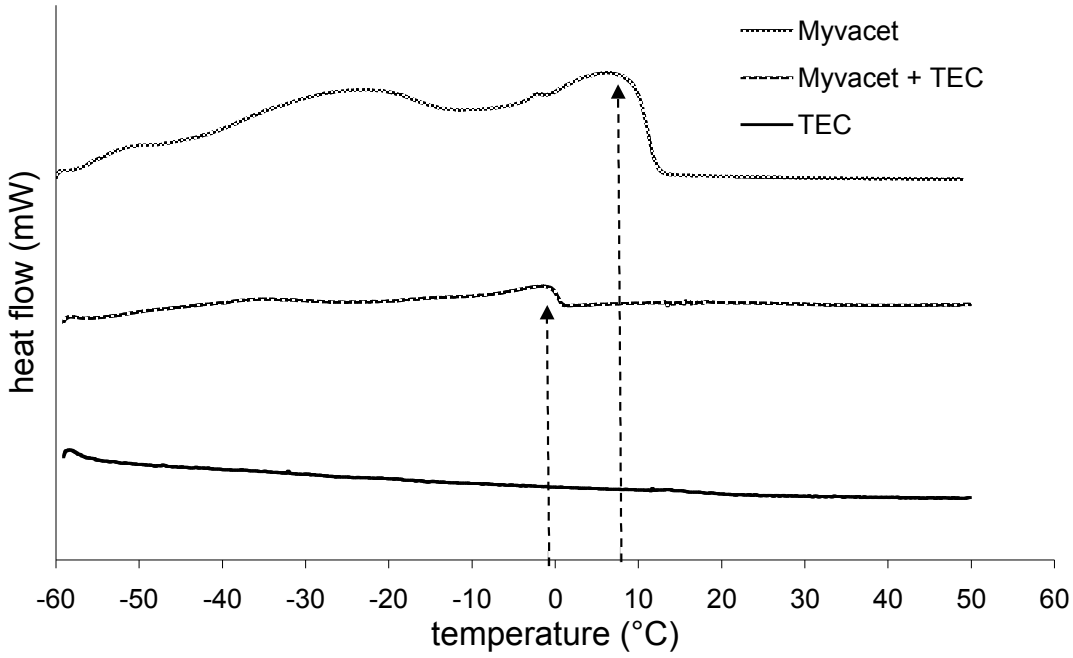

Figure 51: DSC heating curves of TEC and Myvacet® and the mixture of both containing 70% (w/w) TEC and 30% (w/w) Myvacet®

Remembering the Tg investigations of the plasticized powders (see C 3.1.4.2) the results of the free amount of plasticizer can be confirmed. Due to the increase of the mobility plasticizers lower the Tg of a polymer by penetrating and dissolving in the polymer. Investigating the Tg of plasticized powders containing solely Myvacet® as liquid the Tg was decreased to 93.4 °C ± 0.4 °C (7.5 parts (w/w) Myvacet®) respectively 88.5 °C ± 2.1 °C (25 parts (w/w) Myvacet®) indicating that Myvacet® does not dissolve in the polymer. The good compatibility and miscibility of TEC and Myvacet® is demonstrated as no melting peak is observable in the plasticized powder indicating that the mixture is dissolving into the polymer. Additionally, it is shown that Myvacet® acts as solvent for TEC as a freezing point depression is observed.

3.1.5 Summary

An efficient material application is crucial for the dry coating process with regard to the coating efficiency. The coating efficiency is highly influenced by the wetting of the powder and by interparticle forces achieving a higher coating efficiency when stronger interparticle forces between the materials exist. In order to determine the parameters needed to increase the interparticle forces and consequently the coating efficiency, the attractive forces between the coating materials were investigated.

The wettability of the polymer was measured by performing contact angle measurements. By adding Myvacet® to TEC the contact angle is reduced using HPMCAS comprimates as substrate. In contrast, the contact angles of the liquids on HPMCAS/talc comprimates do not show any difference. Additionally, the contact angles on HPMCAS/talc comprimates are two times higher than the contact angles of HPMCAS comprimates. A relation between the coating efficiencies of the formulation in section C 2.1 and the contact angle measurements is not found. Nevertheless, it has to be pointed out that the value of the contact angle is not related to the coating efficiency.

The measurements of the adhesion forces between polymer and plasticized polymer were performed using AFM. No significant differences are observed between the materials except for the sample consisting of HPMCAS and solely Myvacet® where the adhesion force was increased. It was presumed that Myvacet® does not penetrate into the polymer and exerts capillary forces between the particles resulting in a higher adhesion force. This hypothesis corresponds to the high coating efficiency of 87% (see C 2.1). By determining the free amount of plasticizer in the plasticized powders using DSC, the hypothesis is confirmed. The thermogram of the plasticized powder consisting of HPMCAS and Myvacet® shows a melting peak of Myvacet® indicating the presence of free plasticizer. The plasticized powder containing a mixture of TEC and Myvacet® does not show a melting peak indicating that TEC acts as a trigger for the penetration and dissolution of Myvacet®. Nevertheless, regarding the higher coating efficiency of the formulation containing TEC and Myvacet® (84%) in contrast to solely TEC (72%) it can be assumed that Myvacet® prolongates the penetration of the liquid into the polymer. The liquid remains longer on the surface leading to an extended effect of the capillary forces.

Resuming the results the need of a wetting agent is demonstrated. However, its spreadability is not the key parameter for the increase of the coating efficiency. Rather, the property to remain longer on the polymer surface compared to the plasticizer TEC is a prerequisite for a high coating efficiency.

3.2 Film formation

As the film formation of the dry coating process differs completely from conventional coating methods it is of certain interest to elucidate the film formation process and to define a parameter like the minimum film formation temperature (MFT) used for aqueous dispersion based processes in order to describe an efficient film formation. Film formation occurs mainly during the curing phase following the coating phase (see C 1.2). Therefore, the film formation was analyzed with regard to the two process parameters influencing film formation, namely curing temperature and time. After curing samples at different temperatures and time intervals the drug release was determined in 0.1 N HCl. Surface and cross-sectional morphologies of the pellets were examined by scanning electron microscopy and the glass transition temperature of the obtained films was determined by thermomechanical analysis.

3.2.1 Expectation of film formation process and study design

Generally, film formation of the plasticized polymer particles is expected to occur already at temperatures below the pure polymer's glass transition temperature. This is caused by the plasticizer reducing the polymer's Tg which results in elevated mobility and softness of the polymer molecules. Thus, the film formation temperature should be lower in comparison to the glass transition temperature of the pure polymer. In contrast to conventional coating processes, using aqueous polymer dispersions no water with plasticizing quality is in use. Though, due to the absence of water, no temporarily plasticizing effect exists. Nevertheless, it has to be considered, that the liquid plasticizer exert capillary forces as long as it is not taken up completely by the polymer powder. However, the capillary forces exerted by the plasticizer are assumed to be of minor importance in comparison to aqueous dispersion based processes. Especially during the curing phase, when the plasticizer is assumed to have penetrated completely into the polymer particles, the temporarily capillary forces disappear and film formation proceeds under different driving forces. Since the dry coating process is carried out without any solvent respectively dispersion media and no residue plasticizer is left, it can be assumed that film formation conforms to the dry sintering theory of polymers. Dillon et al. [36] introduced dry sintering theory where film formation occurs due to viscous flow and particle deformation. Caused by the visco-elastic behavior of polymers, applied stress induces a combined response of elastic deformation and viscous flow [40].

Considering the decreased viscosity and modulus of the polymer particle by the plasticizer the deformation and the resulting film formation is facilitated since a softer polymer is able to deform and flow easier than a harder one [75]. In order to induce the viscous flow and film formation the temperature needed is supposed to be close to the Tg of the polymer [145].

Keeping this hypothesis in mind and considering the process parameters of the curing phase (see C 3.1.1.2) and the achieved enteric resistance of the formulations (see C 2.2) it can be postulated that the applied product temperature of 55 °C is above the formulation's Tg (49.8 °C ± 3.2 °C) and apparently sufficient for functional film formation. In order to investigate the viability of this hypothesis, pellets were coated using formulation B/C containing HPMCAS and TEC/Myvacet®. As described above (see C 1.2) the polymer and the plasticizer were applied to the pellets simultaneously, except for the beginning of the coating phase when the plasticizer has been sprayed 30 seconds before powder feeding was started. As the film consisting of 75% (w/w) HPMCAS and 25% (w/w) plasticizer obtained from a cast organic solution of the coating components exhibits a Tg of 51.7 °C ± 3.3 °C, the influence of curing temperatures between 25 °C and 95 °C on enteric resistance was investigated. Additionally, the influence of curing time was studied.

3.2.2 Film formation during coating phase

During the coating phase of the dry coating process the product temperature was adjusted as low as possible (25 °C) in order to prevent premature film formation. At the beginning the plasticizer has been sprayed 30 seconds before the feeding of the dry polymer was started. This ensures the wetting of the pellets' surface facilitating the adhesion of the polymer to the surface of the substrate and the cohesion of the polymer particles with each other (see C 3.1). Regarding the scanning electron micrographs (SEM) (Figure 52 (A)) a continuous layering can be detected after ten minutes of applying the coating material.

(A) 10 min. coating

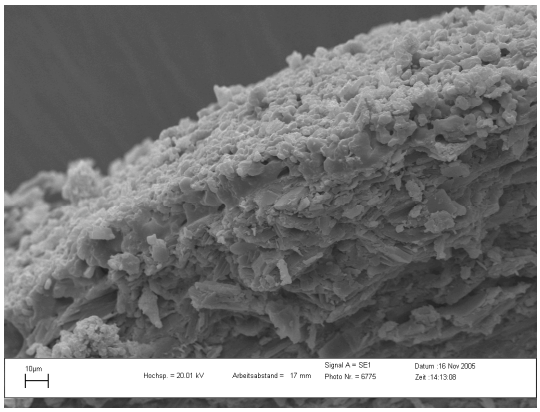

(B) 23 min. coating

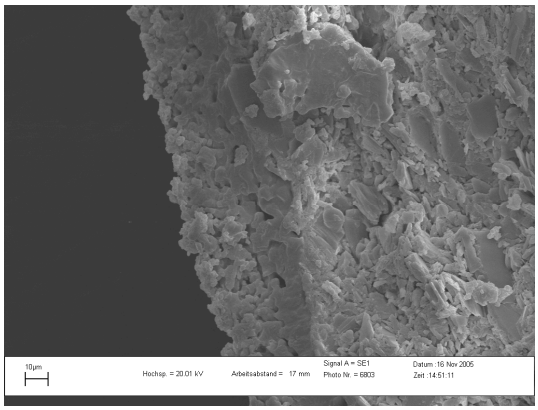

Figure 52: Scanning electron micrograph of dry coated pellets during the coating phase after 10 minutes and after 23 minutes

When the application is accomplished (Figure 52 (B)) the layer of the cohered particles is twice the thickness as after ten minutes. Furthermore, the material layer shows partial film formation of the inner layers. This might be caused by the higher plasticizer concentration on the substrate surface leading to an enhanced softening of the polymer particles of the inner layers with respect to the outer ones. Additionally, capillary forces emerging from the plasticizer, prior to its uptake into the polymer particles, play a role as well. Capillary forces are known as one driving force for film formation [141]. Once the plasticizer is penetrated into the polymer particles the capillary forces are negligible. Another reason may be simply a longer residence time of the inner layered polymer particles which results in enhanced film formation of the inner layers in comparison to the outer ones due to the known time dependency of film formation.

However, the film obtained after the coating step does not result in enteric resistance, which can be shown by the dissolution profile of uncured pellets (Figure 53) caused by poor film formation.

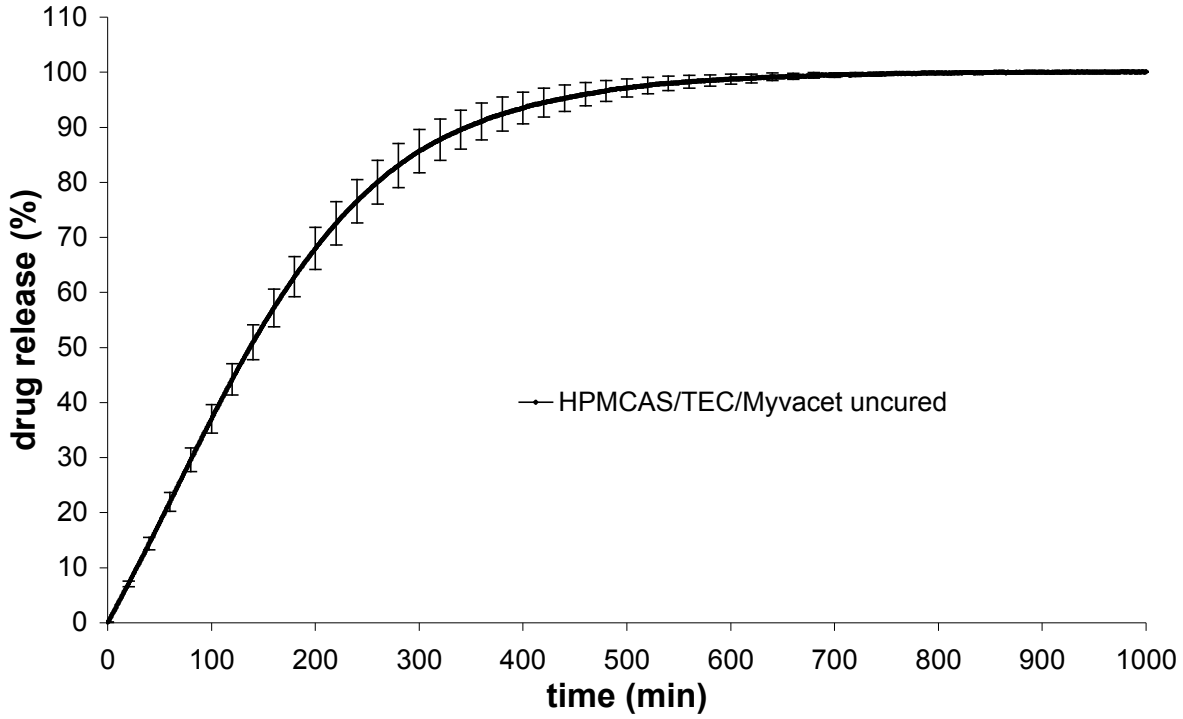

Figure 53: Drug release in 750 ml of 0.1 N-HCl (pH 1) from theophylline pellets coated with HPMCAS, TEC and Myvacet® before the curing step, n = 6, mean ± CI (95%)

The drug is released from uncured pellets steadily obeying a zero order kinetic due to insufficient film formation of the coating material and indicating the necessity of the curing step. After getting in contact with water the HPMCAS particles seem to swell but to retain pores which are able to release the drug from inside. In this context it has to be pointed out, that by using SEM it might not be possible to differentiate whether film formation is sufficient to achieve enteric resistance or whether it is not.

3.2.3 Determination of curing temperature and curing time

As described in literature [3, 17] and as shown above an additional curing phase is needed in order to achieve functional film formation. As mentioned before, the main parameters influencing the curing process are curing temperature and time. In order to determine the curing conditions, needed for film formation, the coated pellets were cured at different temperatures and time intervals. Therefore the pellets were coated in the rotary fluid bed and afterwards cured in an oven. One batch of pellets was coated and used for the investigation ensuring coating uniformity for all samples during curing. The influence of curing temperature on film formation is shown by comparing the drug release after 120

minutes in 750 ml of 0.1 N HCl (pH 1) of coated pellets cured at different temperatures (Figure 54).

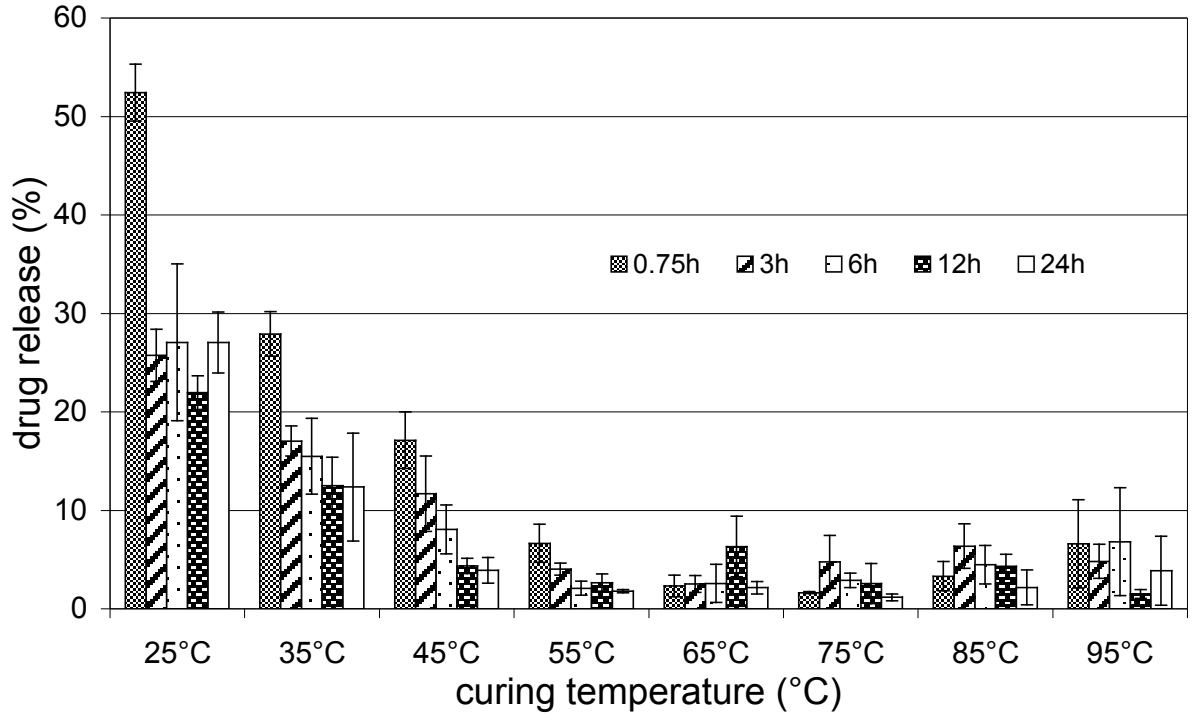

Figure 54: Drug release in 750 ml of 0.1 N HCl (pH 1) of theophylline pellets after curing at 25 °C, 35 °C, 45 °C, 55 °C, 65 °C and 75 °C for 0.75 h, 3 h, 6h, 12 h and 24 h, n = 4, mean ± CI (95%)

Prior to dissolution the coated pellets were cured 0.75 h at eight temperatures starting with 25 °C and increasing in ten degrees steps up to 95 °C. By an increase in curing temperature an enhancement of acid resistance can be observed. Consequently, the drug release of cured pellets is decreasing from 52.4% ± 2.9% at 25 °C to 1.6% ± 0.1% at 75 °C. Due to the stickiness of the film at higher curing temperatures, the film may have been damaged during sample preparation prior to dissolution leading to irregular drug releases between 65 °C and 95 °C curing temperature.

With respect to the requirements of enteric coated articles, according to USP XXIX [142], an enteric resistance can be observed after 0.75 h curing at 55 °C and above; this is in perfect accordance to the expectation that enteric resistance should be obtained by curing close to the Tg. The drug release at 55 °C curing temperature is 6.7% ± 1.9%. Considering the obtained results, film formation improved by increasing the curing temperature, which is also confirmed by scanning electron micrographs.

The micrographs reveal that the surface of pellets cured at lower temperatures is rough and that the film is porous (Figure 55 A-D). Film thickness of pellets cured at 25 °C seems to be similar to uncured pellets. Nevertheless, film formation is superior to uncured pellets according to the results obtained by dissolution studies. Once more it has to be pointed out that the determination of the quality of film formation is limited using SEM.

(A) 25 °C

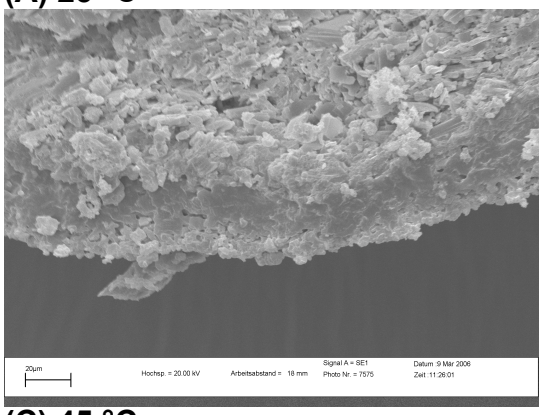

(B) 35 °C

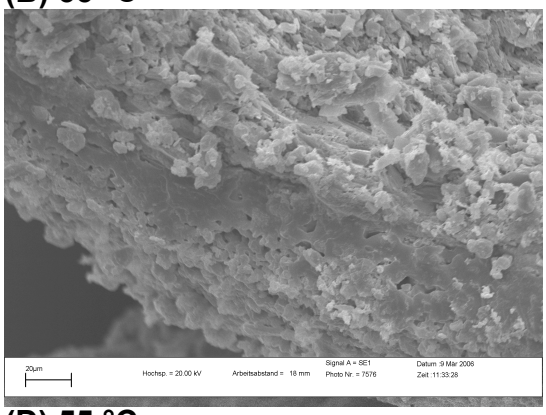

(C) 45 °C

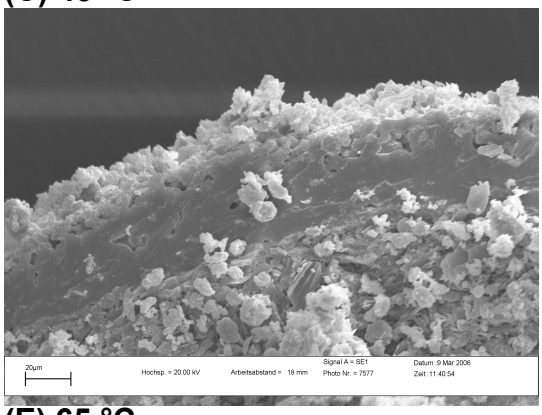

(D) 55 °C

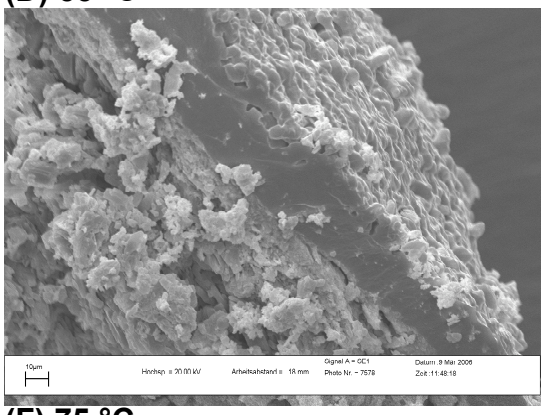

(E) 65 °C

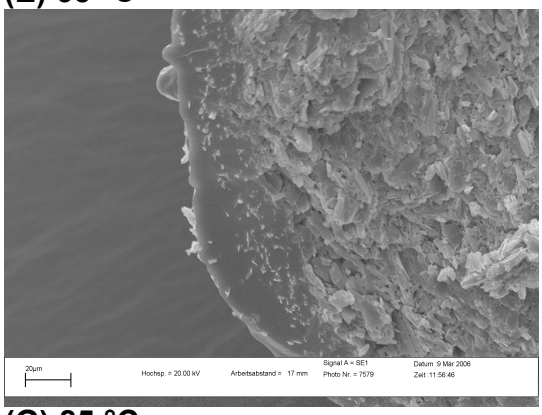

(F) 75 °C

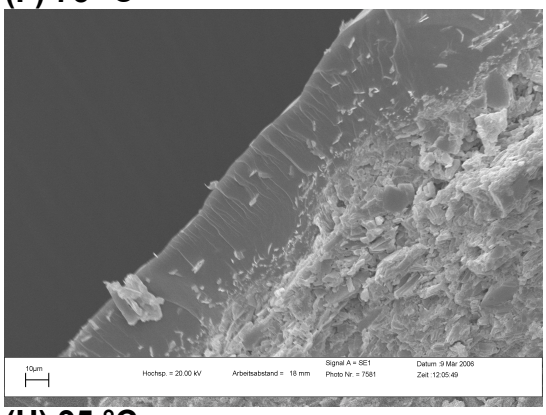

(G) 85 °C

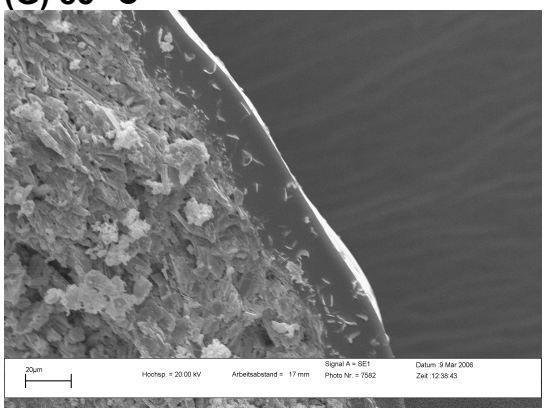

(H) 95 °C

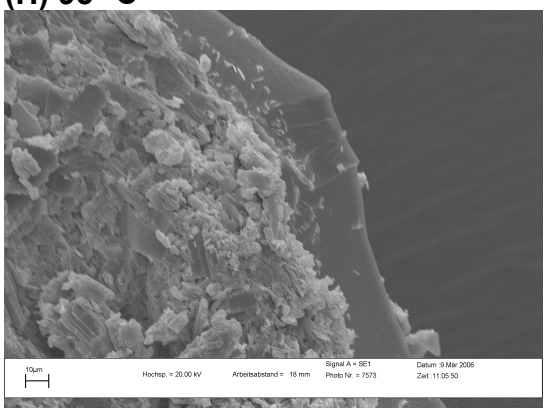

Figure 55: Scanning electron micrographs of dry coated pellets cured at different temperatures for 0.75 h

Furthermore, it can be observed, that film formation starts at the inner layers and continues to the outer ones (Figure 55 B-D). This might be caused by the higher plasticizer concentration on the substrate surface leading to an enhanced softening of the polymer particles of the inner layers with respect to the outer ones. Additionally, capillary forces emerging from the plasticizer prior to its uptake into the polymer particles play a role as well. Furthermore, film formation of the inner part may be caused by the higher residence time of the polymer particles of the inner layers in comparison to the outer ones. By curing at 35 °C, film formation proceeds detected by a decrease of drug release to 27.9% ± 2.2%. A curing temperature of 45 °C results in a decreased drug release of 17.1% ± 2.8%. However, functional film formation is not obtained at these temperatures. At 55 °C, the outer layers still show a porous structure and the surface of the pellets is still rough. However, film formation is already sufficiently good and film thickness already large enough to obtain enteric resistant pellets. At temperatures above 65 °C, film formation is observed in the outer particle layers and the surface becomes increasingly smoother (Figure 55 E-H).

After pointing out that the needed curing temperature to achieve sufficient film formation is close to the Tg and after pointing out its importance regarding the theory of film formation, the influence of the curing time on drug release in 0.1 N HCl was determined. In addition to 0.75 h curing time at the above named temperatures the pellets were cured for 3 h, 6 h, 12 h, and 24 h (Figure 54).

The drug release of pellets cured at 25 °C can be reduced from 52.4% ± 2.9% to 27.9% ± 2.2% by increasing the curing time from 0.75 h to 3 h. However, further prolongations of curing time do not show major changes of the drug release. Pellets cured at 35 °C also indicate a reduced drug release of 17.0% ± 1.5% after 3 h curing in comparison to 0.75 h. After 6 h, 12 h, and 24 h no significant changes are observed. In both cases no enteric resistance according to the USP XXIX [142] is obtained. This is in contrast to the pellets cured at 45 °C, where enteric resistance can be achieved after 12 h curing, determining a drug release of 4.4% ± 0.8%. The higher plasticizer concentration on the substrate may be sufficiently high resulting in film formation slightly below the Tg. At 55 °C curing temperature enteric resistance was obtained already after 0.75 h. Nevertheless the drug release was even more reduced after 3 h and 6 h. This is phenomenological for the film formation process because even above the Tg it takes a certain time for film formation to complete. Pellets cured at higher temperatures do not show major changes when increasing the curing time. Obviously, film formation at this temperature has been accomplished already within 0.75 h. The irregular higher drug releases of the samples cured at 65 °C for 12 h, at 75 °C for 3 h as well as at 85 °C and

95 °C may be due to damages of the film which are caused by sample preparation prior to dissolution.

Considering the results, the efficiency of film formation is increased by higher curing temperature and longer curing time. At 55 °C and above 0.75 h curing time leads to an enteric resistance. Nevertheless by increasing the curing time up to 12 h enteric resistance can be achieved even slightly below the Tg at 45 °C (Figure 54), which can be explained by looking at the material application again (see C 3.1). Conducting the dry coating process the film formation starts at the inner parts of the layering caused by the higher concentration of plasticizer on the pellets' surface that leads to a decrease of Tg. As a function of time, the plasticizer diffuses and migrates from the inner part of the film to the outer polymer layers, according to the plasticizer gradient equilibrating the ratio between polymer and plasticizer in the film and, consequently, enabling further film formation. This results in an increase of the film's thickness, finally leading to enteric resistance, in the case of pellets cured at 45 °C after 12 h curing time.

Looking at the SEM micrographs again, it can be shown that between 25 ° and 35 °C, the porous structure of the polymer coating still remains, although the curing time is increased (Figure 56 A-B) and insufficient film formation is obtained in contrast to the pellets cured at 45 °C and above, where the structure becomes more dense (Figure 56 C-E).

(A) 25 °C, 3 h

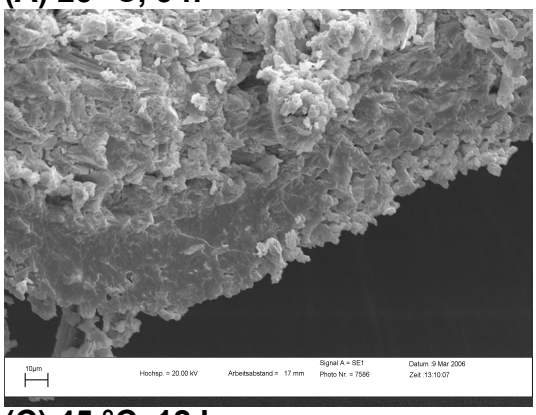

(B) 35 °C, 3 h

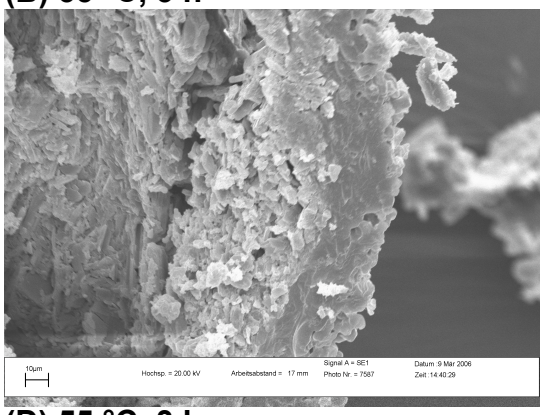

(C) 45 °C, 12 h

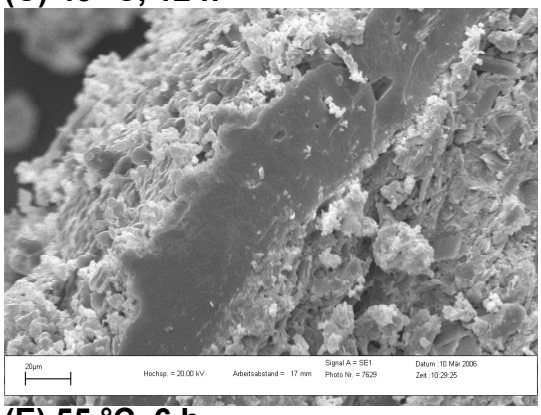

(D) 55 °C, 3 h

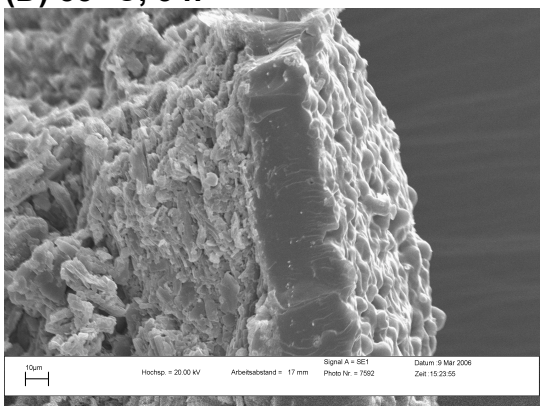

(E) 55 °C, 6 h

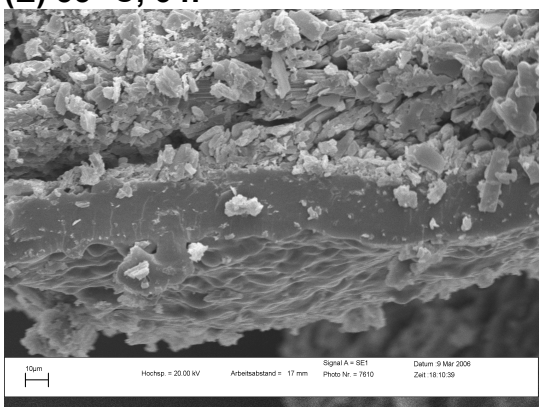

Figure 56: Scanning electron micrographs of dry coated pellets cured at different temperatures and times

Though, due to the dependency of film formation on both, curing temperature and time, it is impossible to define a single value of temperature when film formation occurs. Instead, the necessary conditions to obtain film formation consist always of a pair of curing temperature and time values (Table 22).

CURING TEMPERATURE (°C)	CURING TIME (h)
25 °C	- (> 24)
35 °C	- (> 24)
45 °C	> 12
55 °C	< 0.75
65 °C	< 0.75
75 °C	< 0.75
85 °C	< 0.75
95 °C	< 0.75

Table 22: Curing temperature and curing time conditions which lead to film formation and enteric resistance

3.2.4 Glass transition temperature

The Tg of the dry coated films was also determined using TMA in order to investigate whether it is similar to the one obtained from cast films using organic solutions. In contrast to aqueous dispersion based coatings, isolated films cannot be cast using a MFT bench because of the missing dispersion media. In order to determine the Tg of films produced by the dry coating process, the pellets cured at different temperatures were inserted in a specially designed sample holder (Figure 57). By this exceptional setup the penetration of the sensor into the polymer layer can be determined in situ, namely on the pellet's surface.

Figure 57: TMA sample holder designed to measure the film's glass transition temperature in situ

The temperature range at which the sensor penetrates into the polymer layer is around 38.5 °C after curing at temperatures between 25 °C and 55 °C varying between 37.6 °C ± 1.3 °C (55 °C) and 39.4 °C ± 4.7 °C (45 °C) (Table 23). The temperature of penetration obtained from pellets cured at 65 °C is 43.7 °C ± 1.0 °C; this is in between pellets cured at lower temperatures and pellets cured at 75 °C, 85 °C and 95 °C which exhibit temperatures in the range of 48.2 °C ± 1.8 °C and 50.9 °C ± 1.4 °C.

CURING TEMPERATURE (°C)	Tg (°C) 1. CURING PHASE	Tg (°C) 2. CURING PHASE
25	39.0 ± 3.2	52.9 ± 3.3
35	37.6 ± 1.4	55.7 ± 1.9
45	39.4 ± 4.7	51.5 ± 6.5
55	37.6 ± 1.4	46.1 ± 5.4
65	43.7 ± 1.1	49.3 ± 3.2
75	49.2 ± 2.0	47.4 ± 3.4
85	50.9 ± 1.6	47.9 ± 1.9
95	49.3 ± 3.2	47.9 ± 2.6

Table 23: Glass transition temperatures (Tg) after the first curing at different temperatures and after the second curing at 95 °C, n = 3, mean ± CI (95%)

Remembering the SEMs (Figure 55 A-D), a porous structure and only partly film formation especially of the outer layers was detected after curing at lower temperatures due to the described plasticizer gradient, which promotes the film formation from the inner layers to the outer ones. This may cause a premature penetration of the sensor at temperatures below the glass transition temperature as the porous structure may collapse due to the rising temperature. Consequently the obtained Tg may be too low and therefore may be incorrect. Pellets cured at higher temperatures show higher Tgs meeting the expectations with regard to the SEMs where enhanced film formation and no porous structures are observed.

In order to measure the Tg of the films cured at lower temperatures correctly, the Tg of all films was redetermined after a second curing phase at 95 °C, 1 h expecting complete coalescence. All samples show Tgs between 47.4 °C ± 3.0 °C (75 °C curing temperature) and 55.7 °C ± 1.7 °C (35 °C curing temperature) (Table 23) indicating complete coalescence of the film. A similarity to the Tgs obtained from the pellets cured at 75 °C and above after the first curing phase is obvious. However, as TMA measurements are dependent on the film integrity and homogeneity and as still doubts about integrity and homogeneity of dry coated films might exist, organic solutions of polymer and plasticizer were cast and investigated by TMA. In comparison films consisting of 75% (w/w) HPMCAS and 25% (w/w) plasticizer obtained from a cast organic solution of the coating components exhibits a Tg of 51.7 °C ± 3.3 °C, that confirms exactly the determined Tgs after the second curing.

Considering these results the glass transition temperature corresponds quite well with the temperature range of 45 °C to 55 °C in which satisfied film formation and enteric resistance of the pellets was obtained. Thus, it can be assumed that in contrast to conventional coating processes using aqueous polymer dispersions, a temporarily plasticizing effect does not exist confirming the hypothesis that the film's Tg must be close to the film formation temperature. Summarizing the results, the glass transition temperature of the plasticized polymer has to be considered as a key parameter for the adjusted curing temperature of the dry coating process.

3.2.5 Summary

The key parameter of the film formation of the dry coating process has been found to be the glass transition temperature of the film. This is in contrast to conventional coating processes, where the minimum film formation temperature is the key parameter which is below the film's Tg. Enteric resistance using formulation B/C (HPMCAS (75% (w/w)) and

Myvacet®/TEC (25% (w/w)) is obtained after curing at 55 °C for 0.75 h. Although, film formation is possible below the Tg, when applying highly extended curing times. Curing at 45 °C has to be performed for at least 12 h in order to achieve enteric resistance. Film formation slightly below the Tg is possible because of a plasticizer gradient along the coat. The gradient is caused by spraying the plasticizer 30 seconds before starting powder feeding during the coating phase. This results in a higher plasticizer concentration of the inner layers of the coat relatively to the outer ones. Therefore film formation of the inner layers is possible even slightly below the Tg. As the plasticizer diffuses to the outer layers during curing according to the plasticizer gradient, film formation proceeds in a certain time.

4 Process optimization

The aims of process optimization were the investigation and optimization of key process parameters influencing the process efficiency and enteric resistance. Therefore a design of experiments was created investigating five independent process parameters. The results were evaluated using the software Modde® 7 by multilinear regression.

4.1 Statistical design

A 2^{5-1} fractional factorial design with two additional repetitions on the zero level was used to evaluate the influence of the factors coating temperature (°C), curing temperature (°C), feeding/spraying rate (g/min), air flow (m^3/h) and rotor speed (rpm). The levels of the DOE and the abbreviations of the variables are listed in Table 24.

FACTORS	ABBREVIATION	LEVEL		
		-1	0	+1
Coating temperature (°C)	Temp 1	30	40	50
Curing temperature (°C)	Temp 2	45	55	65
Feeding/spraying rate (g/min)	Coat	5.6/1.75	11.1/3.5	16.7/5.25
Air flow (m^3/h)	Air	50/100	70/120	90/140
Rotor speed (rpm)	Rot	190	230	270

Table 24: Factors and levels of the design of experiments (DOE)

The setting took place according to a CCF design (central composite face design) which enables the determination of main effects and interactions. Quadratic effects locate a minimum or maximum of main effects in the experimental domain. Regarding the feeding/spraying rate it has to be explained that the given ratio of 70% (w/w) HPMCAS and 30% (w/w) plasticizer blend consisting of TEC and Myvacet® was not changed. Additionally, it has to be mentioned that the air flow rate settings between the coating and the curing phase were fixed pairs. For example, carrying out the process at the lower level (50/100 m^3/h), 50 m^3/h was adjusted for the coating phase respectively 100 m^3/h for the curing phase. The responses are the coating efficiency (CE) (%) and the drug release (DR) (%) after 120 minutes in the acid stage.

The quality of the model can be characterized by four parameters (Table 25). The coefficient of determination (R^2) gives information about whether the model fits with the collected data. A high R^2 stands for a well fitted model. However, R^2 is susceptible since each variable (= process run) added to the model increases the value of R^2. Thus, in this study $R^2_{adj.}$ was used to evaluate the model which is adjusted for the degree of freedom and does not increase automatically by adding variables. Q^2 is a measure of prediction about whether new results can be predicted by the findings of the DOE. Q^2 is calculated by cross validation of the given results. The model validity known as 'lack of fit' determines whether the model error is in the same range as the pure error. As 'lack of fit' the probability value (p-value) is used which has to be higher than the probability of error (α = 0.05). Additionally, the reproducibility is characterized by the variations coefficient (VC) of the results at the center point which was performed in triplicate.

	R^2_{adj}	Q^2	p	VC
Coating efficiency (CE)	0.856	0.529	0.069	0.988
Drug release (DR)	0.76	0.632	0.328	0.897

Table 25: Parameters describing the quality of the model

Regarding the parameters it is summarized that the model is of sufficient quality for both responses as the $R^2_{adj.}$ has an acceptable value and the Q^2 values are above 0.5 [42]. Considering the variation coefficient (VC), calculated by the variance of the center point, a high reproducibility of the process can be assumed. Thus, the DOE was used to characterize the dry coating process and to optimize the process settings.

The presented values in Table 25 were determined after having performed a backwards regression for each response separately. Therefore terms were removed stepwise from the model if their p-values are higher than the probability of error (α = 0.05) starting with the highest value. When significant interactions of insignificant main effects were observed, the main factor was not removed whatever p-value it has.

For the coating efficiency (CE) the model could be simplified and is described in equation:

$$CE = Y = \beta_0 + \beta_1 Temp1 + \beta_2 Temp2 + \beta_3 Coat + \beta_4 Air + \beta_5 Rot + \beta_6 Temp2^2 + \beta_7 Air^2 + \beta_8 Temp1 \bullet Temp2 + \beta_9 Temp1 \bullet Coat + \beta_{10} Temp1 \bullet Air + \beta_{11} Temp1 \bullet Rot + \beta_{12} Temp2 \bullet Coat + \beta_{13} Temp2 \bullet Air + \beta_{14} Temp2 \bullet Rot,$$

With respect to the drug release (DR) the following equation is valid:

$$DR = Y = \beta_0 + \beta_1 Temp1 + \beta_2 Temp2 + \beta_3 Coat + \beta_4 Air + \beta_5 Rot + \beta_6 Temp2^2 + \beta_7 Temp1 \bullet Coat + \beta_8 Temp2 \bullet Air$$

where $\beta_1 \ldots \beta_n$ are the regression coefficients and β_0 is constant. Both equations demonstrate that besides the main effects several interactions and quadratic effects are influencing the responses. A detailed characterization of the models is performed in section 4.1.1 and 4.1.2.

4.1.1 Coating efficiency

As mentioned in section 2.1, it is of certain interest to minimize the loss of coating material and, consequently, to increase the coating efficiency (CE). It was shown that a good spreading of the plasticizer on the solid material seemed to enhance the amount of attached material (see C 3.1.2). However, the influence of the process parameters was not investigated.

Regarding the coefficient plot (Figure 58) it is shown that several main effects and also quadratic effects influence the coating efficiency. For the interpretation the significant main effects, namely coating temperature, curing temperature, feeding/spraying rate and rotor speed, will be analyzed with regard to the interactions of the effects. Additionally the quadratic effects of the curing temperature and the air flow will be described.

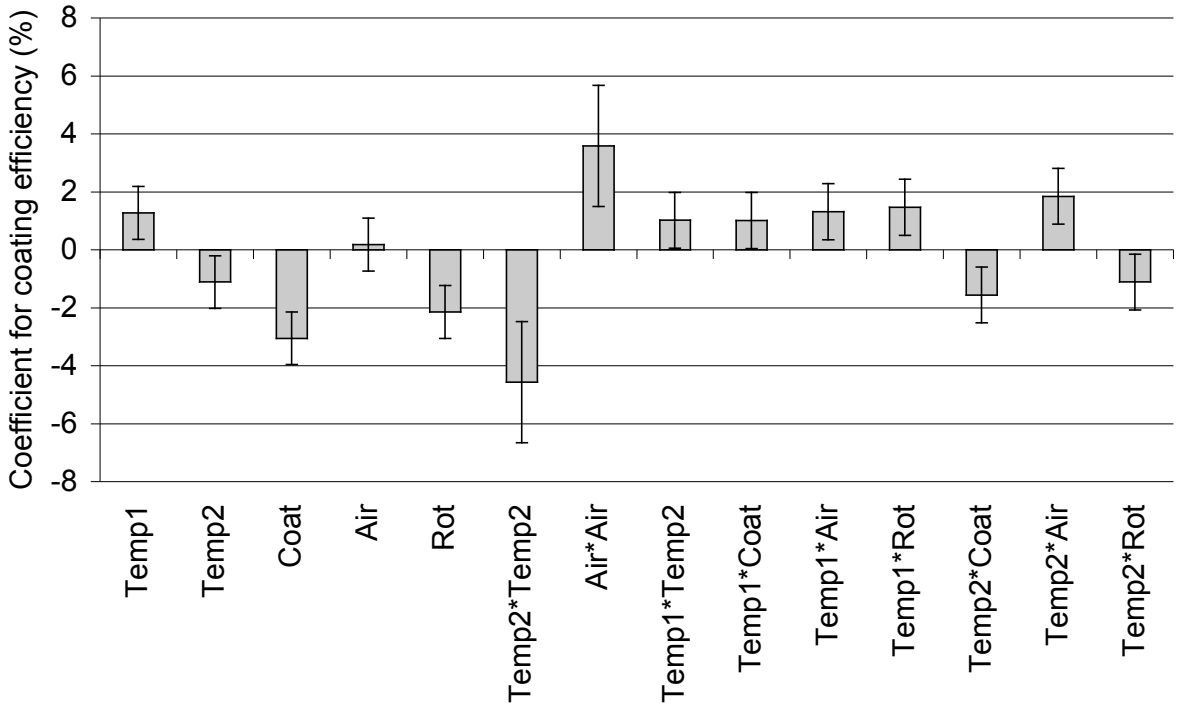

Figure 58: Bar plot of the coefficients for the coating efficiency (CE)

The bar plot reveals that an increased coating temperature increases the coating efficiency. This may be explained by the facilitation of the particle attachment, which is caused by the stickier surface at elevated temperatures closer to the Tg. The feeding and spraying rate of the coating material stands in a reciprocal relation to the coating efficiency achieving a higher coating efficiency when using a low rate during the coating phase. By a longer coating period and a slower application of the material the probability of particles' cohesion and adhesion on the pellet is enhanced. Beside, more time is given to increase the surface stickiness of the particles due to the plasticizer penetration, promoting the attachment of polymer particles (see C 3.2.2). Further it enables the layering of particles, which get detached from the filter and fall down due to filter rocking and pressurization. Additionally, it is observed that a decrease of the rotor speed results in an increase of the coating efficiency. The reduced speed decreases the number of contacts of the pellets with the equipment, which minimizes the abrasion of coating material. Furthermore, the bed movement is slower leading to less friction between the pellets and, consequently, less abrasion.

The effects of the curing temperature and air flow rate have to be considered with regard to the quadratic effect indicating the optimum. Since they are the strongest effects, demonstrated by the high bar plots, and since they interact with each other, they will be described first.

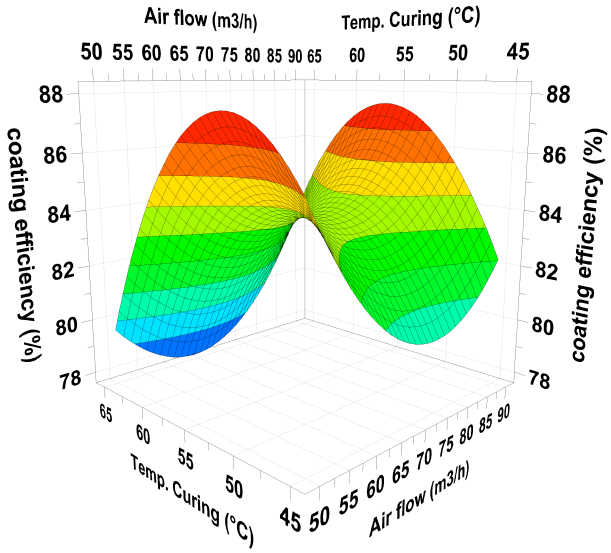

Figure 59: Surface plot of air flow rate and curing temperature, $R^2_{adj.}$ = 0.856

The surface plot shows that the maximum of the curing temperature is located at the center point at 55 °C which is close to the Tg (see C 3.2.4) of the formulation. Below 55 °C curing temperature the coating efficiency is decreased due to the possible abrasion respectively detachment of the polymer particles. At lower curing temperatures the stickiness of the polymer particles is less pronounced and facilitates the detachment of the particles, additionally supported by the increased air flow, which is generally increased during curing in comparison to the coating phase. At curing temperatures of 65 °C the Tg is overstepped and the polymer is in the rubbery state. Consequently, the extreme sticky surface of the film may be rubbed off in the rotor fluid bed. In comparison, by curing at 55 °C the Tg of the film is overstepped as well (see C 3.2.3) and film formation is observed, however, according to the SEMs (3.2.3) the surface of the coated pellets is still corrugated resulting in less stickiness and leading to less abrasion compared to the higher cured samples.

The effect of the air flow on the CE shows a minimum at the center point for which no explanation is found (Figure 59). As mentioned above, during the dry coating process the air flow has different values. During the coating phase the air flow rate is adjusted at a low level, in order to achieve sufficient adhesion of the coating material, and during the curing phase at a higher level, preventing pellet agglomeration due to the stickier polymer at elevated temperatures. This readjustment may cause that the effect of the parameter is blurred and therefore not be interpreted. Unfortunately, by developing the DOE the air flow rate was set up as a single factor in order to keep the number of factors reasonably small. Generally, it was expected that a low air flow rate would increase the coating efficiency because of an enhanced adhesion and cohesion of the coating material. If the factor “air”

was split like the process temperature in two factors, it might have been possible to explain the influence of the air flow. In order to confirm this presumption and clarify the blurred effect, a further DOE has to be performed where the air flow is split in two factors. Hence, due to the gained information, the interaction of the air flow and the coating temperature is not discussed any further.

The following response surface plots show the interactions of factors and describe them regarding both process phases, the coating and the curing phase. Therefore, the interactions of the feeding/spraying rate and the coating respectively curing temperature are depicted in two surface plots. The same was performed with the rotor speed and the process temperatures.

The surface plots of the feeding/spraying rate and the process temperatures are shown in Figure 60. Surface plot (a) depicts the influence of the feeding/spraying rate and the coating temperature on the coating efficiency. As already mentioned above, by feeding/spraying the coating material slowly into the fluid bed an increase in the coating efficiency can be achieved. Due to the longer application time the liquid plasticizer has more time to soften the polymer particle which will facilitate the attachment of further particles. Increasing the coating temperature can enhance this effect, however, the effect is more pronounced at higher feeding/spraying rates in comparison to lower ones. By increasing the temperature an increase of the particles' stickiness is achieved enhancing material layering and partly compensating the effect of the higher feeding/spraying rates.

The surface plot (b) shows the interaction of the feeding/spraying rate and curing temperature. Although these two factors are used in the two different phases of the process an interaction can be observed. As mentioned above a low feeding/spraying rate increases the coating efficiency. At low curing temperatures the effect of an increase of the feeding/spraying rate plays a minor role reducing slightly the coating efficiency. As the temperature is below the polymers' Tg the particles, which are attached to the equipment or rather filter, will get detached by filter rocking and pressurization and fall down on the pellets. Thus, the material can cohere with the coating material on the pellets leading to an increase of the coating efficiency. In contrast, at curing temperatures above the Tg, the coating efficiency is decreased extremely caused by the coalescence of the material attached to the filter and equipment.

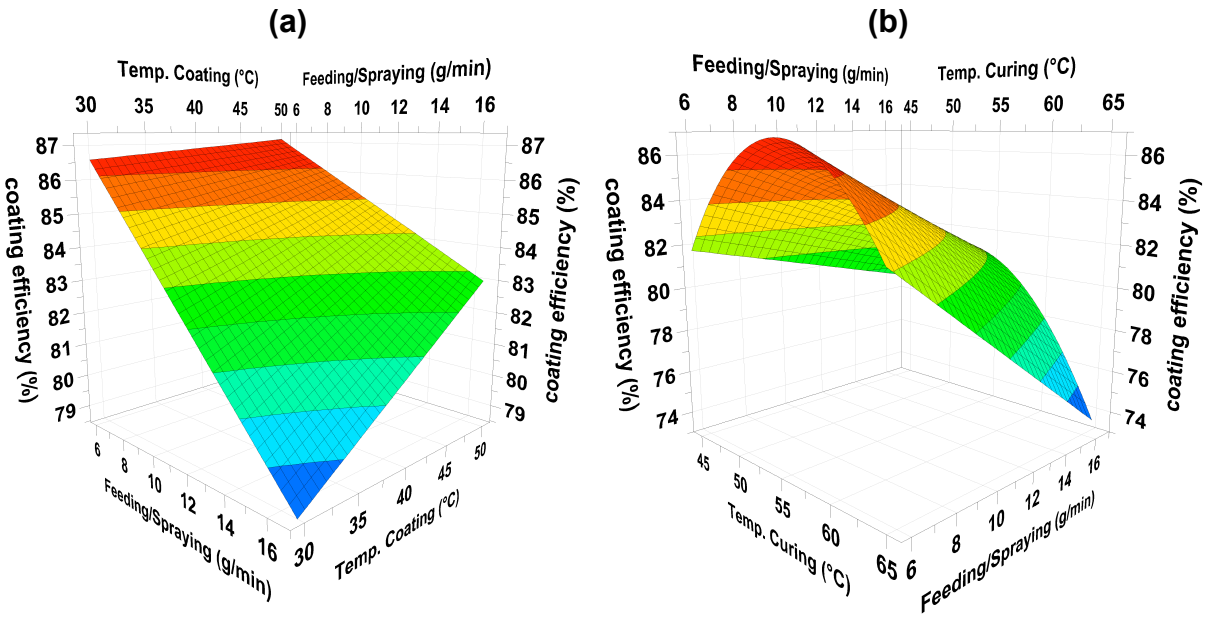

Figure 60: Surface plots of coating temperature and feeding/spraying rate (a) and curing temperature and feeding/spraying rate (b), $R^2_{adj.}$ = 0.856

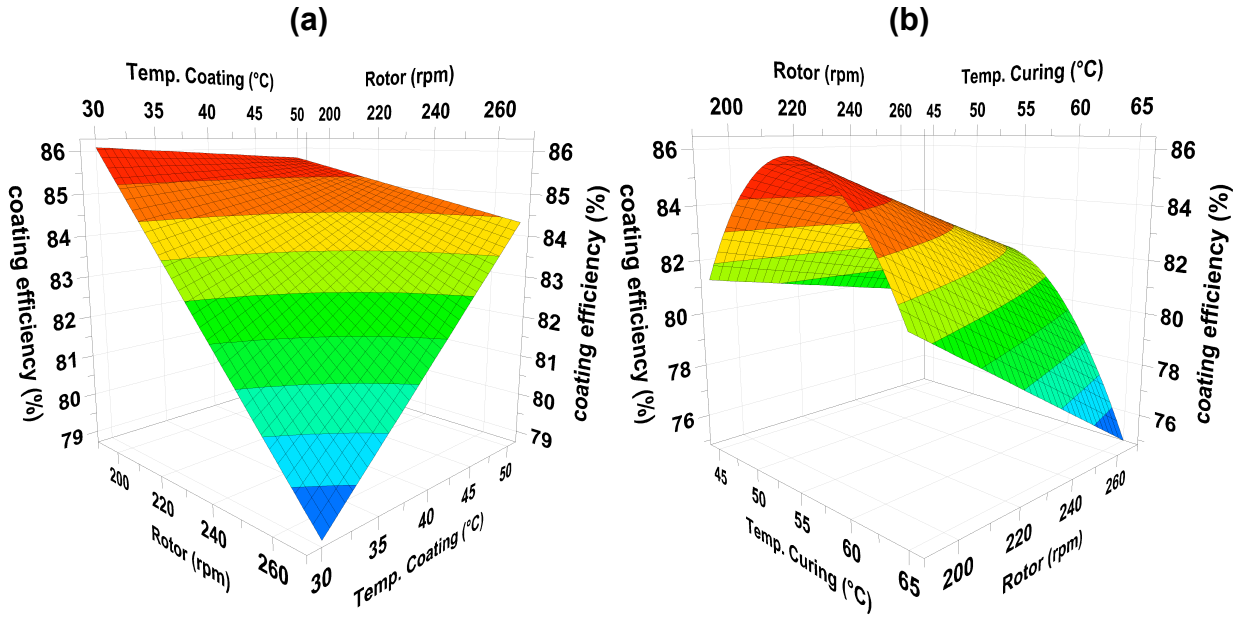

Figure 61: Surface plots of coating temperature and rotor speed (a), and curing temperature and rotor speed (b), $R^2_{adj.}$ = 0.856

Regarding the surface plot of the coating temperature and the rotor speed (Figure 61 (a)) it can be shown that by increasing the rotor speed the coating efficiency decreases, caused by the increased abrasion of the coating material. At higher coating temperatures this effect is pronounced slightly. The probability of material abrasion at high rotor speeds is compensated by the arising stickiness of the polymer at elevated temperature closely below the Tg. In contrast, at low coating temperatures the increase of the rotor speed decreases highly the coating efficiency demonstrating the synergism of the abrasion at higher rotor speeds and the missing stickiness of the polymer. By increasing the coating temperature at a high rotor speed the coating efficiency increases caused by the described stickiness of the polymer whereas at a low rotor speed the coating efficiency is lowered marginally. Altogether it can be summarized that the effect of a high rotor speed and a low coating temperature is outstanding since the coating efficiency is highly decreased in contrast to the other levels of the factors where the coating efficiency changes marginally.

The interaction of the rotor speed and the curing temperature is shown in Figure 61 (b). Similar to the surface plot of the rotor speed and the coating temperature, the reduction of the rotor speed leads to an increase of the coating efficiency caused by less abrasion of the polymer. This effect is most strongly pronounced at the optimum of the curing temperature (55 °C) whereas optimal cohesion of the polymer is achieved at the Tg inhibiting abrasion. At lower curing temperatures an increase of the rotor speed lowers slightly the coating efficiency. Here, the abrasion of the polymer depends only from the bed movement since the temperature is low and the polymer is less sticky. Increasing the rotor speed at high curing temperatures (65 °C) the coating efficiency is more decreased. At an increased rotor speed and high curing temperatures the abraded polymer will coalesce on the coating equipment leading to a higher loss of coating material.

Considering the results it can be summarized that a low feeding/spraying rate and a low rotor speed results in a high coating efficiency with regard to the coating and curing phase of the process. During the coating phase the temperature has a minor influence as the coating efficiency changes marginally by increasing or decreasing the coating temperature, except for the combination of a high feeding/spraying rate or high rotor speed and a low coating temperature. During the curing phase the temperature plays an important role as a high coating efficiency can be achieved at the optimum of the curing temperature at 55 °C, which is the center point of the DOE and is concurrently the Tg of the coating material.

4.1.2 Enteric resistance

As an enteric resistant polymer is used the enteric resistance is an important parameter, which has to be fulfilled, indicating a successful and efficient coating process. In section C 3.2 the film formation which is essential for enteric resistance was investigated and the key parameter of film formation, the Tg, was determined. It was demonstrated that film formation predominantly occurs during curing and that, additionally to the temperature, the time influences film formation. By choosing the drug release (DR) as response the influence of the process parameters on film formation are investigated indirectly. Generally, it is recommended not to choose responses depending on each other. However, it has to be mentioned that the drug release can depend on the coating efficiency. Obtaining higher coating efficiencies the film thickness increases proportionally leading to a higher enteric resistance if film formation occurs at all. Although this relation was expected enteric resistance was chosen as response because it is one major aim of this study besides the coating efficiency.

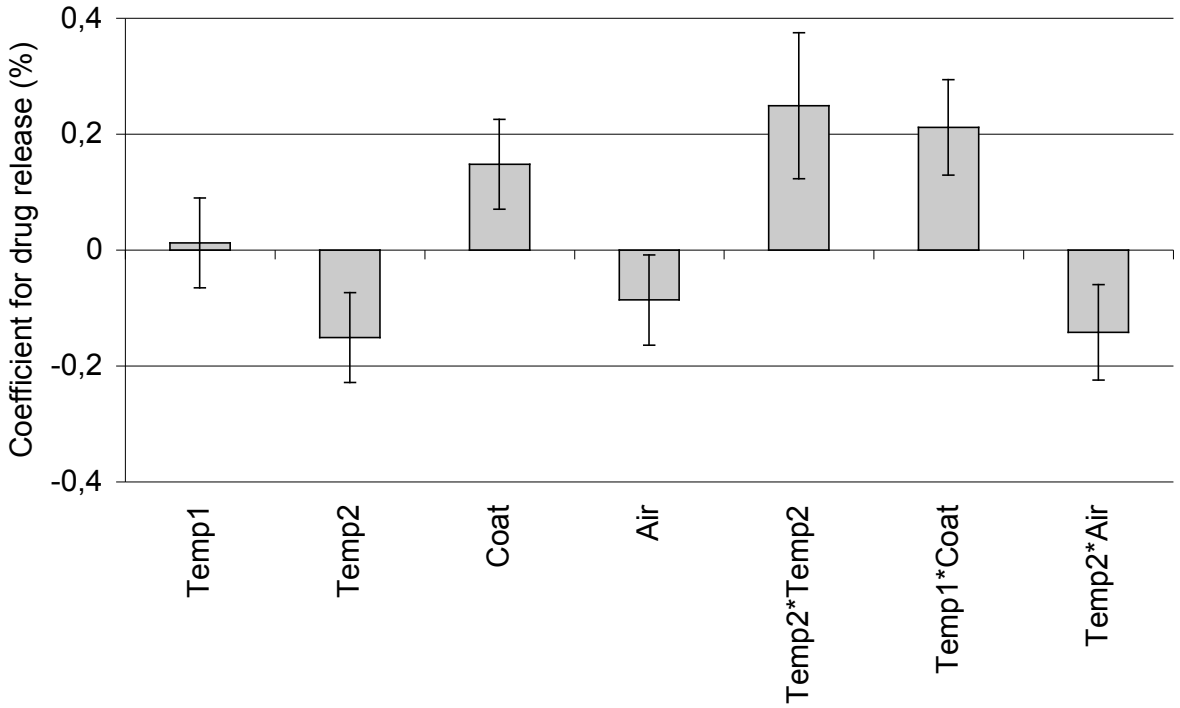

Figure 62: Bar plot of the coefficients of drug release (%)

The coefficient plot (Figure 62) reveals that the curing temperature exerts the strongest effect and indicates an optimum of the curing temperature due to its quadratic effect. It might be expected that the optimum is located at the center point at 55 °C, which confirms the temperature needed for film formation as described in section 3.2. A decreased

feeding/spraying rate leads to a decreased drug release. Remembering the effect of low feeding/spraying rate on the coating efficiency it can be assumed that due to the increased film thickness the drug release is decreased. The third main effect is the air flow rate which reduces the drug release by an increase of the rate. Two interactions, one between the curing temperature and the air flow and the other between the feeding/spraying rate and the coating temperature, are observed and described as follows.

The surface plots of the two interactions are shown in Figure 63. Plot (a) shows the interaction between the feeding/spraying rate and the coating temperature in relation to the drug release. At low feeding/spraying rates a low drug release is achieved not being influenced by the coating temperature. This result corresponds to the results of the coating efficiency. The drug release at fast feeding/spraying rates and low coating temperatures is even more reduced than at low feeding/spraying rates. In contrast a low coating efficiency is observed at the same settings. Furthermore, the drug release is highly increased by elevating the coating temperature at fast feeding/spraying rates and contradicts the effect of the coating efficiency's surface plot. Adjusting the same setting an average coating efficiency is achieved contradicting the high drug release. As mentioned above the drug release is depending on the coating efficiency respectively film thickness. By achieving a high coating efficiency it is expected to achieve a low drug release due to the increase of the film thickness. Regarding the surface plot of the interaction of the feeding/spraying rate and the coating temperature, which is significant for both responses, the prediction is not fulfilled since the surface plots contradict each other.

Amongst this parameter the curing temperature in order to achieve film formation is an important parameter for the drug release. Without achieving a sufficient temperature no film formation will occur and, consequently, the response cannot be analyzed. Due to the chosen levels of the coating and curing temperature of the DOE this temperature is only achieved during the curing phase. In section C 3.2.3 it is shown that for curing times of 0.75 h a temperature of 55 °C is needed in order to obtain enteric resistance. Due to the described plasticizer gradient a certain film formation will be achieved below this temperature. However, this is valid only for the high level of the coating temperature (50 °C) without considering the needed time. Thus, it is questionable if the response 'drug release' can be evaluated without regarding the curing temperature. Unfortunately, the surface plot (a) in Figure 63 does not respect this relation. With respect to this it can be resumed that this interaction does not present an independent effect of the parameters on the drug release.

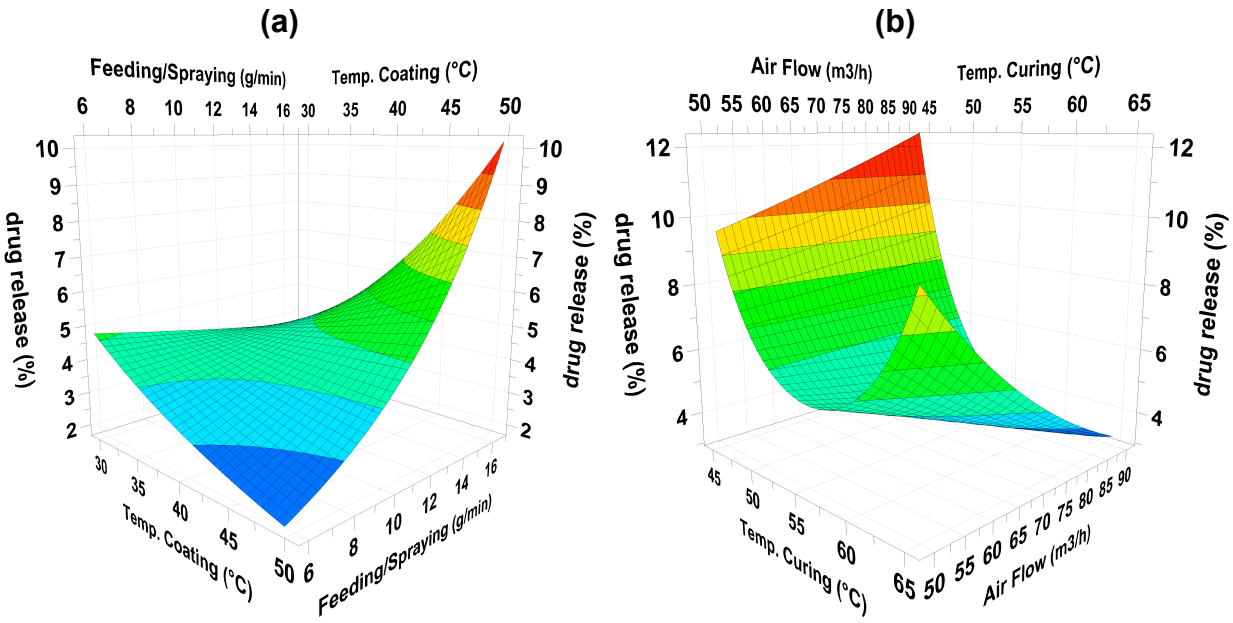

Figure 63: Surface plots of feeding/spraying rate and coating temperature (a) and air flow rate and curing temperature (b), $R^2_{adj.}$ = 0.76

The second interaction is interpretable since the curing temperature, which is needed in order to achieve film formation, is included. The surface plot Figure 63 (b) illustrates the curing temperature and the air flow in relation to the drug release (DR). Here, the effect of the air flow rate can be interpreted since no quadratic effect of this factor exists. Similar to the results of the coating efficiency the curing temperature has an optimum at 55 °C. However, this optimum is only observable at low air flow rates. At high air flow rates and low curing temperatures an increase of the drug release can be detected. At temperatures below the Tg the higher air flow rate detaches the particles from the pellets and further from the equipment, which leads to a thin film. The drug release is increased not meeting the requirements of the USP XXIX [142]. Low drug releases are obtained increasing the temperatures above 55 °C which conforms perfectly to the results of section 3.2.3 determining enteric resistance after curing at 55 °C and higher. Due to the increase of temperature up to the Tg and higher the particles are sticky and cling on the pellets forming an enteric resistant film. Although higher temperatures promote abrasion of coating material which leads to thinner films, a low drug release is obtained. The increase of fluidization by higher air flow rates inhibits pellet agglomeration and abrasion of the polymer particles as the pellets have less contact with each other. Additionally, the air flow streams the pellet bed by emerging from the air slit between the rotor plate and the wall resulting in a decrease of contacts between the pellets and the rotor wall.

Regarding the results it is demonstrated that the drug release is highly influenced by the curing temperature as its quadratic effect has the highest effect in the bar plot. The

optimum of the effect is located at 55 °C which confirms with the temperature needed for film formation after 45 minutes curing (see C 3.2). In combination with the air flow rate it is demonstrated that an increase of the air flow leads to a low drug release at curing temperature at 55 °C and higher observing no optimum in this area of the surface plot.

4.1.3 Summary

Combining the results of the coating efficiency and the drug release it is shown that the curing temperature has the major influence on both parameters. Conforming to the film formation investigations, the optimum of the curing temperature is located close to the Tg at 55 °C. This corresponds to the curing temperature used for the study described in section 1.2. Additionally, the feeding and spraying rate and the rotor speed play a certain role for the efficiency of the process. Generally, low feeding/spraying rates increased the coating efficiency. Nevertheless, it was demonstrated that a high coating temperature could compensate the negative effect of a high feeding/spraying rate. Hence, in order to increase the coating efficiency a slow respectively moderate feeding/spraying rate with regard to the needed time is preferable where the influence of the coating temperature is marginal. Additionally, the rotor speed influences the coating efficiency, which can be increased by decreasing the rotor speed. Similar to the feeding/spraying rate low coating temperatures lead to a low coating efficiency at high rotor speeds and should be avoided.

The main effect of the air flow rate on the drug release interacts with the curing temperature. It is depicted that an increase of the airflow rate leads to a low drug release at curing temperatures below the Tg. At temperatures meeting the Tg or higher a higher air flow rate decreases the drug release resulting in the disappearance of the temperature optimum. Nevertheless, the influence of the air flow has to be considered carefully as the factor was not split in two separate ones for the coating and the curing phase and, has to be investigated in further studies.

5 Process transfer on GPCG 5

The aim of the process transfer was to confirm the process stability and reproducibility of the dry coating process with a focus on its possible industrial use. Therefore the dry coating process was conducted using a GPCG 5 (Glatt GmbH) with a rotor insert together with the gravimetrical powder feeder described in section C 1.1 (see Figure 64).

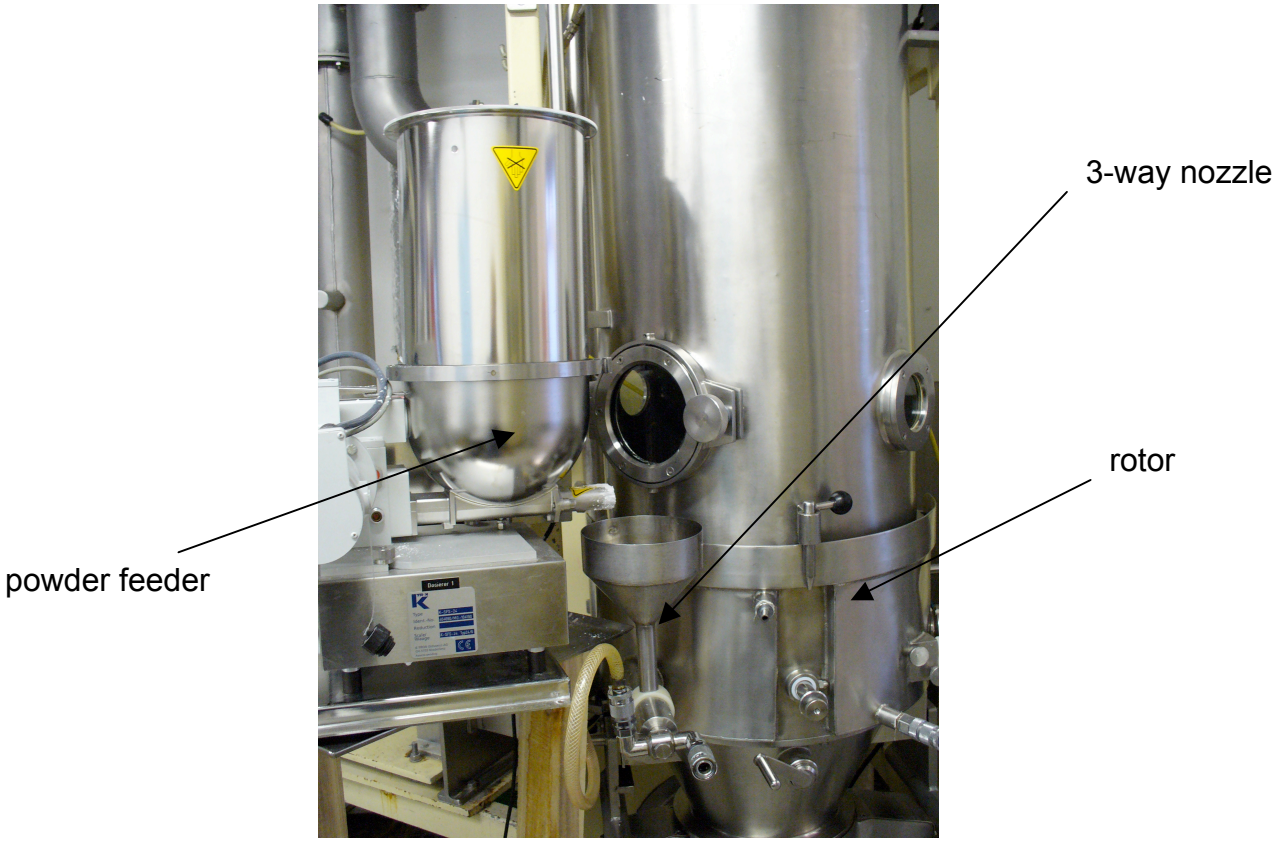

Figure 64: GPCG 5 with the gravimetrically powder feeder and the 3-way nozzle

In literature, the dry coating process was conducted in small batch sizes around 1 kg using the fluid bed and a spheronizer [31, 109] excepting Obara et al., who conducted the dry coating process in the fluid bed with a batch size of 10 kg [101]. Consequently, it is of certain interest to investigate whether the process can be conducted with larger batch sizes than 1 kg in the rotor fluid bed. Certainly, it has to be mentioned that the GPCG 5 is presenting a larger laboratory scale. The pilot scale begins at one-tenth of the production scale [29]. For scaling up to pilot or production batch sizes the powder feeder has to be substituted by a feeder with higher feeding rates.

Prior to the process the parameters used with a GPCG 1.1 were converted to the parameters used with the GPCG 5 by setting the diameters of the rotor plates in relation. The obtained factor was used to calculate the needed feeding rate, air flow rate and rotor

speed. Additionally, the feeding/spraying rate was reduced since the process optimization had resulted in a higher coating efficiency by lower feeding/spraying rates.

PROCESS PARAMETERS	GPCG 1.1	GPCG 5
Rotor speed (rpm)	230	140
Inlet air temperature (°C) Coating /curing phase	43/60	50/65
Product temperature (°C) Coating / curing phase	40/55	42/55
Outlet air temperature (°C) Coating / curing phase	40/54	40/54
Air flow rate (m^3/h) Coating / curing phase	70/120	130/200
Atomizing air pressure (bar)	1.5	2.0
Spray nozzle diameter (mm)	1.2	1.2
Spray rate (g/min)	3.5	9
Powder feed rate (g/min)	11	29
Time coating / curing (min) Coating / curing phase	23/45	60/45

Table 26: Process parameters of the GPCG 1.1 and GPCG 5

The formulation used for the process was formulation B/C containing 70% (w/w) HPMCAS as coating polymer and 30% (w/w) plasticizer mixture of TEC and Myvacet® in a ratio of 70:30. After the complete application of the coating material prior to the curing phase 100.0 g talc were added inhibiting pellet agglomeration during the curing phase. However, the polymer was applied without talc to the pellets. The process was conducted in triplicate with a batch size of 7 kg achieving a complete coverage of the nozzle in order to ensure the ultimate contact of the polymer particles with the pellets. The coating efficiency was determined to be 89.3% ± 4.5% (mean ± CI) being slightly higher than the CE achieved in

the GPCG 1.1. The drug release was analyzed to be 3.6% ± 1.2%. Enteric resistant in the first 120 minutes in the acid stage according to the USP XXIX [142] (Figure 65) was met. Regarding the profile it can be detected that the coated pellets disintegrated immediately in the neutral stage. This is in contrast to formulation A where talc was mixed with HPMCAS leading to a slightly delayed drug release after changing the pH from 1 to 6.8 (see C 2.2.2).

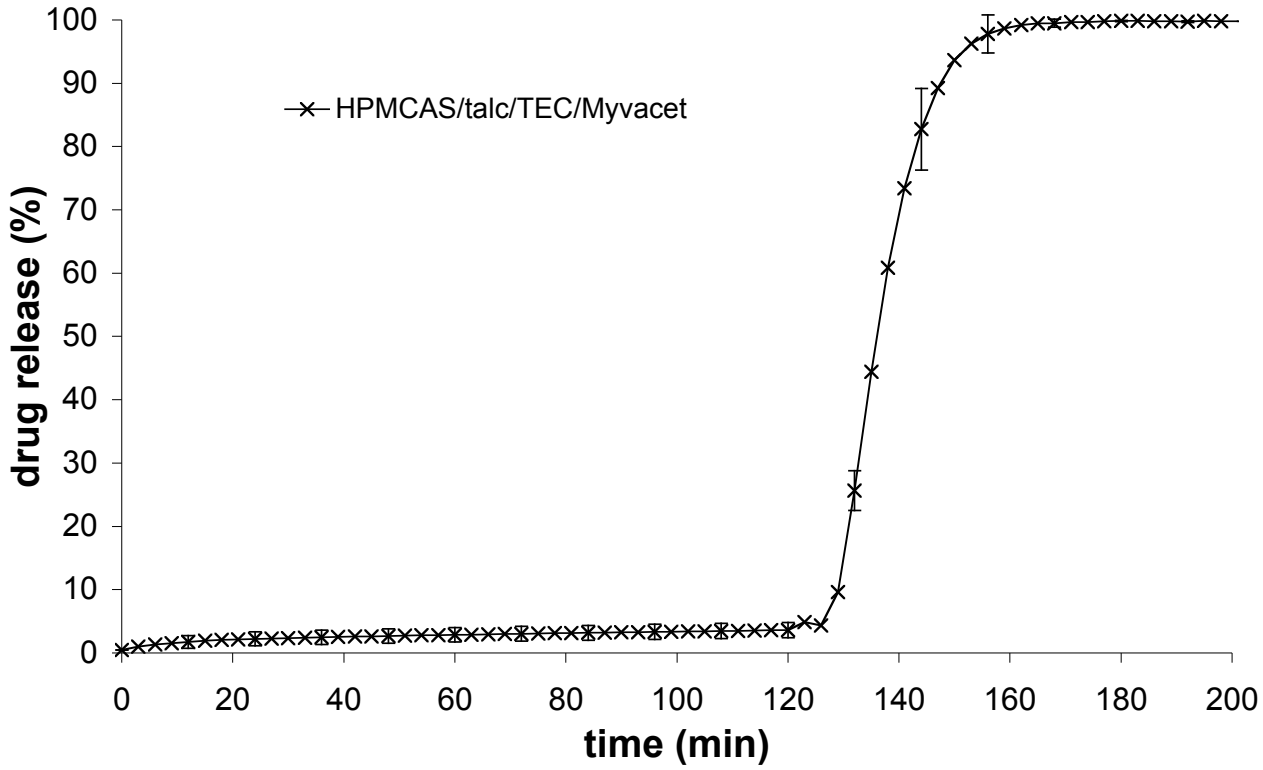

Figure 65: Drug release of theophylline pellets coated with formulation B/C powdered with talc after the coating phase in 750 ml of 0.1 N-HCl (pH 1) for 120 minutes and after addition of 250 ml of $Na_3PO_4 \cdot 12\ H_2O$ solution (65 g/l) (pH 6.8) for further 80 minutes using 40 mg pellets in each vessel, n = 12, mean ± CI (95%)

Considering the results it can be assumed that the dry coating process can be performed in larger rotor fluid beds and that the process might be scale up in order to be conducted in the pilot or rather production scale.

D SUMMARY

The purpose of this study is to develop a novel dry coating technology without the use of a solvent respectively dispersion media. Because of their absence, water or organic solvent do not need to be evaporated which leads to shorter processing times. Hence, the dry coating process exerts short processing times of 70 minutes including the coating phase lasting 23 minutes and the curing phase which takes place immediately after the coating phase for 45 minutes. During the coating phase the coating polymer is applied separately from the liquid plasticizer getting immediately in contact with the liquid on the to be coated pellets. Afterwards the pellets are cured in the second phase in order to obtain a functional coating. The dry coating process is realized in the rotary fluid bed by mounting a gravimetrical powder feeder in alignment to the three way nozzle of the fluid bed equipment, dosing the dry coating powder to the nozzle. The three way nozzle transports the powder together with the liquid plasticizer into the pellet bed. Conducting the process with this set up a simultaneous and close application of the coating material into the dense pellet bed of the rotor is ensured, avoiding an excessive loss of polymer powder and resulting in a layering of the coating material. Due to the dense spiral movement of the fluid bed, the layering of the polymer particles is enhanced by clinging them tightly to the pellet, which minimizes the loss of powder. The plasticizer facilitates on the one hand the adhesion of the polymer to the surface and on the other hand the film formation of the particles. After the material is applied completely onto the cores film formation is induced due to an increase in temperature. Conducting the dry coating process the curing occurs in the rotary fluid bed preventing pellet agglomeration, which may occur during curing in an oven.

As polymer micronized HPMCAS powder (Aqoat®) is used in order to achieve enteric resistant coatings. Different plasticizers, namely TEC and Myvacet®, and the anti tacking agents talc and silicon dioxide are composed with the polymer. The varying formulations are characterized focusing on the coating efficiency, the enteric resistance and the storage stability with respect to drug release and agglomeration tendency. The formulations containing Myvacet® exhibit high coating efficiencies achieving the highest coating efficiency when solely Myvacet® was used as plasticizer. However, this formulation does not show any film formation and, hence, enteric resistance. It is shown that all formulations containing TEC as plasticizer are enteric resistant meeting the requirements of the USP XXIX [142] and indicating that TEC is needed to achieve functional films. Thus, these formulations are used for further characterizations. The stability testing according to the ICH guidelines [67] demonstrates storage stability of the formulations with regard to the

drug release. However, without an anti tacking agent the coated pellets tend to tack together leading to agglomeration of the bulk and further to film's damage when desagglomerating the bulk. By adding an anti tacking agent this phenomenon is prevented. Talc which is mixed together with the polymer prior to the coating process and silicon dioxide, applied to the coated and cured pellets as a top powder, are compared, both inhibiting excellently the agglomeration. However, after 12 months storage at 60% RH ± 5% RH the pellets top powdered with silicon dioxide start to agglomerate. Due to the exhausted capacity of silicon dioxide to sorb water from the environment aging occurs resulting in a higher tackiness. Nevertheless, considering the simplification of the formulation and the probability to substitute talc in the coating formulation, this formulation is used for further studies focusing on the mechanical view of the coating material application and film formation.

The dry coating process was analyzed regarding the coating phase and the curing phase separately. The scope of the investigation is to elucidate the material application during the coating phase and to determine the parameters needed to achieve a high coating efficiency. The film formation and its key parameter during the curing phase are investigated.

The characterization of the coating phase is essential for the dry coating process in order to understand the material application and to determine the parameters influencing this phase. Since the polymer powder and the liquid plasticizers are applied together to the pellets different interparticle forces play a role for the adhesion and cohesion of the materials. Cohesion force measurements using an atomic force microscope and contact angle measurements give tendencies but cannot elucidate the essential parameter for the adhesion and cohesion. It is shown that the addition of Myvacet® to TEC results in a reduction of the surface tension and in lower contact angles on the polymer. The cohesion force is not enhanced by mixing Myvacet® with TEC in contrast to the use of Myvacet® without TEC where an increase of the cohesion forces is observed. Furthermore, it is detected that Myvacet® does not penetrate into the polymer without TEC as trigger. Although Myvacet® is classified as plasticizer, in this study it takes plays as solely wetting agent since it does not penetrate into the polymer and consequently has no plasticizing effect on it. This result leads to the presumption that Myvacet® is able to exert capillary forces between the polymer particles explaining the increase of the cohesion forces and corresponding to the highest coating efficiency of the formulation of HPMCAS and Myvacet®. Accordingly, due to the lower compatibility of the mixture of TEC and Myvacet® with the polymer, the liquid is assumed to remain longer on the surface prior to penetration leading to an prolonged effect of the capillary forces and explaining the increase of the

coating efficiency. Consequently, the good spreadability of the wetting agent Myvacet® is not the key parameter of the coating efficiency. It is resumed that the properties to remain on the surface of the polymer and to build up strong capillary forces play the major role. After the plasticizer penetration van der Waals forces ensures the maintenance of the adhered and cohered material.

During the curing phase film formation takes place due to the increase of temperature. The film formation is characterized with regard to the curing temperature and curing time determining enteric resistance according to the USP XXIX [142] after curing at 55 °C for 0.75 h. Furthermore, the Tg of the film is determined at 55 °C elucidating that the key parameter of the film formation of the dry coating process is the glass transition temperature of the film. However, film formation is observed at lower curing temperatures. By starting the spraying of the liquid plasticizer 30 seconds prior to the feeding of the powder, a plasticizer gradient is obtained resulting in film formation starting at the inner layers due to an elevated plasticizer to polymer ratio and proceeding to the outer layers of the film. Thus, film formation is achieved below the Tg, when extending curing times.

The process parameters influencing the coating efficiency and enteric resistance are determined and optimized by a 2^{5-1} design of experiments. It is shown that the curing temperature has the major influence on both responses observing the optimum at 55 °C. This is according to the curing temperature chosen during the process development and determined as key parameter for film formation. Besides, it is demonstrated that after the coating material is applied completely and the curing phase is induced, the CE is still susceptible. Low feeding/spraying rates and rotor speeds increase the efficiency of the process regarding both, the coating efficiency and the enteric resistance. Higher enteric resistance is obtained at higher air flow rates at temperatures meeting the Tg or higher.

The dry coating process is transferred on a larger rotary fluid bed (GPCG 5) demonstrating the suitability of the process to be used for larger batch sizes. According to the results of the process optimization the feeding/spraying rate is adjusted lower resulting in a higher coating efficiency compared to the smaller batch size. The coated pellets are enteric resistant meeting the requirements of the USP XXIX [142].

Summarizing the results this study shows that the dry coating is a serious alternative to conventional coatings. By undertaking small changes in the equipment a highly efficient process can be performed with respect to its short processing times. Despite the lower coating efficiency the dry coated pellets are on a par with conventional coated pellets.

E EXPERIMENTAL PART

1 Characterization of coated dosage forms

1.1 Particle size measurement

The particle size distribution was determined using laser light diffraction (Helos/KF-Magic, Sympatec GmbH, Clausthal-Zellerfeld, Germany) including a dry dispersing system (Rodos, Sympatec GmbH, Clausthal-Zellerfeld, Germany). The powder was applied on the Vibri feeder (Sympatec GmbH) transporting the powder to the dry dispersing system. This disperses the dry powder using the venturi effect. The atomizing air was adjusted at 2.0 bar and the negative (venturi) pressure at 60 mbar. The results were analyzed by Windox 4.0 software (Sympatec GmbH). The value of the median (x_{50}) is the average of three measurements.

1.2 Surface tension

The surface tension of the plasticizers was determined using the tensiometer K100 (Kruess GmbH, Hamburg, Germany) equipped with the Wilhelmy plate. The surface tension γ_L is calculated using the following equation:

$$\gamma_L = \frac{F}{l \cdot \cos\varphi} \qquad \textbf{Eq. 24}$$

Whereas F stands for the force acting on the balance, l is the length of the plate and φ is the contact angle. The plate is made of roughness platinum and is optimally wetted so that the contact angle is virtually 0°. This means that the term cos φ has a value of approximately 1, thus only the measured force and the length of the plate need to be taken into consideration. The liquids were measured three times determining 10 values in each measurement.

1.3 Coating efficiency / Coating level

The coating efficiency was calculated by dividing the actually achieved weight gain of the coated pellets by the theoretically achievable weight gain of the coated pellets. The results were expressed in percent being the mean value of three batches.

The coating level was calculated by dividing the weight of the applied polymer by the weight of the uncoated cores.

1.4 Batch division

For the stability and agglomerations tendency investigations the batches of formulation A – D were divided as shown on the flowchart (Figure 66). Storing the samples from each batch as shown it was ensured that the different characterizations were carried out with the same batch. The amount of material was limited to 1 kg leading to the chosen number of measurement' s repetition.

For the enteric resistance 5 g pellets were stored for the complete storing interval and samples were withdrawn each point of measurement. The samples for investigating the agglomeration tendency were stored separately in defined vials (d = 4 cm) using four at one testing. The flowability was measured in triplicate after storing for 24 h at 60% RH ± 5% RH after preparation.

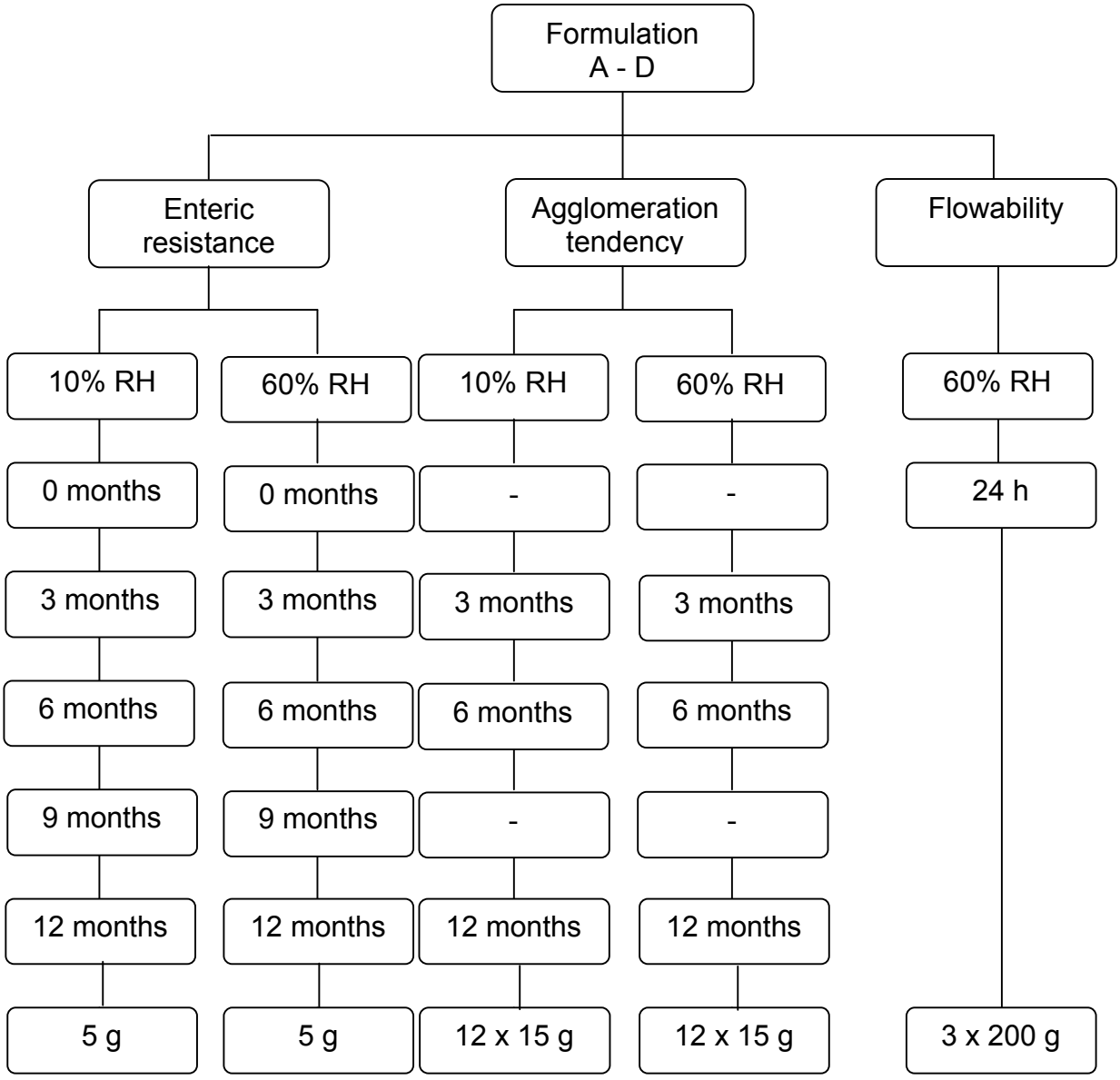

Figure 66: Batch division of formulation A – D for stability and agglomeration tendency investigations

1.5 Enteric resistance

The in vitro drug release was conducted according to the USP XXIX method A [142] rotating paddle method (Sotax AT6, Sotax GmbH, Loerrach, Germany). The dissolution was studied at 37 °C ± 0.5 °C in 750 ml of 0.1N-HCl (pH 1) for 120 minutes and after addition of 250 ml of $Na_3PO_4 \cdot 12\ H_2O$ solution (65 g/l) (pH 6.8) for further 80 minutes using 40 mg pellets in each vessel. The paddle rotation was adjusted at 50 rpm. The drug release was analyzed spectrophotometrically at 272 nm using a continuous flow-through

system attached to the UV spectrophotometer (Lambda 2, Perkin Elmer, Rodgau-Juegesheim, Germany) transporting the liquid with a peristaltic pump (50 rpm) (IPC, Ismatec, Glattbrugg, Schweiz) with modified PVC tubings (Tygon R 3603, Norton, USA). The drug release of each batch was determined from six samples calculating the mean and the CI (95%).

1.6 Agglomeration tendency

1.6.1 Determination of residues

Samples of pellets (15 g) were stored in vials of 4 cm diameter at 25 °C ± 2 °C and 60% RH ± 5% RH respectively 10% RH ± 5% RH. After different storage intervals the samples were passed through a sieve of a vibrational sieving machine (AS 200 control, Retsch, Haan, Germany) with a mesh size of 1600µm adjusting an amplitude of 0.35 mm. Every minute the mass of residues on the sieves was determined until the weight was constant three times respectively the sample was sieved 15 minutes. The determined residues were the mean of four measurements ± CI (95%).

1.6.2 Determination of flowability

The flowability was determined using a ring shear tester (Dr. Dietmar Schulze Schuettgutmesstechnik, Wolfenbuettel, Germany) with the cell typ MV10, v1.1 having a filling volume of 267.04 cm^3 and a waffle structure at the base and the lid of the cell. By pouring the pellets out of a vial the material was filled into the cell. The overlaying material on the cell was removed and the surface was smoothed using a card without applying any shear stress to the sample. The weight was determined prior to the measurement. During the measurements the normal stress of preshear was adjusted at 5000 Pa. Shearing proceeds at 1000, 2000, 3000, 4000 Pa shear stress. The normal and determined shear stresses where incipient flow occurs were plotted in a σ, τ - diagram. The curve through the points of incipient flow is the yield locus. The ratio of the consolidation stress σ_1 to the unconfined yield strength σ_c is called the flowability. The analysis of the results is performed using the software RST – Control 95, Version 1.0 (Dr. Dietmar Schulze Schuettgutmesstechnik). The measurement was repeated twice and the mean ± CI (95%) was calculated.

2 Coating material application and film formation

2.1 Differential scanning calorimetry

The determination of free plasticizer of plasticized powders were performed using the DCS 821e (Mettler Toledo GmbH, Giessen, Germany). As reference an empty aluminum pan was used. The calibration of temperature and heat flow was conducted using indium. The analysis was performed with sealable 40 µl aluminum pans using approximately 5 mg sample. The measurement was carried out applying a continuous flow of nitrogen adjusting a flow rate of 50 ml/min. The sample was frozen to –60 °C with a freezing rate of 10 °C/min, kept 30 minutes constant and heated up to 50 °C setting 2 °C/min as heating rate. The analysis of the results was performed using the STAR^e – Software version 6.01 (Mettler Toledo GmbH). All measurements were carried out in triplicate calculating the mean ± CI (95%). The shown thermograms are always the second measurement.

2.2 Thermo mechanical analysis

The Tg of HPMCAS powder and plasticized powders containing HPMCAS, triethyl citrate and Myvacet® were obtained by thermo mechanical analysis (Mettler TMA 40 with Star^e-Software, Mettler Toledo, Giessen, Germany). The powders were compressed to compacts (20 mg, diameter: 5 mm) using a torque hand press (6 Nm) ensuring a smooth surface similar to the film's surface. After the TMA was calibrated with indium, the analysis has been carried out in triplicate under nitrogen atmosphere over a range of –20 °C to 120 °C at a heating rate of 10 °C/min (mean ± CI (95%)).

2.3 Contact angle measurement

The contact angles were determined by the sessile drop method using the DSA 100 (drop shape analysis system DSA 100, Kruess GmbH, Hamburg, Germany). Tablets of the powders (diameter: 13 mm, weight: 0.2 g) were compressed using an IR press (628 N/cm^3, hydraulic IR press, Perkin Elmer, Germany). The achieved flat-faced compacts were placed on an adjustable platform and the liquid was dropped on the tablet with a micrometer syringe (5 µl). A video of 30 seconds was recorded and the last image was used for the determination of the contact angle using DSA 1 software (DSA 1.90.0.014/ C002, Kruess GmbH). The determination of the contact angle was carried out by the circle fit method (Figure 67) measuring the curvature of the circle which is formed by the shape of the liquid drop (n = 8).

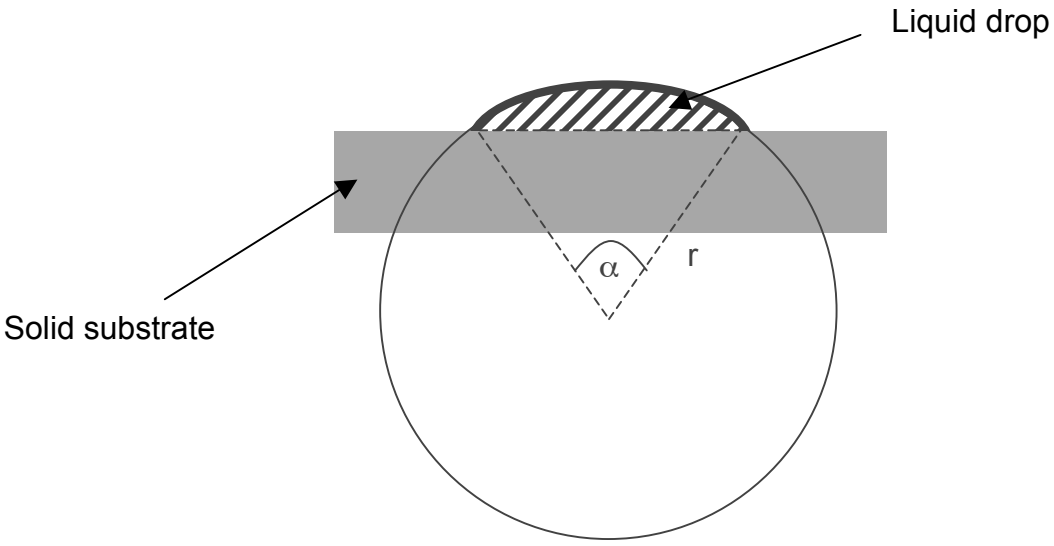

Figure 67: Contact angle determination using the circle fit method

The drop contour is fitted to a segment of a circle A and the circle segment is determined using the following equation:

$$A = \frac{r^2}{2}\left(\frac{\pi\alpha}{180°} - \sin\alpha\right) \qquad \textbf{Eq. 25}$$

whereas r is the radius of the circle and α the angle of the segment. Than the contact angle can be calculated by the height-width relationship of the enclosing rectangle.

2.4 Atomic force microscopy

2.4.1 Design

The measurements were performed using an atomic force microscope (AFM) JPK NanoWizard which is controlled by the JPK NanoWizard SPM control software version 3.0.18 (JPK Instruments AG, Berlin, Germany). The microscope is isolated by a vibration isolation table TS – 150 (TableStable, Scientific Instruments, Ammerbuch, Germany) in order to protect the AFM against vibration and by an acoustic chamber, due to the influence of sound waves, during the measurement. Above the microscope a CCD camera (inverse Axiovert 200, Carl Zeiss Lichtmikroskopie, Goettingen, Germany) is mounted which allows to watch the cantilever and the sample during the measurement. The base whereupon the substrate is placed can be adjusted by the x, y – microscrews. The AFM consists of several components (Figure 68).

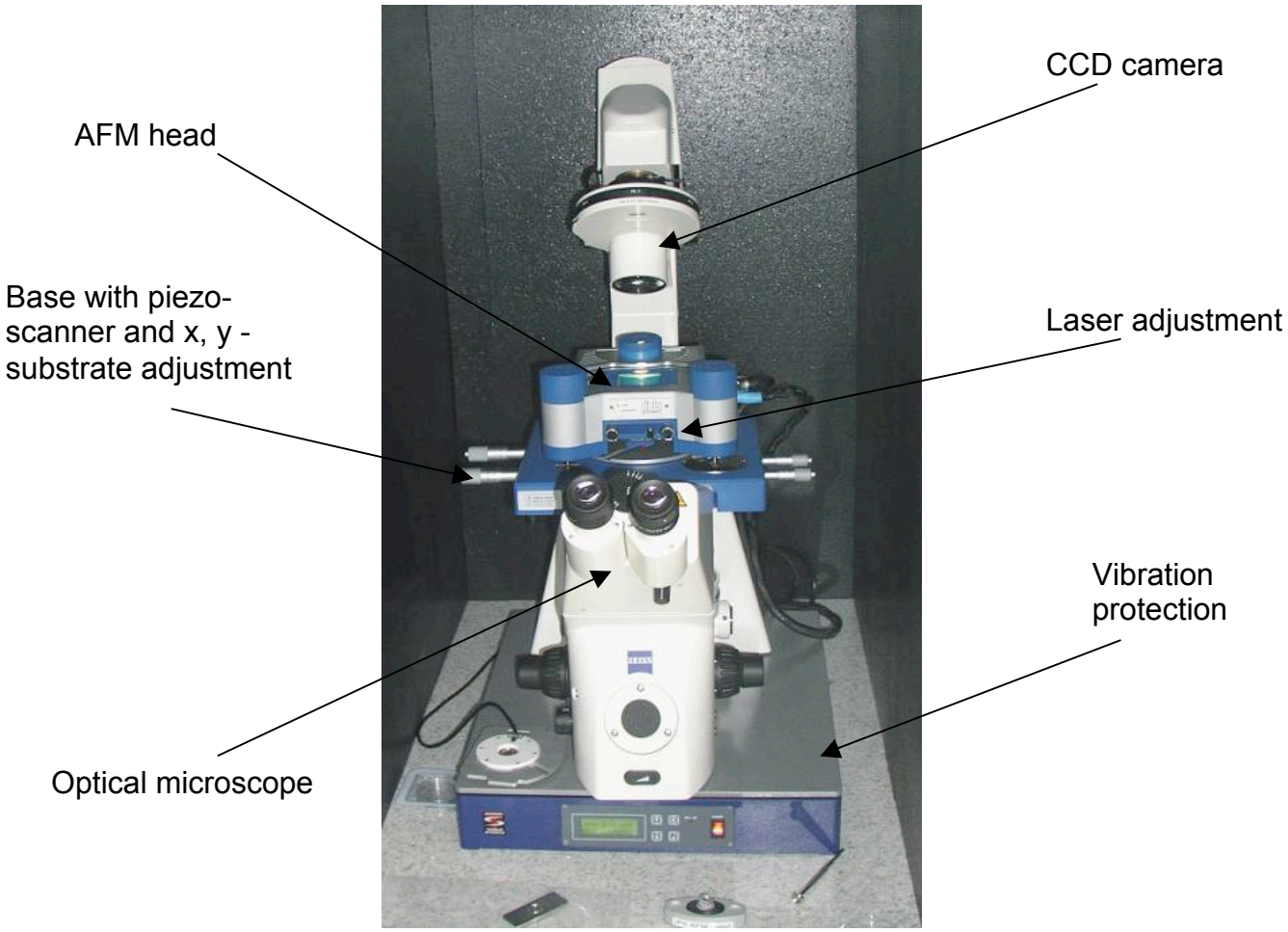

Figure 68: JPK NanoWizard AFM

The used scanner has a scan area of 100 µm x 100 µm in x, y – direction and 5 µm in z-direction. On the scanner the head is laying equipped with the sample holder, laser mirror and photodiode detector. The cantilever is inserted in a holder which ensures that the cantilever tip is angled to the substrate due to its seating with a 11° incline. A clip is fixing the cantilever from the back (Figure 69).

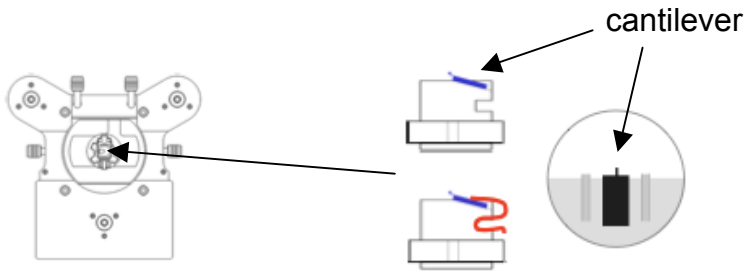

Figure 69: AFM head (upside down) and cantilever holder with cantilever and clip (top view and square view)

Prior to the measurement the head was lowered stepwise until detecting the substrate's surface. The measurements were performed at defined conditions (22 °C ± 1 °C, 40% RH ± 5% RH).

2.4.2 Substrate preparation

The powders were compressed to compacts (20 mg, diameter: 5 mm) using a torque hand press (6 Nm) in order to achieve a macroscopically smooth surface. Additionally, samples were prepared in the same way and afterwards cured above the Tg for 24 hours ensuring coalescence of the polymer and, consequently, a smooth surface.

2.4.3 Tip preparation

For the surface plots rectangular silicium nitride cantilevers were used in order to determine the roughness of the substrates (NP-S, Veeco, Santa Barbara, USA) with a nominal tip radius of 30 nm and a nominal length of 160 µm and a nominal width of 50 µm (Veeco). The spring constant was calculated with 0.42 N/m. For ensuring a maximum reflection of the laser during the measurements the cantilever was sputtered with gold.

Conducting adhesion force measurements probes were utilized with four v-shaped, gold sputtered cantilevers using the thick legged with 100 µm length and the highest stiffness (NP–OW, Veeco, Santa Barbara, USA) (Figure 70). The cantilever was fixed to the holder of a micro-manipulator (3D oil-hydraulic manipulator MMO–203, Narishige Group, New York, USA) with double-sided adhesive tape. The particles, which were spread on an object slide, were attached to the cantilever tip by moving down and up the cantilever with the micro-manipulator. Afterwards the attached particles were cured for 2 h in an oven at 150 °C achieving sintering of the particles on the cantilever. After the measurement of each substrate the particle's intactness was controlled using the optical microscope installed below the AFM (Figure 68).

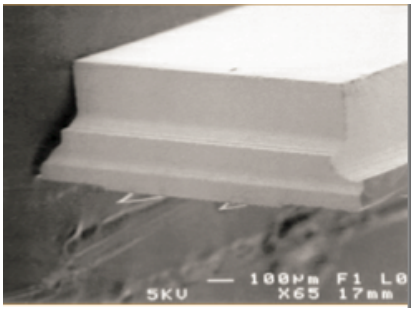

Figure 70: SEM of a cantilever NP–OW

2.4.4 Determination of spring constants

The spring constant calibration of the cantilever is a critical process. First of all, the exact value of the spring constant enters all force calculations. Secondly, all present experimental methods for the calibration of the spring constant suffer from uncertainties in the order of 10% to 20% of the measured value. The spring constant of an end-loaded cantilever of rectangular cross section is

$$k = \frac{Ewd^3}{4l^3} \qquad \textbf{Eq. 26}$$

where E is the elastic modulus of the component material, a is the cantilever thickness, w its width and l its length. Width and length are given by the supplier with an error of less than 1%, whereas E and a can only be determined with an accuracy of around 10 - 15%. Thus, the obtained value is just a guideline for the order of magnitude of the spring constant. Several spring calibration methods are known in literature which is approved for v-shaped cantilevers [18]. In this work force distance curves of the unprepared cantilevers were performed against a reference material with hard and inert properties (glass). The slope of the curve's linear segment is used to determine the spring constant. Performing this technique it has to be ensured that the tip of cantilever gets in contact with the reference material as the lower part of the cantilever gets stiffer which leads to incorrect determined spring constants.

2.4.5 Determination of surface topography

The substrates were scanned in tapping mode with a rectangular cantilever in order to determine the quality of smoothness. Areas of 1 µm x 1 µm were investigated adjusting a

scan rate of 0.5 Hz. The measurements were performed at 4 different domains ensuring conformity of the substrate's surface.

2.4.6 Determination of adhesion and cohesion forces

In a force measurement, the sample is periodically moved up and down at constant speed by applying a voltage to the piezoelectric translator onto which the sample is mounted. During this process the vertical deflection of the cantilever (against which the sample is pushed) is measured. The direct result of a measurement with the atomic force microscope is a plot of the cantilever deflection, in (V), as a function of the piezo displacement, in (nm). This has to be converted to a plot of the force, in (N), as a function of separation between probe and sample, in (nm).

The investigations were conducted by performing force volume plots of 32 x 32 (1024 total) force curves on a 1 µm x 1 µm scan area. Therefore two respectively three plots were scanned lying next to each other. Additionally, three different scan areas on the substrate were selected randomly. In order to ensure that the piezo scanner always moves up to a defined deflection of the cantilever a relative trigger was set achieving that the same force affects on the measurement. The scan rate was adjusted at 6 Hz. The analysis of the curves was carried out using a self-designed software (M. Kappl, Max Planck Institute for Polymer Research, Mainz, Germany). Each force volume plot was scanned, calibrated and the adhesion force was calculated from the deflection of the cantilever at the point of retraction according to Hook's law for the cantilever spring:

$$F_a = k \bullet \delta_C \qquad \textbf{Eq. 27}$$

where δ_c is the deflection of the cantilever and k the spring constant of the cantilever.
For comparability, the determined adhesion forces from the force volume plots of different plots were approved statistically by variance analysis. The mean of 8 force volume plots was used to calculate the mean interparticle force ± CI (95%).

2.5 Scanning electron microscopy

Pellets were quick-freezed with liquid nitrogen and broken in pieces. The pieces were fixed on a brass plate using adhesive tape prior they were sputter coated with gold for 240 s (Agar Manual Sputter Coater, Agar Scientific Ltd., Stansted, Essex, England). Afterwards

the samples were examined by observing their surface and cross-sectional morphologies with a scanning electron microscope (LEO VP 1430, Carl Zeiss NTS GmbH, Oberkochen, Germany) under vacuum adjusting 20 kV operating voltage.

2.6 Thermo mechanical analysis

The glass transition temperature (Tg) of dry coated pellets was obtained by thermo mechanical analysis (Mettler TMA40 with Star^e-Software, Mettler Toledo, Giessen, Germany) as described in E 2.2. Sample preparation was accomplished by adjusting the pellets in a sample holder (Figure 57). The analysis was carried out under nitrogen atmosphere between –20 °C to 120 °C at a heating rate of 10 °C/min after calibrating the TMA with indium as substrate. The determination of the samples' Tg was performed in triplicate.

3 Process optimization

The DOE was analyzed using Modde 7 (Umetrics® AB, Umeå / Malmoe, Sweden). The process settings of section C4.1 are shown in Figure 71. The experiments were conducted at random. The responses are the coating efficiency (%) and the drug release according to the requirements of the USP enteric coated articles (%).

EXP NO	TEMP. COATING (°C)	TEMP. CURING (°C)	FEEDING/ SPRAYING (g/min)	AIR FLOW (m^3/h)	ROTOR (rpm)	COATING EFFICIENCY (%)	DRUG RELEASE (%)
1	30	45	5,6	50	270	87,84	7,07
2	50	45	5,6	50	190	85,1	4,34
3	30	65	5,6	50	190	89,43	13,05
4	50	65	5,6	50	270	83,19	5,04
5	30	45	16,7	50	190	87,74	10,84
6	50	45	16,7	50	270	83,15	27,79
7	30	65	16,7	50	270	66,87	5,11
8	50	65	16,7	50	190	79,48	19,86
9	30	45	5,6	90	190	85,24	21,68
10	50	45	5,6	90	270	85,24	4,12
11	30	65	5,6	90	270	81,37	4,62
12	50	65	5,6	90	190	91,81	1,67
13	30	45	16,7	90	270	74,92	13,86
14	50	45	16,7	90	190	83,66	19,3
15	30	65	16,7	90	190	79,85	2,06
16	50	65	16,7	90	270	80,73	5,88
17	30	55	11,15	70	230	80,59	2,53
18	50	55	11,15	70	230	84,43	6,53
19	40	45	11,15	70	230	78,73	9,41
20	40	65	11,15	70	230	78,85	6,46
21	40	55	5,6	70	230	85,69	1,96
22	40	55	16,7	70	230	83,56	12,81
23	40	55	11,15	50	230	85,3	5,11
24	40	55	11,15	90	230	88,58	3,99
25	40	55	11,15	70	190	84,18	3,32
26	40	55	11,15	70	270	84,5	5,16
27	40	55	11,15	70	230	83,41	4,55
28	40	55	11,15	70	230	84,12	4,81
29	40	55	11,15	70	230	84,42	3,1

Figure 71: Worksheet of the design of experiments (CCF)

4 Process transfer / Determination of process parameters

The process parameters feeding/spraying rate, air flow and rotor speed have to be modulated for the scale up. Therefore the radii of the rotor plates were set in relation. The feeding/spraying rate was adjusted at 9 g and 29 g/minute calculated by equation 28 (Eq. 28)

$$\left(\frac{r_2}{r_1}\right)^2 = k_1 \qquad \textbf{Eq. 28}$$

where r_2 is the radius of the rotor plate in the larger GPCG 5 of 48 cm and r_1 the radius of the GPCB 1.1 of 30 cm resulting in a factor k_1 of 2.56 which is multiplied with the rates adjusted if using the GPCG 1.1.

For the air flow rate the equation 28 was modulated to equation 29 where k_2 was calculated to be 1.62.

$$\left(1+\left(\frac{r_1}{r_2}\right)\right) = k_2 \qquad \textbf{Eq. 29}$$

The rotor speed was converted by calculating the speed in m/s and recalculated with the larger radius.

F SUPPLY SOURCE OF MATERIALS

Acetone p.a.	Riedel de Haën, Seelze, Germany
Aerosil® 200	Degussa AG, Duesseldorf, Germany
HCl (1 N)	Merck KgaA, Darmstadt, Germany
HPMCAS (Aqoat®)	Shin-Etsu Chemical Co., Niigata, Japan
AMG (Myvacet® 9 – 45 K)	Kerry Bio – science, Almere, The Netherlands
Na_3PO_4 • 12 H_20	Fluka Chemie GmbH, Buchs, Switzerland
Talc	Erbsloeh KG, Krefeld, Germany
TEC	Merck KgaA, Darmstadt, Germany
Theophylline pellets	Klinge Pharma, München, Germany

G BIBLIOGRAPHY

[1] Afrin, R., Arakawa, H., Osada, T. and Ikai, A. Extraction of membrane proteins from a living cell surface using the atomic force microscope and covalent crosslinkers, *Cell Biochemistry and Biophysics*. 39: 101-117 (2003)

[2] Ando, M., Kojima, S., Ozeki, Y., Nakayama, Y. and Nebashima, T. Development and evaluation of a novel dry-coated tablet technology for pellets as a substitute for the conventional encapsulation technology, *International Journal of Pharmaceutics*. 336: 99 - 107 (2006)

[3] Andresen, E. T. Bedeutung der Temperung für die Arzneistofffreisetzuung aus Diffusionspellets mit Ethylcelluloseüberzügen aus wässriger Dispersion sowie deren Stabilität, *Ph. D. Thesis, Duesseldorf, Germany* (2001)

[4] Aveyard, R., Clint, J. H. and Nees, D. Theory for the determination of line tension from capillary condensation, *Journal of the American Chemical Society*. 93: 4409 - 4411 (1997)

[5] Avis, K. E., Shukla, A. J. and Chang, R.-K., The evolution of coating solid dosage forms of drugs, In: Pharmaceutical uni Operations: Coating (Drug Manufactoring Technology Series), CRC press LLC, Boca Raton, USA (1998)

[6] Baettig, M. J. Untersuchung zur Herstellung von Pellets in der Rotorwirbelschicht unter Berücksichtigung einer kontinuierlichen Arbeitsweise, *Ph. D. Thesis, Basel, Switzerland* (1996)

[7] Bando, H. and McGinity, J. W. Physicochemical properties of enteric films prepared from aqueous dispersions and organic solutions, *International Journal of Pharmaceutics*. 313: 43-48 (2006)

[8] Bauer, K. H., Froemming, K.-H. and Führer, C., Lehrbuch der Pharmazeutischen Technologie, Wissenschaftliche Verlagsgesellschaft mbH Stuttgart, Stuttgart, Germany (2006)

[9] Bauer, K. H., Lehmann, K., Osterwald, H. P. and Rothgang, G. Überzogene Arzeiformen, *Wissenschaftliche Verlagsgesellschaft mbH, Stuttgart, Germany* (1998)

[10] Begat, P., Morton, D. A. V., Staniforth, J. N. and Price, R. The cohesive-adhesive balances in dry powder inhaler formulations I: Direct quantification by atomic force microscopy, *Pharmaceutical Research*. 21: 1591-1597 (2004)

[11] Begat, P., Morton, D. A. V., Staniforth, J. N. and Price, R. The cohesive-adhesive balances in dry powder inhaler formulations II: Influence on fine particle delivery characteristics, *Pharmaceutical Research*. 21: 1826-1833 (2004)

[12] Berard, V., Lesniewska, E., Andres, C., Pertuy, D., Laroche, C. and Pourcelot, Y. Dry powder inhaler: influence of humidity on topology and adhesion studied by AFM, *International Journal of Pharmaceutics*. 232: 213-224 (2002)

[13] Binnig, G., Gerber, C., Stoll, E., Albrecht, T. R. and Quate, C. F. Atomic Resolution with Atomic Force Microscope, *Europhysics Letters*. 3: 1281-1286 (1987)
[14] Binnig, G. and Rohrer, H. Scanning Tunnel Microscopy *IBM Journal of Research and Development*. 30: 355-369 (1985)
[15] Bodmeier, R., Guo, H. X. and Paeratakul, O., Process and formulation factors affecting the drug release from pellets coated with the ethylcellulose-pseudolatex, Aquacoat, In: Aqueous Polymeric Coatings for Pharmaceutical Dosage Forms, Marcel Dekker, New York, 55 - 80 (1997)
[16] Bodmeier, R. and Paeratakul, O., Suspension and Dispersible Dosage Froms of Multiparticulates, In: Multiparticulate Orla Drug Delivery, Marcel Dekker, Ney York, 143 - 159 (1994)
[17] Bodmeier, R. and Paeratakul, O. The Effect of Curing on Drug-Release and Morphological Properties of Ethylcellulose Pseudolatex-Coated Beads, *Drug Development and Industrial Pharmacy*. 20: 1517-1533 (1994)
[18] Bonaccurso, E. Investigation of electrokinetic forces on single particles, *Ph.D. Thesis, Siegen, Germany* (2001)
[19] Bouffard, J., Dumont, F. B. and Legros, R. Optimization and scale - up of a fluid bed tangential spray rotorgranulation process, *International Journal of Pharmaceutics*. 335: 54 - 62 (2007)
[20] Brown, G. L. Formation of films from polymer dispersions, *Journal of Polymer Science*. 12: 423-434 (1956)
[21] Buckton, G. The assessment and pharmaceutical importance, of the solid/liquid interface: a review with respect to powders, *International Journal of Pharmaceutics*. 44: 1 - 8 (1988)
[22] Buckton, G. and Newton, J. M. Assessment of the wettability and surface energy of a pharmaceutical powder by liquid penetration, *Journal of Pharmacy and Pharmacology*. 37: 605-609 (1985)
[23] Buckton, G. and Newton, J. M. Assessment of the Wettability of Powders by Use of Compressed Powder Discs *Powder Technology*. 46: 201-208 (1986)
[24] Butt, H.-J., Graf, K. and Kappl, M., Liquid surfaces, In: Physics and Chemistry of Interfaces, Wiley-VCH Verlag GmbH & Co. KGaA, Weinheim, Germany (2006)
[25] Butt, H.-J., Graf, K. and Kappl, M., Surface forces, In: Physics and Chemistry of Interfaces, Wiley-VCH Verlag GmbH & Co. KGaA, Weinheim, Germany (2006)
[26] Butt, H. J. Measuring electrostatic, van der Waals, and hydration forces in electrolyte solutions with an atomic force microscope, *Biophysical Journal*. 60: 1438-1444 (1991)
[27] Butt, H. J., Cappella, B. and Kappl, M. Force measurements with the atomic force microscope: Technique, interpretation and applications, *Surface Science Reports*. 59: 1-152 (2005)

[28] Cates, M. E., Haw, M. D. and Holmes, C. B. Dilatancy, jamming, and the physics of granulation, *Journal of Physics: Condensed Matter*. 17: 2517-2531 (2005)
[29] Center for Drug Evaluation and Research, C. Guidance for Industry: Immediate release solid oral dosage forms, scale-up and postapproval changes: chemistry, manufacturing, and controls, in vitro dissolution testing, and in vivo bioequivalence documentation (1995)
[30] Cerea, M., Maroni, A., Vecchio, C., Palugan, L., Zema, L. and Gazzaniga, A. Dry-Coating Process for the Preparation of HPMCAS Enteric-Coated Soft-Gelatin Capsules, *Proc. AAPS Annual Meeting and Exposition*. (2006)
[31] Cerea, M., Zheng, W. J., Young, C. R. and McGinity, J. W. A novel powder coating process for attaining taste masking and moisture protective films applied to tablets, *International Journal of Pharmaceutics*. 279: 127-139 (2004)
[32] Chan, L. W., Wong, T. W., Chua, O. C., York, P. and Heng, P. W. S. Anti-tacking Action of Polyvinylpyrrolidone on Hydroxypropylmethylcellulose, *Chemical & Pharmaceutical Bulletin*. 51: 107 - 112 (2003)
[33] Cole, G., Hogan, J. and Aulton, M., Pharmaceutical Coating Technology, Taylor & Francis, Padstow, U.K. (1995)
[34] Davis, M., Ichikawa, I., Williams, E. J. and Banker, G. S. Comparison and evaluation of enteric polymer properties in aqueous solutions, *International Journal of Pharmaceutics*. 28: 157-166 (1986)
[35] Degussa AG. Eudragit® Methacrylate Poylerms for Pharmaceutical Applications, *Product brochure* (2006)
[36] Dillon, R. E., Matheson, L. A. and Bradford, E. B. Sintering of Synthetic Latex Particles, *Journal of Colloid Science*. 6: 108-117 (1951)
[37] Dobler, R. E., Pith, T., Lambla, M. and Holl, Y. Coalescence mechanism of polymer colloids: I. Coalescence under the influence of particle-water interfacial tension, *Journal of Colloid and Interface Science*. 152: 1 - 11 (1992)
[38] Ducker, W. A., Senden, T. J. and Pashley, R. M. Direct measurement of colloidal forces using an atomic force microscope, *Nature*. 353: 239-241 (1991)
[39] Ebewele, R. O., Thermal Transitions in Polymers, In: Polymer Science and Technology, CRC Press, Boca Raton, USA, 89 (2000)
[40] Eckersley, S. T. and Rudin, A. Mechanism of Film Formation from Polymer Latexes, *Journal of Coatings Technology*. 62: 89-100 (1990)
[41] Eger, K., Troschuetz, R. and Roth, H. J., Arzneistoffanalyse, Wissenschaftliche Verlagsgesellschaft, Stuttgart, Germany (1999)
[42] Eriksson, L., Johansson, E., Kattaneh - Wold, N., Wikstroem, C. and Wold, S. Design of Experiments, *Umetrics Umea*. 87 (2000)

[43] European Pharmacopoeia. Wirkstofffreisetzung aus festen Arzneiformen, 286 - 289 (2007)
[44] Eve, J. K., Patel, N., Luk, S. Y., Ebbens, S. J. and Roberts, C. J. A study of single drug particle adhesion interactions using atomic force microscopy, *International Journal of Pharmaceutics*. 238: 17-27 (2002)
[45] Felton, L. A. and Baca, M. L. Influence of curing on the adhesive and thermomechanical properties of an applied acrylic polymer, *Pharmaceutical Development and Technology*. 6: 53-59 (2001)
[46] Felton, L. A. and McGinity, J. W. Influence of insoluble excipients on film coating systems, *Drug Development and Industrial Pharmacy*. 28: 225-243 (2002)
[47] Felton, L. A. and McGinity, J. W. Influence of plasticizers on the adhesive properties of an acrylic resin copolymer to hydrophilic and hydrophobic tablet compacts, *International Journal of Pharmaceutics*. 154: 167-178 (1997)
[48] Felton, L. A., Shah, N. H., Zhang, G., Infeld, M. H., Malick, A. W. and McGinity, J. W. Physical-mechanical properties of film-coated soft gelatin capsules, *International Journal of Pharmaceutics*. 127: 203-211 (1996)
[49] Fetscher, A. Weichmachereinfluß auf die Wirkstofffreisetzung und die thermo-mechanische Eigenschaft von magensaftresistenten Filmbildnern auf Polyacrylatbasis, *Ph. D. Thesis, Tuebingen, Germany* (1998)
[50] Frenkel, J. Viscous flow of crystalline bodies under the action of surface tension, *Journal of Physics*. 9: 385 - 391 (1945)
[51] Frohoff-Huelsmann, M. A. Waessrige Ethylcellulosedispersionen mit Hydroxypropylmethylcellulose als Ueberzugsmaterial fuer Arzneistoffpellets, *Ph. D. Thesis, Duesseldorf, Germany*. (1999)
[52] Fukumore, Y., Coating of multiparticulates using polymeric dispersions, In: Multiparticulate oral drug delivery, Marcel Dekker, New York, (1994)
[53] Genovesi, A., Spadoni, A., Funaro, C. and Vecchio, C. Evaluation of a Novel Dry Coating Method using Powder Layering GS - IMA Technology, *Proc. 4th World Meeting ADRITELF/APGI/APV, Florence, Italy* (2002)
[54] http://www.glatt.com/d/01_technologien/01_04_08.htm, Glatt GmbH, (2006)
[55] Goodhart, F. W., Harris, M. R., Murthy, K. S. and Nesbitt, R. U. An evaluation of aqeous film - forming dispersions for controlled release, *Pharmaceutical Technology*. 8: 64 - 71 (1984)
[56] Gordon, M. and Taylor, J. S. Ideal Copolymers and the 2Nd-Order Transitions of Synthetic Rubbers .1. Non-Crystalline Copolymers, *Journal of Applied Chemistry*. 2: 493-500 (1952)

[57] Guo, H. X., Heinamaki, J., Karjalainen, M., Juhanoja, J., Khriachtchev, L. and Yliruusi, J. Compatibility of aqueous enteric film coating with pellets containing waxy maize starch and lactose, *Stp Pharma Sciences*. 12: 198-200 (2002)
[58] Gutierrez-Rocca, J. C. and McGinity, J. W. Influence of aging on the physical-mechanical properties of acrylic resin films cast from aqueous dispersions and organic solutions, *Drug Development and Industrial Pharmacy*. 19: 293-301 (1993)
[59] Heim, L.-O., Blum, J. r., Preuss, M. and Butt, H.-J. r. Adhesion and Friction Forces between Spherical Micrometer-Sized Particles, *Physical Review Letters*. 83: 3328 (1999)
[60] Hogan, J. E. Aqueous versus organic solvent film coating, *International Journal of Pharmaceutical Technology & Production*. 3: 17 - 20 (1982)
[61] Hogan, J. E., Film - coating Materials and their Properties, In: Pharmaceutical coating technology, Taylor & Francis, London, UK 6 - 52 (1995)
[62] Hogan, J. E., Modified release coatings, In: Pharmaceutical Coating Technology, Taylor & Francis, London, UK, 409 - 438 (1995)
[63] Hooton, J. C., German, C. S., Allen, S., Davies, M. C., Roberts, C. J., Tendler, S. J. B. and Williams, P. M. An atomic force microscopy study of the effect of nanoscale contact geometry and surface chemistry on the adhesion of pharmaceutical particles, *Pharmaceutical Research*. 21: 953-961 (2004)
[64] Hooton, J. C., German, C. S., Allen, S., Davies, M. C., Roberts, C. J., Tendler, S. J. B. and Williams, P. M. Characterization of particle-interactions by atomic force microscopy: Effect of contact area, *Pharmaceutical Research*. 20: 508-514 (2003)
[65] Ichikawa, H., Uemura, T., Fukumori, Y., Sato, K., Abe, H. and Naito, M. Dry particle Coating with Polymerc Nanopowders for Fabricating Prolonged-Release Microparticles with Multi-Layered Structure, *Proc. AAPS Annual Meeting and Exposition*. (2006)
[66] Ikai, A. and Afrin, R. Toward mechanical manipulations of cell membranes and membrane proteins using an atomic force microscope: An invited review, *Cell Biochemistry and Biophysics*. 39: 257-277 (2003)
[67] International Conference on Harmonization of Technical Requirements for Registration of Pharmaceuticals for Human Use, I., Stability Testing of New Drug Substances and Products, Q1A (R2), www.ich.org/LOB/media/MEDIA419.pdf (2003)
[68] Iyer, U., Hong, W.-H., Das, N. and Ghebre -Sellassie, I. Comparative evaluation of three organic solvent and dispersion based ethylcellulose coating formulations, *Pharmaceutical Technology*. 14: 68 - 86 (1990)
[69] Jagota, A. and Dawson, P. R. Simulation of the Viscous Sintering of Two Particles, *Journal of the American Ceramic Society*. 73: 173-177 (1990)
[70] Jenike, A. W. Storage and Flow of Solids, *Bull. No. 123, Engng. Exp. Station, Univ. Utah, Salt Lake City*. (1964)

[71] Kablitz, C. D., Harder, K. and Urbanetz, N. A. Dry coating in a rotary fluid bed, *European Journal of Pharmaceutical Sciences*. 27: 212-219 (2006)
[72] Kablitz, C. D. and Urbanetz, N. A. Characterization of the film formation of the dry coating process, *European Journal of Pharmaceutics and Biopharmaceutics*. doi:10.1016/j.ejpb.2007.1002.1023 (2007)
[73] Kappl, M. and Butt, H. J. The colloidal probe technique and its application to adhesion force measurements, *Particle and Particle Systems Characterization*. 19: 129-143 (2002)
[74] Karisson, E. B., The Nobel Prize in Physics 1901 - 2000, In: The Nobel Prize: The First 100 Years, Imperial College Press, London, UK (2001)
[75] Keddie, J. L., Meredith, P., Jones, R. A. L. and Donald, A. M. Kinetics of the film formation in acrylic latices studied with multiple - angle - of - incidence ellipsometry and environmental SEM, *Macromolecules*. 28: 2673 - 2682 (1995)
[76] Kerry Bio-Science. Product Data Sheet Myvacet 9-45 K, *Product brochure*. (2007)
[77] Keshikawa, T. and Nakagami, H. Film Formation with Coating Systems of Aqueous Suspensions and Latex Dispersions of Ethylcellulose, *Chemical & Pharmaceutical Bulletin*. 42: 656-662 (1994)
[78] Kidney, J., Dominguez, M., Taylor, P. M., Rose, M., Chung, K. F. and Barnes, P. J. Immunomodulation by theophylline in asthma. Demonstration by withdrawal of therapy, *Am. J. Respir. Crit. Care Med.* 151: 1907-1914 (1995)
[79] Kleinebudde, P. Pharmazeutische Pellets durch Extrudieren/Sphaeronisieren, *Professorial dissertation, Kiel, Germany* (1997)
[80] Knop, K. Herstellung von Pellets in einer durch Druckluft rotierenden Wirbelschicht, Vergleich mit der konventionellen Wirbelschicht, *Ph. D. Thesis, Duesseldorf, Germany* (1988)
[81] Lecomte, F., Siepmann, J., Walther, M., Macrae, R. J. and Bodmeier, R. Polymer blends used for the coating of multiparticulates: Comparison of aqueous and organic coating techniques, *Pharmaceutical Research*. 21: 882-890 (2004)
[82] Lehmann, K., Chemistry and Application Properties fo Polymethacrylate Coating Systems, In: Aqueous Polymer Coating for Pharmaceutical Dosage Forms, Marcel Dekker, New York, USA (1998)
[83] Lehmann, K. and Dreher, D. Anwendung waessriger Kunststoffdospersionen zum Ueberziehen von Arzneiformen, *Pharmazeutische Industrie*. 34: 894 - 899 (1972)
[84] Lide, D. R., CRC Handbook of Chemistry and Physics, CRC Press, Boca Raton, USA (2000)
[85] Lifshitz, E. M. The Theory of Molecular Attractive Forces Between Solids, *Soviet Phys. JETP*. 2: 73 - 83 (1956)

[86] Lippold, B. C. and Monells Pagés, R. Film formation, reproducibility of production and curing with respect to release stability of functional coatings from aqueous polymer dispersions, *Pharmazie*. 56: 5-17 (2001)
[87] Lippold, B. C. and Monells Pagés, R. Control and stability of drug release from diffusion pellets coated with the aqueous quaternary polymethacrylate dispersion Eudragit® RS 30 D, *Pharmazie*. 56: 477-483 (2001)
[88] Lohrmann, M. Untersuchungen zu interaprtikulären Wechselwirkungen von Lactose und Mannitol als Carrier für Pulverinhalatoren, *PH.D Thesis, Duesseldorf, Germany* (2006)
[89] Lohrmann, M., Kappl, M., Butt, H. J., Urbanetz, N. and Lippold, B. C. Adhesion forces in interactive mixtures for dry powder inhalers - Evaluation of a new measuring method, *European Journal of Pharmaceutics and Biopharmaceutics*. in press: (2007)
[90] M. Goetzinger and Peukert, W. Haftkraftverteilungen von rauen Haftsystemen am Beispiel Kugel-Platte, *Chemie Ingenieur Technik*. 75: 1848-1852 (2003)
[91] Maejima, T. and McGinity, J. W. Influence of film additives on stabilizing drug release rates from pellets coated with acrylic polymers, *Pharmaceutical Development and Technology*. 6: 211-221 (2001)
[92] Magonov, S. N. and Reneker, D. H. Characterization of polymer surfaces with atomic force microscopy, *Annual Review of Materials Science*. 27: 175-222 (1997)
[93] Malm, C. J. and Waring, C. E., Cellulose esters containing dicarbosylic acid groups and process of making same, Us - patent no: 2093462, (1937)
[94] Maloney, T. C. Messen der Porengrößenverteilung mittels DSC, *UserCom*. 2: 15-.19 (2000)
[95] Matthée, K. and Knop, K. Bestimmung von Glassübergangstemperaturen an Pulverpresslingen mittels TMA, *Usercom, Information für Awender von Mettler Tolede Thermoanalysen - Systemen*. 21: 11 - 13 (2005)
[96] McGinity, J. W., Aqueous Polymeric Coatings for Pharmaceutical dosage forms, Marcel Dekker, New York, USA (1997)
[97] Mueller, R. Systematische Untersuchung zur Einstellung der Prozess Parameter im Scale-Up Prozess für die Bohle Film Coater, *Ph. D. Thesis, Duesseldorf, Germany* (2007)
[98] Mykhaylova, V. and Urbanetz, N. A. New Nanoparticle-Micorparticle Formulations for Use in Dry Powder Inhalers, *Proc. DPhG, Joint Meeting, Marburg, Germany* (2006)
[99] Nagai, T., Sekigawa, F., Hoshi, N. and McGinity, J. W., Applications of HPMC and HPMCAS aqueous film coating of pharmaceutical dosage forms, In: Aqueous Polymeric Coatings for Pharmaceutical Dosage Forms, Marcel Dekker, New York, USA, 81-152, (1998)
[100] Naidich, Y. V. and Lavrinenko, I. A. Capillary adhesion forces between solid particles with an intermediate liquid layer at the contact, *Powder Metallurgy and Metal Ceramics*. 6: 709-710 (1967)

[101] Obara, S., Maruyama, N., Nishiyama, Y. and Kokubo, H. Dry coating: an innovative enteric coating method using a cellulose derivative, *European Journal of Pharmaceutics and Biopharmaceutics*. 47: 51-59 (1999)
[102] Obara, S. and McGinity, J. W. Influence of processing variables on the properties of free films prepared from aqueous polymeric dispersions by a spray technique, *International Journal of Pharmaceutics*. 126: 1-10 (1995)
[103] Oh, J. K., Tomba, P., Ye, X. D., Eley, R., Rademacher, J., Farwaha, R. and Winnik, M. A. Film formation and polymer diffusion in poly(vinyl acetate-co-butyl acrylate) latex films. Temperature dependence, *Macromolecules*. 36: 5804-5814 (2003)
[104] Ohm, A. Untersuchung zur Benetzung und Lösungsgeschwindigkeit von Arzneistoffpartikeln, *Ph. D. Thesis, Duesseldorf, Germany* (1984)
[105] Okhamafe, A. O. and York, P. Studies of interaction phenomena in aqueous-based film coatings containing soluble additives using thermal analysis techniques, *Journal of Pharmaceutical Sciences*. 77: 438-443 (1988)
[106] Osterwald, H., Eisenbach, C. D. and Bauer, K. H. Effectiveness and optimal use of plasticizers in film coatings, *Acta Pharmaceutica Technologica*. 28: 34-43 (1982)
[107] Pearnchob, N. and Bodmeier, R. Coating of pellets with micronized ethylcellulose particles by a dry powder coating technique, *International Journal of Pharmaceutics*. 268: 1-11 (2003)
[108] Pearnchob, N. and Bodmeier, R. Dry polymer powder coating and comparison with conventional liquid-based coatings for Eudragit (R) RS, ethylcellulose and shellac, *European Journal of Pharmaceutics and Biopharmaceutics*. 56: 363-369 (2003)
[109] Pearnchob, N. and Bodmeier, R. Dry powder coating of pellets with micronized Eudragi (R) RS for extended drug release, *Pharmaceutical Research*. 20: 1970-1976 (2003)
[110] Pearnchob, N., Dashevsky, A. and Bodmeier, R. Improvement in the disintegration of shellac-coated soft gelatin capsules in simulated intestinal fluid, *Journal of Controlled Release*. 94: 313-321 (2004)
[111] Pearnchob, N., Dashevsky, A., Siepmann, J. and Bodmeier, R. Shellac used as coating material for solid pharmaceutical dosage forms: understanding the effects of formulation and processing variables, *Stp Pharma Sciences*. 13: 387-396 (2003)
[112] Pearnchop, N. Evaluation of new film coatings processes and materials, *Ph.D. Thesis, Berlin, Germany* (2002)
[113] Petereit, H. U., Assmus, M. and Lehmann, K. Glyceryl Monostearate As A Glidant in Aqueous Film-Coating Formulations, *European Journal of Pharmaceutics and Biopharmaceutics*. 41: 219-228 (1995)
[114] Petersen, C., Heldmann, C. and Johannsmann, D. Internal stresses during film formation of polymer latices, *Langmuir*. 15: 7745-7751 (1999)

[115] Podczeck, F. The Influence of Particle Size Distribution and Surface Roughness of Carrier Particles on the in vitro Properties of Dry Powder Inhalations, *Aerosol Science and Technology*. 31: 301 - 321 (1999)
[116] Podczeck, F. and Newton, J. M. Development of an ultracentrifuge technique to determine the adhesion and friction properties between particles and surfaces, *Journal of Pharmaceutical Sciences*. 84: 1067-1071 (1995)
[117] Podczeck, F., Newton, J. M. and James, M. B. Influence of Relative Humidity of Storage Air on the Adhesion and Autoadhesion of Micronized Particles to Particulate and Compacted Powder Surfaces, *Journal of Colloid and Interface Science*. 187: 484-491 (1997)
[118] Podczeck, F., Newton, J. M. and James, M. B. The influence of chemical structure on the friction properties between particles and compacted powder surfaces, *Journal of Materials Science*. 31: 2213-2219 (1996)
[119] Porter, S. C. Controlled-Release Film Coatings Based on Ethylcellulose, *Drug Development and Industrial Pharmacy*. 15: 1495-1521 (1989)
[120] Porter, S. C. and Bruno, C. H., Coating of solid dosage forms, In: Pharmaceutical dosage forms: Tablets, Marcel Dekker, New York, USA, 77 - 160 (1990)
[121] Rabinovich, Y. I., Esayanur, M. S. and Moudgil, B. M. Capillary Forces between Two Spheres with a Fixed Volume Liquid Bridge: Theory and Experiment, *Langmuir*. 21: 10992-10997 (2005)
[122] Riesen, R. and Schawe, J. Die Glasübergangstemperature gemessen mit verschiedenen TA-Techniken, Teil 2: Ermittlung der Glasübergangstemperatur, *Usercom, Information für Awender von Mettler Tolede Thermoanalysen - Systemen*. 18: 1 - 5 (2003)
[123] Roxal Microscopical Society. How a SEM works, *homepage RMS* (2007)
[124] Satas, D. and Tracton, A. A., Coating Technology Handbook, Marcel Dekker, New York, USA (2001)
[125] Sauer, D., Zheng, W., Coots, L. B. and McGinity, J. W. Influence of processing parameters and formulation factors on the drug release from tablets powder-coated with Eudragit® L 100-55, *European Journal of Pharmaceutics and Biopharmaceutics*. doi: 10.1016/j.ejpb.2007.02.021 (2007)
[126] Schmidt-Mende, T. Freisetzuung aus magensaftresistent überzogenen Arzneiformen, *Ph. D. Thesis, Duesseldorf, Germany* (2001)
[127] Schubert, H., Handbuch der Verfahrenstechnik, Wiley-VCH, Weinheim, (2003)
[128] Schulze, D. Flowability and Time Consolidation Measurements Using a Ring Shear Tester, *Powder handling & processing*. 3 (1996)
[129] Schulze, D. Measuring powder flowability: a comparison of test methods Part II, *Powder and Bulk Engineering*. 10 (1996)

[130] Schulze, D. Measuring powder flowability: A comparison of test methods. Part I, *Powder and Bulk Engineering*. 10: 45-61 (1996)
[131] Schulze, D. Zur Fliessfaehigkeit von Schuettguetern - Definition und Meflverfahren, *Chem.-Ing.-Tech.* 67: 60-68 (1995)
[132] Sheetz, D. P. Formation of fillms by drying of latex, *Journal of Applied Polymer Science*. 9: 3759 - 3773 (1965)
[133] Shin-Etsu Chemical Co., L., Hydroxypropyl Methylcellulose Acetat Succinat - Aqoat®, Product brochure (2005)
[134] Siepmann, F., Siepmann, J., Walther, M., MacRae, R. and Bodmeier, R. Aqueous HPMCAS coatings: Effects of formulation and processing parameters on drug release and mass transport mechanism, *European Journal of Pharmaceutics and Biopharmaceutics*. 63: 262-269 (2006)
[135] Specht, F., Saugestad, M., Waaler, T. and Muller, B. W. The application of shellac as an acidic polymer for enteric coating, *Pharmaceutical Technology Europe*. 10: 20-28 (1998)
[136] Staniforth, J. N., Rees, J. E., Lai, F. K. and Hersey, J. A. Interparticle forces in binary and ternary ordered powder mixes, *Journal of Pharmacy and Pharmacology*. 34: 141 - 145 (1982)
[137] Steward, P. A., Hearn, J. and Wilkinson, M. C. An overview of polymer latex film formation and properties, *Advances in Colloid and Interface Science*. 86: 195-267 (2000)
[138] Terebesi, I. Alternative polymers and processes for coating, *Ph. D. Thesis, Berlin, Germany* (2006)
[139] Tobiska, S. and Kleinebudde, P. Coating uniformity and coating efficiency in a Bohle Lab-Coater using oval tablets, *European Journal of Pharmaceutics and Biopharmaceutics*. 8: 39 - 46 (2003)
[140] Tomas, J. Zur Produktgestaltung kohaesiver Pulver - Mechanische Eigenschaften, Kompressions- und Flieflverhalten, *Chemie Ingenieur Technik*. 75: 651-661 (2003)
[141] Toussaint, A. and De Wilde, M. A comprehensive model of sintering and coalescence of unpigmented latexes, *Progress in Organic Coatings*. 30: 113-126 (1997)
[142] USP XXIX, Enteric Coated Articles - Method A, 2685 – 2686 (2006)
[143] Valdrè, G., Antognozzi, M., Wotherspoon, A. and Miles, M. J. Influence of properties of layered silicate minerals on Adsorbed DNA surface affinity, self-assembly and nanopatterning, *Philosophical Magazine Letters*. 84: 539 - 545 (2004)
[144] Vanderhoff, J. W., Tarkowski, H. L., Jenkins, M. C. and Bradford, E. B. Theoretical consideration of the interfacial forces involved in the coalescence of latex particles, *Journal of Macromolecular Chemistry*. 1: 361 (1966)

[145] Voyutsskii, S. S. Amendment to the papers by Bradford, Brown and co-workers: "Concerning mechanisms of film formation from high polymer dispersions", *Journal of Polymer Science*. 32: 528-530 (1958)
[146] Wang, J. and Ghebre -Sellassie, I., Aqueous Polymeric Dispersions as Film Formers, In: Pharmaceutical Dosage Forms: Disperse System, Marcel Dekker, New York, USA, 129 - 162 (1998)
[147] Watts, A., Sauer, D. and McGinity, J. Properties of Hard Gelatn Capsules Coated with an Acrylic Polymer by a Dry Powder Coating Process, *Proc. AAPS Annual Meeting and Exposition*. (2006)
[148] Wheatley, T. A. and Steuernagel, C. R., Latex Emulsions for Controlled Drug Delivery, In: Aqueous Polymeric Coatings for Pharmaceutical dosage forms, Marcel Dekker, New York, USA, 1 - 54 (1997)
[149] Wu, S. H. W., Wyatt, D. M. and Adams, M. W., Chemistry and Application of Cellulosic Polymers for Enteric Coatings of Solid Dosage Forms, In: Aqueous Polymeric Coatings for Pharmaceutical Dosage Forms, Marcel Dekker, New York, USA, 385 - 418 (1997)
[150] Young, P. M., Price, R., Tobyn, M. J., Buttrum, M. and Dey, F. The influence of relative humidity on the cohesion properties of micronized drugs used in inhalation therapy, *Journal of Pharmaceutical Sciences*. 93: 753-761 (2004)
[151] Zang, L., Nanoscale Exploration and Single-Molecule Imaging, Southern University of Illinois, Carbondale, USA (2004)
[152] Zhao, C. L., Wang, Y. C., Hruska, Z. and Winnik, M. A. Molecular Aspects of Latex Film Formation - An Energy-Transfer Study, *Macromolecules*. 23: 4082-4087 (1990)
[153] Zheng, W., Cerea, M., Sauer, D. and McGinity, J. Properties of theophylline tablets powder-coated with methacrylate ester copolymers, *Journal of Drug Delivery Science and Technology*. 14: 319-325 (2004)
[154] Zhu, J., Luo, Y., Ma, Y., Zhang, L., Huang, J., Lum, S. and Chow, K. Dry Powder Coating of Pharmaceutical Tablets by Electrostatic Pan Coating, *Proc. AAPS Annual Meeting and Exposition*. (2006)